

University of Alberta

Near-neutral pH Stress Corrosion Crack Initiation under Simulated Coating
Disbondment

by

Abdoulmajid Eslami

A thesis submitted to the Faculty of Graduate Studies and Research
in partial fulfillment of the requirements for the degree of

Doctoral of Philosophy

in

Materials Engineering

Department of Chemical and Materials Engineering

©Abdoulmajid Eslami

Fall 2012

Edmonton, Alberta

Permission is hereby granted to the University of Alberta Libraries to reproduce single copies of this thesis and to lend or sell such copies for private, scholarly or scientific research purposes only. Where the thesis is converted to, or otherwise made available in digital form, the University of Alberta will advise potential users of the thesis of these terms.

The author reserves all other publication and other rights in association with the copyright in the thesis and, except as herein before provided, neither the thesis nor any substantial portion thereof may be printed or otherwise reproduced in any material form whatsoever without the author's prior written permission.

To Prophet Muhammad, the Messenger of Peace and Mercy.

Abstract

This research is aimed at understanding near-neutral pH SCC initiation under disbonded coatings of pipeline steels, and the effect of different environmental and operational factors on crack initiation. Understanding near-neutral pH stress corrosion cracking (SCC) could answer many of the primary questions on crack initiation of SCC which have not yet been answered. It could also assist the development of effective mitigative measures dealing with thousands of kilometers of pipelines containing this form of cracking, in addition to preventive action for future pipeline installations.

Near-neutral pH SCC usually occurs under polyethylene tape (PE tape) coated pipelines, at locations where the coating becomes disbonded and/or damaged. Ground water can then penetrate under the damaged/disbonded coating, become trapped and form a suitable environment for corrosion and cracking. Despite extensive studies on this topic the details of crack initiation mechanisms in addition to the exact role of environmental and operational factors on crack initiation are not thoroughly understood. Most previous laboratory tests have been done in aggressive loading conditions and ignored the effect of coatings and cathodic protections (CP).

In order to simulate the conditions responsible for crack initiation, a novel testing setup capable of simulating the synergistic effects of coating disbondment, cathodic protection and cyclic loading was implemented. Using this setup and

long term laboratory tests near-neutral pH SCC initiation mechanisms and the effect of some environmental and operational factors on crack initiation were investigated. It was found that near-neutral pH SCC initiation does not necessarily occur in near-neutral pH environments as commonly believed. Depending on the level of CP and CO₂ in the underground environment, different localized environments with varying pH values from near-neutral to high values above 10 can form under the disbonded coatings. This significantly affected the corrosion and near-neutral pH SCC initiation mechanisms. These investigations brought out new findings about the effect of environment and operations on near-neutral pH SCC initiation.

Acknowledgments

First and foremost, I would like to express my special thanks to my supervisors, Prof. Weixing Chen and Prof. Reg Eadie, for their guidance, patience and continuous support throughout the course of my doctoral program. It has been a great pleasure to conduct research under their supervision. I am also thankful to the members of the examining committee, Dr. Winston Revie, Dr. Xiodong Wang, and Dr. Jingli Luo. Special thanks to examining committee chair Dr. Dave Mitlin.

My special thanks to the Department of Chemical and Materials Engineering members at the University of Alberta. Special thanks to Walter Boddez, Richard Cooper, Clark Bicknell, Tina Barker, Shiraz Merali, and Kevin Heidebrecht from the technical support group. Also, I acknowledge my colleagues, Hishang Wang, Mohammad Hassan Marvasti, Afolabi Egbewande, Hao Li, Tianfei Wang, Jared Schoepp, and Dr. Yongwang Kang.

This work was financially supported by NSERC, TransCanada Pipelines Limited and Spectra Energy. I gratefully acknowledge their funding.

I would like to thank my parents for all accomplishments I have made throughout my life. Many thanks to my brother Dr. Mohsen Eslami, a former U of A graduate, for his guidance and encouragement throughout the course of my studies. Beyond words I would like to thank my wife Bi Bi Fatemeh for her love, support, and understanding. She has made my PhD studies our first priority during the past years. Finally I would like to thank Yasaman, our beautiful newborn girl, whom has made life more enjoyable during the final months of my PhD.

Table of Contents

Chapter 1: Background and Literature Review	1
1.1. Research background	2
1.2. Literature review	4
1.2.1. Oil and gas transmission pipelines.....	4
1.2.2. Stress corrosion cracking on oil and gas pipelines	4
1.2.3. Field understanding of near-neutral pH SCC.....	6
1.2.3.1. A Potent Environment.....	7
1.2.3.2. Susceptible pipe	9
1.2.3.3. Stress	10
1.2.4. Laboratory research on near-neutral pH SCC.....	11
1.2.5. Testing techniques used for near-neutral pH SCC initiation studies ..	16
1.2.5.1. Mechanical Tests	17
1.2.5.2. Weight loss corrosion tests	18
1.2.5.3. Electrochemical tests	18
1.2.6. Research findings on near-neutral pH SCC initiation.....	19
1.2.6.1. Effect of mechanical factors on near-neutral pH SCC initiation .	20
1.2.6.2. Metallurgical and microstructural factors affecting near-neutral pH SCC initiation.....	23
1.2.6.3. Environmental factors affecting near-neutral pH SCC initiation	28
1.2.7. Current understanding of near-neutral pH SCC initiation mechanism	36
1.3. Research objective and thesis structure.....	38

1.4. References	40
Chapter 2: Design of a Comprehensive Test Setup for Simulating Field Conditions Responsible for Near-neutral pH SCC	48
2.1. Introduction	49
2.2. Design of a comprehensive test setup for simulating near-neutral pH SCC	50
2.2.1. The Corrosion cell.....	50
2.2.2. Specimen.....	53
2.2.3. Other considerations	54
2.3. Summary	55
Chapter 3: Near-neutral pH Stress Corrosion Crack Initiation under a Simulated Coating Disbondment: Effect of Time and Maximum Stress	56
3.1. Introduction	57
3.2. Experimental	58
3.2.1. Specimen, solution and corrosion cell	58
3.2.2. Stress corrosion cracking initiation tests.....	60
3.2.3. Characterization	61
3.3. Results and discussion	62
3.3.1. C2 solution	62
3.3.2. Potential distribution.....	62
3.3.3. pH distribution	63
3.3.4. Stress corrosion cracking initiation in Test A.....	64
3.3.5. Stress corrosion cracking initiation in Test B	68

3.3.6. SCC initiation mechanism	73
3.4. Conclusions.....	74
3.5. References.....	75
Chapter 4: Near-neutral pH Stress Corrosion Crack Initiation under the Simulated Coating Disbondment: Effect of CO₂ and R-ratio	77
4.1. Introduction.....	78
4.2. Experimental	79
4.2.1. Specimen, solution and corrosion cell	79
4.2.2. Stress corrosion cracking initiation tests.....	80
4.2.2.1. CO ₂ variation in the tests	80
4.2.2.2. R-ratio	80
4.2.2.3. Characterization	81
4.3. Results and discussion	81
4.3.1. pH and potential distribution	81
4.3.2. Stress corrosion cracking initiation tests.....	84
4.3.3. Effect of R-ratio	92
4.3.4. The role of anodic dissolution, CP, and hydrogen in crack initiation mechanisms.....	95
4.4. Conclusions.....	95
4.5. References.....	96
Chapter 5: Near-neutral pH Stress Corrosion Crack Initiation under the Simulated Coating Disbondment: Effect of Oxygen.....	99
5.1. Introduction.....	100

5.2. Experimental	101
5.2.1. Specimen, solution and corrosion cell	101
5.2.2. Stress corrosion cracking initiation tests.....	101
5.2.3. Electrochemical test	102
5.2.4. Characterization	103
5.3. Results and Discussion.....	103
5.3.1. The Reference Test (Test A).....	103
5.3.1.1. CP and pH distribution	103
5.3.1.2. General observation	104
5.3.1.3. Stress corrosion cracking initiation.....	106
5.3.2. Effect of oxygen on near-neutral pH SCC Initiation (Test B)	106
5.3.2.1. CP and pH distribution	106
5.3.2.2. General observations.....	107
5.3.2.3. Stress corrosion cracking initiation.....	108
5.4. Summary and Conclusion	114
5.5. References	116
 Chapter 6: Corrosion of Pipeline Steel under the Simulated Coating	
Disbondment.....	118
6.1. Introduction.....	119
6.2. Experimental	120
6.2.1. Specimen and solution	120
6.2.2. Corrosion cell and coupon holder	121
6.2.3. Corrosion tests	122

6.2.3.1. Electrochemical test	122
6.2.3.2. Weight loss corrosion tests	123
6.2.4. Characterization	123
6.3. Results and Discussions	124
6.3.1. X-65 pipeline steel	124
6.3.2. Corrosion of X-65 pipeline steel	125
6.3.2.1. Electrochemical tests	125
6.3.2.2. Weight loss corrosion test without considering coating disbondment at OCP (Test A)	127
6.3.2.3. Weight loss corrosion test considering coating disbondment at OCP (Test B).....	128
6.3.2.4. Weight loss corrosion test considering coating disbondment and CP (Test C)	131
6.4. Conclusions.....	134
6.5. References.....	135
Chapter 7: Electrochemical Processes under Simulated Coating	
Disbondments	137
7.1. Introduction.....	138
7.2. Experimental	140
7.2.1. Pipeline steel and soil solution.....	140
7.2.2. Corrosion cell.....	140
7.2.3. Test conditions and measurements	141
7.3. Results and Discussions	142

7.3.1. Reference Test.....	142
7.3.1.1. pH distribution	142
7.3.1.2. CP potential distribution	144
7.3.2. Effect of level of applied CP.....	145
7.3.2.1. pH distribution	145
7.3.2.2. CP potential distribution	147
7.3.3. Effect of exposed steel surface area	148
7.3.3.1. pH distribution	148
7.3.3.2. CP potential distribution	149
7.3.4. Effect of disbondment gap size.....	150
7.3.4.1. pH distribution	150
7.3.4.2. CP potential distribution	151
7.3.5. Effect of various factors	152
7.3.6. Effect of coating disbondment material	154
7.3.7. Corrosion and near-neutral pH SCC initiation.....	155
7.4. Conclusions.....	155
7.5. References.....	156
Chapter 8: Conclusions, Research Impact, and Recommendations	159
8.1. Conclusions.....	160
8.1.1. Near-neutral pH SCC initiation under the simulated coating disbondment and effect of environmental and operational factors	160
8.1.2. Corrosion of pipeline steel under the simulated coating disbondment	162

8.1.3. Electrochemical conditions under coating disbondments of pipelines	163
8.2. Research Impact	164
8.3. Recommendations	165
Appendix A: Experimental Setups	167
A.1. Mechanical loading testing frame	168
A. 2. Potentiostat	168
A.3. Reference Electrodes	169
A.3.1. Permanent reference electrode	169
A.3.2. Portable reference electrode	169
A.4. Micro-electrodes used for determining the pH inside coating disbondments	170
A.5. Oxygen probe used for determining oxygen concentration in soil solution	170
A.6. Conductivity probe used for determining the conductivity and resistivity of soil solutions	171
Appendix B: Experimental Procedures	172
B.1. Nickel plating procedure for cross sectional characterization	173
B.2. References	173

List of Tables

Table 1.1: Chemical composition of common near-neutral pH simulated soil solutions used in laboratory simulations [4, 36, and 47].	16
Table 2.1: Comparison between field conditions responsible for near-neutral pH SCC and laboratory test conditions.	49
Table 2.2: Novel test setup capabilities in simulating field conditions responsible for near-neutral pH SCC.	55
Table 3.1: Chemical composition of the X-65 pipeline steel used in this study, API specification for X-65 is also given.	59
Table 3.2: C2 solution chemistry [20].	59
Table 3.3: Near-neutral pH SCC initiation tests.	60
Table 3.4: Chemical composition of the rust remover solution.	61
Table 4.1: Near-neutral pH SCC initiation tests.	81
Table 4.2: Corrosion Rate of X-65 pipeline steel in simulated soil solution at different pH values [17].	89
Table 5.1: SCC initiation tests performed in this study.	101
Table 6.1: Weight loss corrosion tests performed in this study.	123
Table 7.1: Experimental conditions of tests investigated in this study.	142
Table 7.2: Different stages of the tests investigated in this study, representing CP and CO ₂ cycles*.	142
Table 7.3: Resistivity of the near-neutral and high-pH solutions.	145
Table 7.4: CO ₂ permeability and electrical resistivity of the materials used for the simulated coating disbondment in this study, T=25 °C [28, 29].	155

List of Figures

Figure 1.1: PE tape coating disbondments on a pipe surface [3].	2
Figure 1.2: Causes of pipeline ruptures on major Canadian pipelines (figure reproduced from reference [10]).	4
Figure 1.3: SCC pipeline failure site: Lowther, Ontario, August 1985 [1].	5
Figure 1.4: Typical cross sectional image of: (a) near-neutral pH SCC, (b) high-pH SCC [1].	6
Figure 1.5: Necessary elements for near-neutral pH SCC occurrence (figure reproduced from reference [1]).	7
Figure 1.6: Stress and crack distribution on pipe body [1].	10
Figure 1.7: Different stages of SCC (figure reproduced from reference [24]).	12
Figure 1.8: Crack growth rate da/dn as a function of $\Delta K^2 K_{max}/f^{0.1}$ in two simulated soil solutions: (a) C2 solutions, and (b) NOVATW solution [36].	15
Figure 1.9: Surface residual stress versus normalized distribution of pitting and cracking after cyclic loading experiments [53].	22
Figure 1.10: A comparison of axial residual stress along the gage length before and after cyclic loading in air [53].	23
Figure 1.11: Summary graph showing effect of microstructure and yield strength on near-neutral pH SCC initiation, investigated by SSR tests and cyclic loading tests.	27
Figure 1.12: Relation between pH and percentage of CO_3^{2-}/HCO_3^- species (figure reproduced from reference [86]).	30
Figure 2.1: Schematic showing coating disbondment on a pipe section.	50

Figure 2.2: Schematic of the corrosion cell designed for simulating near-neutral pH SCC.	51
Figure 2.3: Schematic of the tensile specimen and coupon holder.	54
Figure 3.1: Cathodic protection levels at different positions from OM, at different time intervals.	63
Figure 3.2: pH distribution of the soil solution inside the shielding at different positions from OM, at different time intervals.	64
Figure 3.3: Typical surface morphologies of the tensile specimen after Test A, at locations: (a) close to OM, (b) between OM and the far end, (c) remote from the OM.	65
Figure 3.4: (a) Average pit diameter based on position from OM in Test A, (b) percent pit surface coverage based on position from OM in Test A.	66
Figure 3.5: EDX spectra showing the composition of the non-metallic inclusion.	67
Figure 3.6: Typical surface morphologies of the tensile specimen after Test B at locations: (a) close to OM, (b) between the OM and the far end, (c) remote from the OM.	69
Figure 3.7: (a) Average pit diameter based on position from OM in Test B, (b) percent pit surface coverage based on positions from OM in Test B.	70
Figure 3.8: Average pit depth as a function of position from OM in Test A and Test B.	71
Figure 3.9: Secondary Scanning Electron Microscope (SEM) image showing the cross section of the sample after Test B, at 10 cm from the OM.	72

Figure 3.10: Secondary Scanning Electron Microscope (SEM) image showing the cross section of the sample after Test B, at 15 cm from the OM.....	73
Figure 3.11: Schematic showing SCC initiation mechanism from: (a) surface of pits (surface view), (b) Bottom of pits (cross section view).....	74
Figure 4.1: Digital camera image showing a polyethylene tape coating disbondment on pipe surface.	78
Figure 4.2: pH variation inside the shielding at different positions from the OM in: (a) Test A, (b) Test B, and (c) Test C.	82
Figure 4.3: Potential distribution prior and after applying CP at different positions from the OM (cm).....	83
Figure 4.4: Typical surface morphologies of the tensile specimen after Test A, at: (a) close to OM, (b) between OM and the far end, (c) remote from the OM.	85
Figure 4.5: A semi-quantitative distribution of the number of corrosion pits at different positions from the OM after Test A.	86
Figure 4.6: Typical surface morphologies of the tensile specimen after Test B at: (a) close to OM, (b) between the OM and the far end, (c) remote from the OM.	87
Figure 4.7: (a) Typical image showing surface micro-cracks formed after Test B inclined 45° inclined to the loading direction (b) a surface micro-crack formed along a scratch line.....	88
Figure 4.8: A semi-quantitative distribution of the number of corrosion pits and surface micro-cracks at different positions from the OM after Test B.	88
Figure 4.9: Typical surface morphologies of the tensile specimen after Test C at: (a) close to OM, (b) between the OM and the far end, (c) remote from the OM.	90

Figure 4.10: A semi-quantitative distribution of the number of corrosion pits and surface micro-cracks at different positions from the OM after Test C.	91
Figure 4.11: High magnification image showing the formation of several sub-micrometer pits in and around the surface micro-cracks after Test C.	92
Figure 4.12: Typical image showing branched micro-cracks initiated at the mouth of a large pit after Test D. Circle shows branched micro-cracks which were initiated at and branched out from the mouth the pit during the test.	93
Figure 4.13: Typical image showing the cross section of the sample after Test D. Circle shows the cross section of a pit with a sharp tip formed during the test....	94
Figure 4.14: Average pit depth as a function of position from the OM in Test A and Test D.	94
Figure 5.1: Digital camera image of the test setup used of electrochemical polarization tests.	102
Figure 5.2: Open Circuit Potential (OCP) and CP potential distribution at different positions from the OM and at the beginning of Test A (the Reference Test).....	104
Figure 5.3: pH variation at different positions from the OM in Test A (the Reference Test).	104
Figure 5.4: Digital camera image of the specimen inside the corrosion cell at the end of Test A (the Reference Test).	105
Figure 5.5: Open Circuit Potential and CP potential distribution at different positions from the OM, at the beginning of Reference Test and Test B (the test with 1% oxygen).	107

Figure 5.6: Digital camera image of the specimen inside the corrosion cell at the end of Test B (the test with 1% oxygen).....	108
Figure 5.7: (a) Average pit diameter at different positions from the OM in Test A (the Reference Test), (b) Average pit diameter at different positions from the OM in Test B (the test with the effect of 1% oxygen).	109
Figure 5.9: Typical image of the specimen surface showing a pit at 9 cm from the OM in: (a) Test A (the Reference Test), (b) Test B (the test with the effect of 1% oxygen).	111
Figure 5.10: A relatively long micro-crack initiated from the mouth of a pit at 8 cm from the OM in Test B (the test with the effect of 1% oxygen).	112
Figure 5.11: Typical pit formed at 10 cm from the OM in: (a) Test A (the Reference Test), (b) Test B (the test with the effect of 1% oxygen).	113
Figure 5.12: Average pit depth as a function of position from the OM in Test A (the Reference Test), compared to Test B (the test with the effect of 1% oxygen).	114
Figure 5.13: Effect of oxygen on crack initiation on pipeline steel surface under the coating disbondment.	115
Figure 6.1: Typical image of coating disbondments formed on a seam weld of a pipe section.	119
Figure 6.2: (a) Schematic of the corrosion cell with the shielding, (b) schematic of the coupon holder with coupons.	122
Figure 6.3: Typical microstructure of the X-65 pipeline steel investigated in this study.....	125

Figure 6.4: Diagram of the potentiodynamic scanning for the X-65 pipeline steel at different pH values.....	125
Figure 6.5: Digital camera image showing X-65 pipeline steel surface 3after the potentiodynamic polarization scan at different pH values: (a) at pH=6.29, and (b) at pH=11.	126
Figure 6.6: (a) Typical image of the steel surface after Test A (30 day test without considering coating disbondment at OCP), (b) high magnification image showing selective corrosion of ferrite after Test A.	128
Figure 6.7: Corrosion rate of X-65 pipeline steel after the 30 day weight loss corrosion tests at OCP condition at different positions from the OM inside the simulated coating disbondment compared with test at OCP where no coating disbondment was used.	129
Figure 6.8: Typical images showing the X-65 pipeline steel microstructure at: a) close to OM, b) far end from the OM, after the 30 day weight loss corrosion test.	130
Figure 6.9: pH distribution under the simulated coating disbondment at different positions from the OM.	131
Figure 6.10: Potentials distribution at different positions from the OM, before and after a CP of $-1.2V_{SCE}$ was applied to the OM.....	132
Figure 6.11: Effect of CP on corrosion mitigation under the coating disbondment at different positions from the OM, compared with OCP tests at situation with and without the shielding effect of the simulated coating disbondment after the 30 day weight loss corrosion tests.	132

Figure 6.12: Schematic showing corrosion rate of pipeline steel at different positions under a coating disbondment as a function of: (a) amount of CO₂ (reactants), (b) level of CP. 134

Figure 7.1: pH variation at different positions from the OM, in the Reference Test. Stage I experiences CP and gas containing 5%CO₂/N₂, stage II experiences CP while the gas has been turned off, stage III again experiences CP and gas containing 5% CO₂/N₂, stage Iv experiences gas containing 5%CO₂/N₂ while the CP has been turned off, and Stage v experiences no CP and gas supply. 143

Figure 7.2: CP potential distribution in the Reference Test, at different positions from the OM in near-neutral pH and localized high and environment compared to the open circuit potential (OCP). 144

Figure 7.3: pH variation at different positions from the OM when CP potentials of: (a) -1.2 V_{SCE}, (b) -1.00 V_{SCE}, and (c) -0.8 V_{SCE} was applied to the OM. Gas containing 5%CO₂/N₂ is being supplied in stages I, and is turned off at the beginning of stage II, and turned on again in stage III. 146

Figure 7.4: CP potential distribution at different positions from the OM in near-neutral pH environment, when CP potentials of -1.2 VSCE, -1.00 VSCE and -0.8 VSCE were applied to the OM, compared to the OCP. 147

Figure 7.5: pH variation at different positions from the OM in: (a) the Reference Test, (b) the test with double exposed steel surface area. Gas containing 5%CO₂/N₂ is being supplied in stages I, and is turned off at the beginning of stage II, and turned on again in stage III. 148

Figure 7.6: OCP and CP potential distribution at different positions from the OM in near-neutral pH environment in the test with double the surface area compared to the Reference Test.	149
Figure 7.7: pH variation at different positions from the OM in: (a) the Reference Test , (b) in the test with reduced disbondment gap size. Gas containing 5%CO ₂ /N ₂ is being supplied in stages I, and is turned off at the beginning of stage II, and turned on again in stage III.	150
Figure 7.8: OCP and CP potential distribution at different positions from the OM in near-neutral pH environment in the test with reduced disbondment gap size compared to the Reference Test.....	151
Figure 7.9: CP potential distribution around the OM of the simulated coating disbondment: a) in the Reference Test, b) in the test with reduced disbondment gap size.....	152

Chapter 1: Background and Literature Review

1.1. Research background

Near-neutral pH stress corrosion cracking has been a major integrity threat for oil and gas transmission pipelines worldwide. The first pipeline failure due to near-neutral pH SCC was recognized in 1985. In that year, three ruptures occurred on pipelines in Ontario operated by TransCanada Pipelines (TCPL). Examination of the failed pipe sections indicated that the failures were the result of stress corrosion cracking (SCC). This SCC exhibited different characteristics than the typical high-pH SCC that had been studied since 1960s. This new form of SCC was called near-neutral pH SCC [1].

Today, several thousand kilometers of major oil and gas pipelines suffer from near-neutral pH SCC. It has been responsible for a considerable number of pipeline failures during the past years [1]. The cracking is ten times more likely to occur under polyethylene tape (PE) coated pipelines than on asphalt or coal tar coated pipes [2]. It is most likely to occur in regions where the disbonded PE tape coating forms a long wrinkle shaped structure which could be filled with ground water (Figure 1.1).

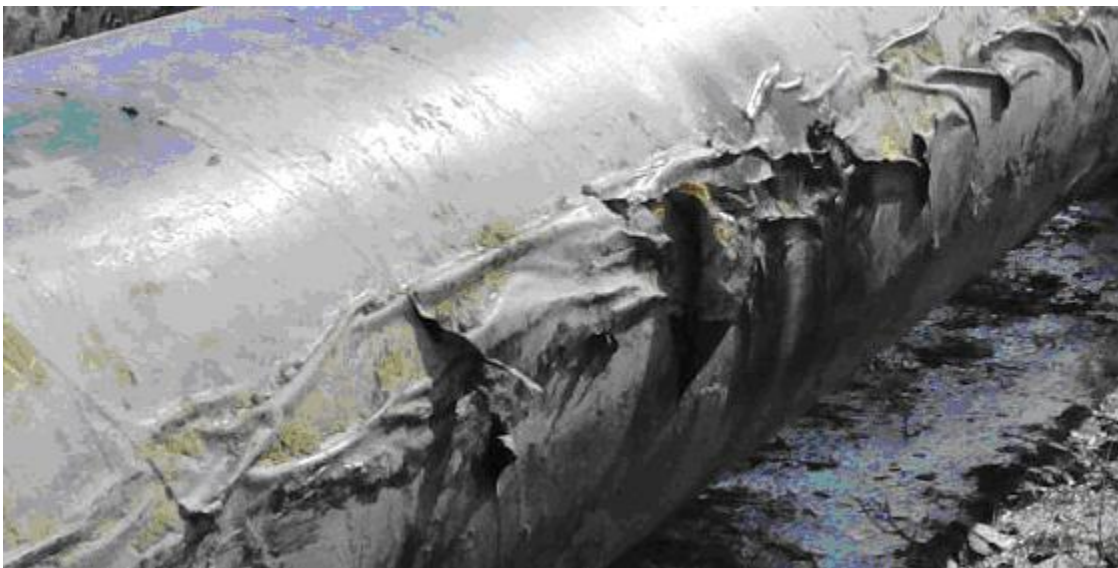


Figure 1.1: PE tape coating disbondments on a pipe surface [3].

Extensive field investigations have shown that near-neutral pH SCC is characterized by wide transgranular cracks [2, 4], and occurs in dilute near-neutral pH soil environments with a pH around 6.5 [5, 6, 7]. It has been indicated that factors like cathodic protection (CP) and coating condition, soil solution chemistry and dissolved gases, steel microstructure and pipe surface condition, and stresses from pipe manufacturing and operation could affect near-neutral pH SCC occurrence and severity [1].

Laboratory research on near-neutral pH SCC was conducted from the initial days of its discovery. Despite extensive laboratory investigations, its exact initiation mechanism(s), and the true effect of environment and pipe operation on crack initiation are not well understood. This might be due to complicated field conditions causing this form of cracking, and/or simplifications done in laboratory tests. For instance, most researchers have underestimated or ignored one or more of the following aspects during their laboratory investigations:

- True stress condition
- Coating disbondment
- Cathodic protection
- Variable environment
- Required time for crack initiation

Understanding the exact mechanism(s) of near-neutral pH SCC initiation, in addition to the true effect of environment, materials, and operating conditions on near-neutral pH SCC is significantly important to the pipeline industry and academia. While it could save millions of dollars for the pipeline industry, it would also solve a challenging industrial issue after years of research on this topic.

Section 1.2 will provide a comprehensive review of the literature pertinent to this area of research.

1.2. Literature review

1.2.1. Oil and gas transmission pipelines

There are more than 540 000 kilometers of buried oil and gas transmission pipelines in Canada alone [1]. They carry a variety of products such as natural gas, crude oil, propane as well as refined gasoline and jet fuel [1]. In order to prevent leaks or ruptures from environmental and mechanical damage, pipelines are regularly inspected and monitored. Despite these efforts, leaks and/or ruptures have been still occurring during past years [1, 8, 9].

Pipeline integrity threats are different in their nature and severity (Figure 1.2). Depending on the type, location and extent of each type of damage, integrity actions are performed. According to the National Energy Board (NEB), the major threats to pipeline integrity are corrosion and cracking [10].

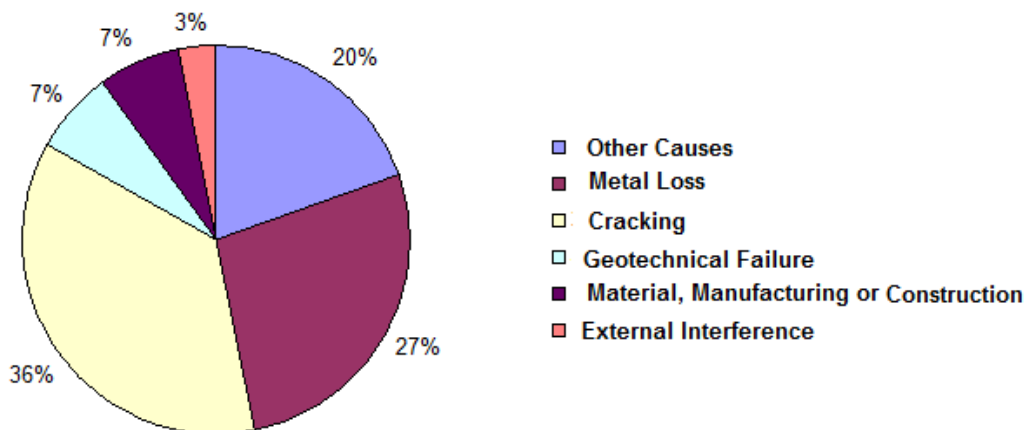


Figure 1.2: Causes of pipeline ruptures on major Canadian pipelines (figure reproduced from reference [10]).

1.2.2. Stress corrosion cracking on oil and gas pipelines

Stress corrosion cracking has been identified as one of the environmental assisted forms of cracking [1]. SCC has been an industrial threat for oil and gas transmission pipelines worldwide. Pipelines in Australia, Iran, Iraq, Italy,

Pakistan, Saudi Arabia, Russia, Canada and the United States have all experienced SCC [2, 11-13].

Stress corrosion cracks are not visible with the naked eye once initiated. They grow in both the surface and depth directions, and form colonies of cracks. If they reach a critical depth, they would cause pipeline leak or rupture. This might cost pipeline companies tens of thousands of dollar in repair and excavation costs, in addition to environmental damage and risk to the public. Figure 1.3, shows a SCC pipeline failure site [1].



Figure 1.3: SCC pipeline failure site: Lowther, Ontario, August 1985 [1].

Stress corrosion cracking is categorized in two general forms i.e., high-pH (classical) SCC, and near-neutral (non-classical) pH SCC. High-pH SCC was first reported in the mid-1960s [12]. It is intergranular in the steel microstructure with minor corrosion on crack walls [1]. It occurs in concentrated carbonate-bicarbonate soil solutions with pH values above 9 [1]. The mechanism of high-pH SCC is associated with continuous rupture and formation of passive films at the crack tip and along the grain boundaries [7, 14-16]. Near-neutral pH SCC, the non-classical form of SCC, is the more recent form of cracking identified on Canadian pipelines in the mid 1980s [2]. It appears transgranular in the

microstructure with evidence of corrosion on the crack walls. Figure 1.4 shows typical cross sectional images of high-pH and near-neutral pH SCC cracks [1].

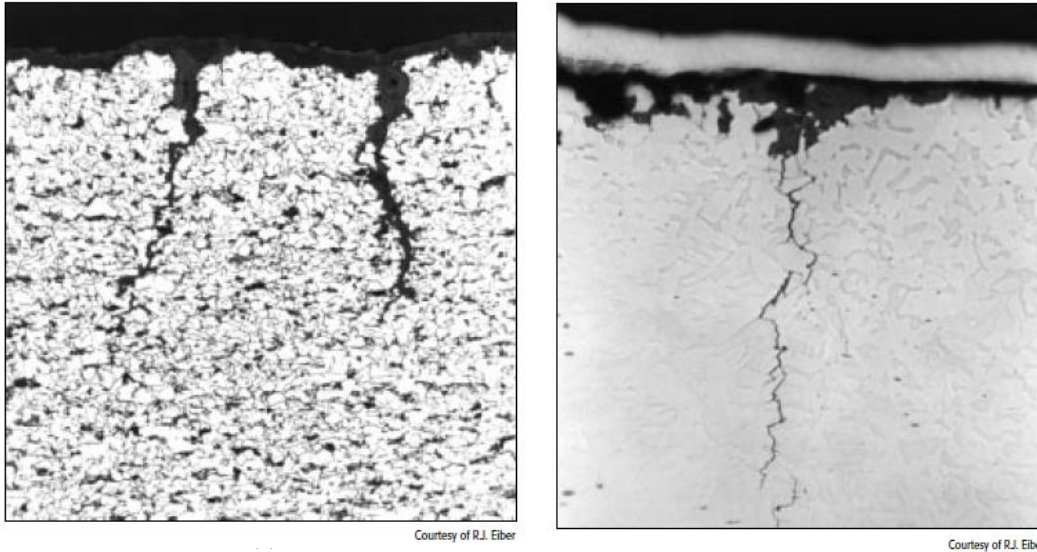


Figure 1.4: Typical cross sectional image of: (a) near-neutral pH SCC, (b) high-pH SCC [1].

As opposed to the high-pH SCC, there is much less understanding of near-neutral pH SCC. This might be due to the complicated field conditions causing this form of cracking, or simply because it is the more recently discovered form of cracking. In the following sections an overview of the current understanding of near-neutral pH SCC, from field and laboratory investigations, is provided.

1.2.3. Field understanding of near-neutral pH SCC

Near-neutral pH SCC has been identified as one of the environmentally assisted forms of cracking [1]. Field investigations have shown that a potent environment, a susceptible pipe and tensile stresses are the required elements for this form of cracking [1]. This is schematically shown in Figure 1.5, and explained in following sections.

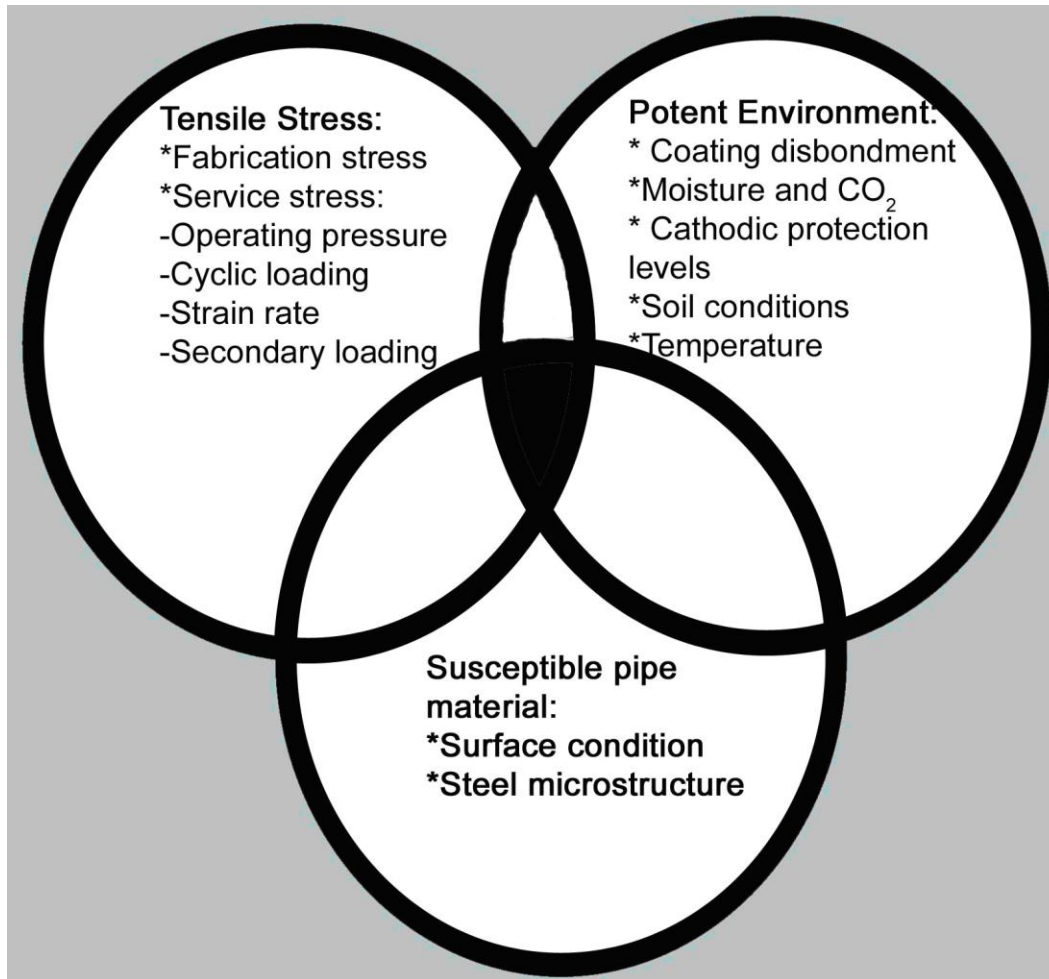


Figure 1.5: Necessary elements for near-neutral pH SCC occurrence (figure reproduced from reference [1]).

1.2.3.1. A Potent Environment

Coating disbondment, cathodic protection (CP), soil conditions, and temperature are the main indicators of a potent environment for near-neutral pH SCC [1].

a) Coating disbondment and cathodic protection

Failure of the pipeline coating is the primary source of SCC and corrosion [3]. In an ideal situation if the coating fails, CP would protect the pipe surface from corrosion and cracking. Unfortunately this is not always the case. Near-neutral pH SCC usually occurs under polyethylene (PE) tape coated disbondments, at locations where the coating gets damaged and/or disbonded [1]. If this occurs, ground water could penetrate and become trapped under the coating disbondment.

Due to the high resistivity of ground water and the shielding effect of the coating, CP cannot reach the pipe surface and a suitable environment for corrosion and cracking could be formed.

Near-neutral pH SCC has not been a serious problem for pipe coatings which do not shield CP (such as the epoxy coated pipes), nor those which tend to peel off once disbonded (such as the coal tar coating). In both situations, CP can reach the pipe surface and protect it from corrosion and SCC [17].

The exact level of CP penetration under coating disbondments could not be determined by regular methods used for measuring the pipe to soil potentials [18, 19]. Therefore, since corrosion and SCC are observed under tape coating disbondments, it is generally assumed that these locations are free from CP [6]. However this might not be true, since there is evidence of some CP penetration under tape coating disbondments [1].

b) Soil conditions

As long as the coating is perfectly attached to the pipe surface, soil conditions would not affect near-neutral pH SCC. Once the coating is damaged and/or disbonded, soil conditions could become active. Drainage, pH, dissolved gases, bacteria, and temperature are some of the soil parameters which have been studied during field investigations [1].

Field investigations have shown that near-neutral pH SCC occurs in soils with a pH range of 5.5-7.5 [1]. However, this pH might not represent the exact pH value under the tape coated disbondments at the time of the SCC and corrosion occurrence.

Near-neutral pH SCC has been observed occurring more often in poorly drained soils where reducing conditions are maintained [2]. These soils contain low

concentrations of carbonate-bicarbonate, with the presence of other species, including chloride, sulphate, and nitrates.

There are different types of dissolved gases (such as N₂, CO₂, O₂, and H₂S) in the underground environment. They come from different sources: CO₂ is mainly generated by the decay of organic matter in the soil environment, O₂ could penetrate from above ground, and H₂S could be generated by bacterial activity [2]. While field investigations have shown an increase in SCC severity with increased bacterial activity [2], due to the complicated field conditions there is no proof about the exact role of dissolved gases on near-neutral pH SCC.

Despite rupture levels being exceeded close to compressor and pump stations where the pipe and soil temperatures are higher, field investigations have not seen any direct relations between soil temperature and near-neutral pH SCC occurrence [2].

1.2.3.2. Susceptible pipe

All pipe steels used for oil and gas transmission pipelines are susceptible to near-neutral pH SCC [1]. These pipeline steels are low carbon steels which vary in strength and microstructure. They usually follow the API X-series standards [20]. Over time manufacturing companies have improved both microstructure and load bearing capacity of the pipe steels. X-80 and X-100 are examples of the more recent pipe grades which have been used for oil and gas transmission pipelines [21]. Due to complexity of field conditions causing near-neutral pH SCC, it is difficult to determine which pipe grades are more susceptible to near-neutral pH SCC. For instance, the lower SCC severity observed on some of the most recent pipes grades might be due to metallurgical factors, better coating systems, or improvement in CP protection systems [22].

1.2.3.3. Stress

Stress exists on the pipe body in two main directions, i.e. longitudinal and circumferential. Near-neutral pH SCC cracks are usually observed perpendicular to these directions (Figure 1.6).

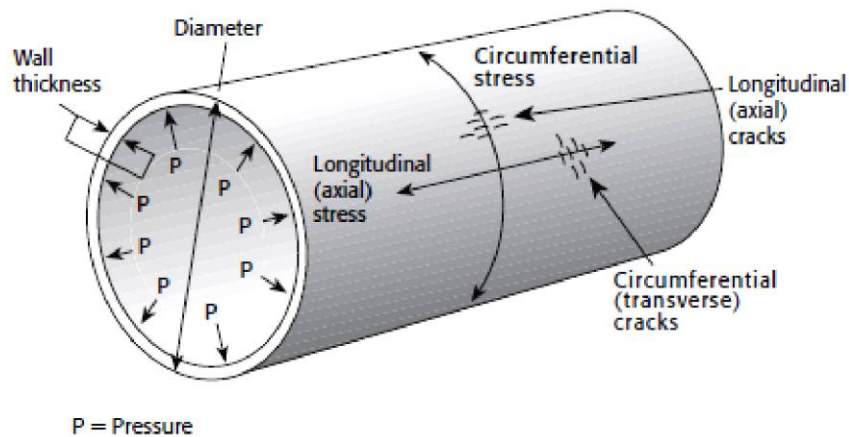


Figure 1.6: Stress and crack distribution on pipe body [1].

Different sources of stress exist on the pipe body. They consist of, but are not limited to [1]:

a) Stresses from pipe contents

Stresses caused by pipe contents cause internal operating pipeline pressure. The internal operating pipeline pressure causes hoop and longitudinal stresses on the pipe body. Hoop stress is the primary source of stress on the pipe body. It is common to express stresses from pipe contents in terms of percentage of SMYS¹, calculated from the hoop stress [1].

Pipe contents are pumped at different pressure levels. This causes stress fluctuations on the pipe body. The level of stress fluctuations is presented by R-ratio ($R = \text{minimum stress} / \text{maximum stress}$). A study done by CEPA² indicated that the lowest R-ratio is generally around 0.7 for liquid pipelines, while it is

¹ Specified Minimum Yield Stress

² Canadian Energy Pipeline Association

around 0.9 for gas pipelines. Both liquid and gas pipelines could experience R-ratios below 0.5 during operation, with much higher fluctuations for liquid pipelines [23]. Field investigations have shown a higher percentage of SCC colonies at distances close to pump stations [2, 3]. This might be due to the higher stress and increased stress fluctuations at these locations [2, 3].

b) Stresses from pipe manufacturing and installation

Stresses from pipe manufacturing and installation are usually caused during welding and from the bending of pipe joints. They appear on the pipe body as residual stresses, and could exceed 25 percent of the SMYS of the pipe material [1]. Field investigations have shown higher number of near-neutral pH SCC crack colonies close to weld lines [3]. While this might be due to coating disbondment and the stress concentration effect of the geometry at these locations, it may also be due to the higher levels of residual stresses close to weld lines. Higher numbers of SCC colonies were also observed at pipe bends, which could also be due to higher level of residual stresses at these locations [3].

c) Stresses from soil and ground movements

It is very difficult to determine the exact level of stress on buried pipelines caused by soil weight and ground movements. In some cases the stresses might be minor, while in others situations when combined with other sources of stresses; they might exceed the pipeline load bearing capacity and cause pipeline failure [1].

1.2.4. Laboratory research on near-neutral pH SCC

There has been significantly less research on near-neutral pH SCC as compared to high-pH SCC. Parkins [24] explained near-neutral pH SCC occurring in four stages i.e., development of conditions necessary for crack initiation, initiation of cracks, growth of the initiated cracks, and final failure of the pipeline (Figure 1.7).

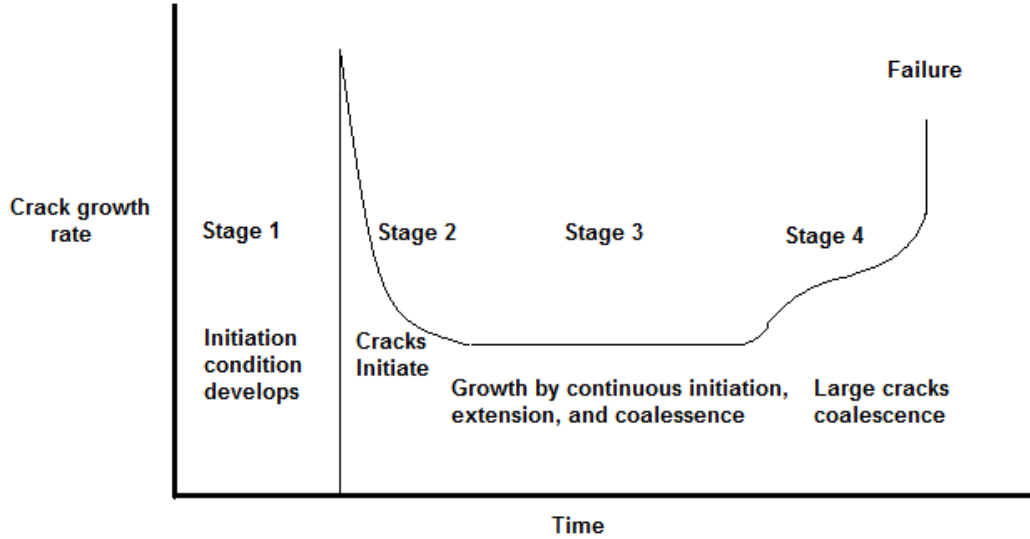


Figure 1.7: Different stages of SCC (figure reproduced from reference [24]).

As can be seen from Figure 1.7, crack initiation and growth are involved in the majority of the pipeline life time. This has encouraged researchers to focus their studies on these two main categories using different testing techniques in laboratories.

Crack growth studies have been carried out since recognition of near-neutral pH SCC in mid 1980's. Researchers have investigated different aspects of crack growth through laboratory research [25-37]. Recent studies have shown that hydrogen, anodic dissolution, cyclic stress, and low temperature creep play critical roles in near-neutral pH SCC growth mechanism(s) [29, 36 and 37]. While the exact growth mechanism is still subject to investigation, different growth models applicable to near-neutral pH SCC have been developed [29, 31, 36, 38, 39, and 40]. Due to the importance of these models and since they contain mechanistic understandings, an introduction to the more common models is presented below:

a) Paris Model

The Paris Model [41] is one of the simplest models of its kind. It correlates the crack growth rate per fatigue cycle, to the level change of stress intensity factor over the stress cycle. It is presented as:

$$\frac{da}{dn} = C_f \cdot \Delta K^m \quad (1-1)$$

Where $\frac{da}{dn}$ is the crack growth per cycle, ΔK is the amplitude of stress intensity over the stress cycle, C_f is the crack propagation fatigue coefficient (a material property), and m is the crack propagation fatigue exponent (also a material property).

As can be seen from Equation (1-1), the Paris model is a fatigue based model, which is purely dependent on material properties and loading parameters. It does not consider the effect of the environment. This model has shown limited success in fitting to near-neutral pH SCC data [36].

b) Crack Tip Strain Rate Model

Beavers et al. used the following formula to correlate the strain rate produced at the crack tip with the loading frequency and stress ratio [38]:

$$\varepsilon^0 = 4f(1 - R) \quad (1-2)$$

Where ε^0 is the crack tip strain rate, f is the loading frequency, and R is the stress ratio.

Beavers believed the above formula could be used to determine condition of crack dormancy or propagation. A careful examination of the above model with near-

neutral pH SCC data showed poor correlation [38, 40]. This might be due to the fact that this model, like the Paris model, has only considered fatigue as the driving force for near-neutral pH SCC.

c) Superposition Model

According to this model the crack growth rate in near-neutral pH SCC can be modeled as the superposition of fatigue crack growth in air, and SCC crack growth in constant load inside a corrosive environment [42-45]. This is shown in the following formula:

$$\frac{da}{dn}(total) = \frac{da}{dn}(fatigue) + \frac{1}{f} \frac{da}{dt}(scc) \quad (1-3)$$

Where $\frac{da}{dn}$ is the crack growth per cycle, f is the frequency of loading, and $\frac{da}{dt}$ is the crack growth per time of the cycle.

While improvements in correlating with near-neutral pH SCC laboratory testing data was observed using this model [44], it did not correlate well with near-neutral pH SCC field data [36].

d) True Corrosion Fatigue Model

A more recent and advanced model is the Through Corrosion Fatigue Model, introduced by Chen et al. [36]. In this model the crack growth behavior of the pipeline steel in near-neutral pH SCC is modeled as a function of fatigue and environment. The general formula for this model is:

$$\frac{da}{dn} = \Delta K^2 K_{max} / f^\alpha \quad (1-4)$$

Where $\frac{da}{dn}$ is the crack growth per cycle, ΔK is the change of stress intensity over the stress cycle, K_{\max} is the maximum stress intensity during the cycle, f is the loading frequency, and α is a factor that depends on the corrosivity of the environment. In addition to predicting the crack growth rate, the Through Corrosion Fatigue Model is capable of determining a threshold as a function of loading and environment where crack dormancy could occur (see Figure 1.8).

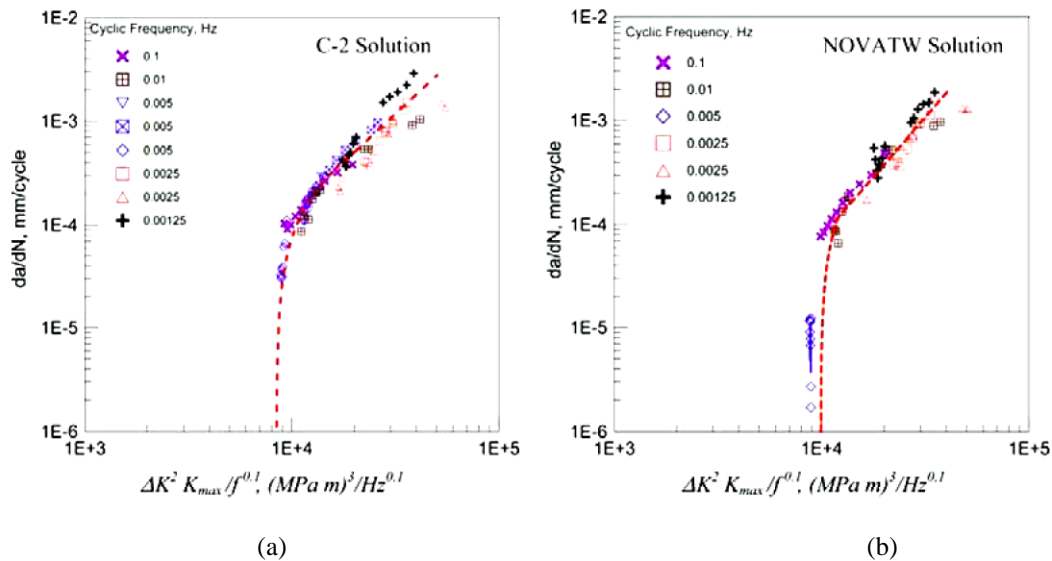


Figure 1.8: Crack growth rate da/dn as a function of $\Delta K^2 K_{\max} / f^{0.1}$ in two simulated soil solutions: (a) C2 solutions, and (b) NOVATW solution [36].

The potential value of this model in correlating with laboratory test data, and its ability to correlate with field data is still under investigation [29, 36, and 46]; but it has shown excellent applicability to date.

Similarly to crack growth studies, near-neutral pH initiation studies have been carried out from the early stages of near-neutral pH SCC recognition. The studies have investigated mechanism(s) of near-neutral pH SCC initiation, in addition to studying the effect of different mechanical, metallurgical, and environmental factors on near-neutral pH SCC initiation. Different testing techniques have been used for the studies. Relative to the subject of this thesis, the remainder of this literature review will be focused on introducing the common testing techniques

used for the near-neutral pH SCC initiation studies, followed by a review on important findings on near-neutral pH SCC initiation, Also, some of the knowledge gaps pertinent to this area are introduced.

1.2.5. Testing techniques used for near-neutral pH SCC initiation studies

Near-neutral pH SCC initiation laboratory studies are usually performed in simulated soils solutions, representing the ground water found around SCC sites. The simulated soil solutions are mainly dilute calcium-carbonate solutions with a pH around neutral. Chemical composition of three common near-neutral pH simulated soil solutions, used for laboratory simulations is presented in Table 1.1.

Table 1.1: Chemical composition of common near-neutral pH simulated soil solutions used in laboratory simulations [4, 36, and 47].

Concentration Solution	g/L KCl	g/L NaHCO ₃	g/L CaCl ₂	g/L MgSO ₄	g/L CaCO ₃	pH (with 5%CO ₂ , 95%N ₂)
NS4	0.122	0.483	0.181	0.131	-	6.3
NOVATW	0.015	0.437	-	-	0.23	7.11
C2	0.0035	0.0195	0.0255	0.0274	0.0606	6.29

Real soil solutions might have some components which have not been considered in the simulated soil solutions. One of these components is bacteria. Fang et al. explained the discrepancy between the results obtained from near-neutral pH SCC tests in laboratory to that observed in field by the possible effect of bacteria [48]. Despite this, the simulated soil solutions are quite reliable in terms of simulating near-neutral pH SCC soil conditions. In this regard, Beavers and Harle [22] showed that anodic potentiodynamic polarization curves for real soil extracts were similar to that observed for simulated NS4 solution.

The laboratory testing techniques used for near-neutral pH SCC initiation studies could be categorized, but not limited to the following; mechanical tests, weight loss corrosion tests, and electrochemical tests. Each is briefly introduced in the following sub-sections.

1.2.5.1. Mechanical Tests

Slow strain rate (SSR) tests and cyclic loading tests are the most common type of mechanical testing techniques used for near-neutral pH SCC investigations. While cyclic loading tests are a more appropriate form of testing in terms of being capable of simulating the actual pipe stress conditions, both testing techniques have been used during the past years for near-neutral pH SCC simulations. Standard and non-standard specimens such as Compact Tension (CT) specimens, round/flat tensile testing specimens, and full scale and curved specimens could be used for these tests [33, 47, 49-51].

In SSR tests [52] the specimen is subjected to a simulated soil environment under slow constant strain rate, usually up to failure. This test is accompanied with necking and extensive plastic deformation around the necking region [22]. The susceptibility to near-neutral pH SCC could be determined in SSR tests by determining the ratio of reduction in the specimen cross sectional area measured in the corrosive environment (RA_{SCC}) to that compared to air (RA_{air}) [4, 6]. While SSR tests are relatively simple and fast, they have been criticized for using aggressive loading conditions that misrepresent the actual pipe stress conditions [4, 22].

Cyclic loading test is the other common type of mechanical testing technique, more capable of simulating actual pipe stress conditions (see section 1.2.3.3). For each cyclic loading test, the following parameters should be known:

- R-ratio
- Maximum stress (σ_{\max})
- Frequency (f)

Both crack initiation and growth studies may be carried out using cyclic loading tests. If non-aggressive loading conditions are used, it might take up to several months for cracks to be initiated in cyclic loading tests [53]. By using pre-cracked specimens and monitoring crack growth rates by potential drop systems, crack growth studies could take a much shorter time [54].

1.2.5.2. Weight loss corrosion tests

Weight loss corrosion tests are usually performed in order to determine the corrosion rate of a specific pipeline steel in various soil environments [36, 55], or the corrosion rates of different pipeline steels in a particular environment [37]. The corrosion rate presents an average corrosion rate for the testing period, and is usually expressed in units like $\text{mg}/(\text{cm}^2 \cdot \text{sec})$ or mm/sec . In addition to the corrosion rate obtained from the weight loss corrosion tests, micro-structural changes after corrosion exposure could be studied [55].

1.2.5.3. Electrochemical tests

Electrochemical tests are an accelerated type of test which have been extensively used in near-neutral pH SCC studies in order to assist understanding of crack initiation and growth. While they are valuable in terms of instantaneous estimation of the corrosive environment, they might not reflect the true corrosion behavior of pipeline steels which have been exposed to corrosive environment for long time periods. Polarization techniques, hydrogen permeation tests and EIS¹ measurements are the most common type of electrochemical tests used for near-neutral pH SCC initiation and growth studies. A brief introduction to these

¹ Electrochemical Impedance Spectroscopy

testing techniques is presented below (more details can be found in references 56, 57, and 58).

Polarization tests are performed by potentiodynamic or potentiostatic techniques. For each technique a three electrode system consisting of a working, reference, and a counter electrode is used. Depending on availability and application, different types of reference and counter electrodes could be used. In potentiostatic testing techniques the steel potential is kept constant for a known time frame, and current density is recorded as a function of time. In potentiodynamic testing technique, the testing unit scans the potential on pipeline steel at a known rate, and records the current density. Using these testing techniques, the corrosion rate of pipeline steel, corrosion potential, and existence of oxide films could be investigated. Selecting the proper scan rate in potentiodynamic polarization tests is important, since it can affect the results [57].

In hydrogen permeation tests, the level of hydrogen entry into steel microstructure can be investigated. The most common type of testing method for obtaining the level of hydrogen entry into the steel microstructure is the Davanathan-Stachurski testing technique [58]. In this testing technique, a thin specimen (on the order of mm thickness) is placed in between two corrosion cells. On one side of the specimen surface, hydrogen is generated and diffuses through the metal which is then oxidized on the other side of the specimen. The rate of hydrogen permeation is proportional to the measured current density on the oxidizing surface.

EIS measurements have also been used in near-neutral pH SCC studies mainly in order to determine the characteristic of soil solutions and/or surface deposits, or investigating corrosion reaction mechanisms [59, 60, and 61].

1.2.6. Research findings on near-neutral pH SCC initiation

Near-neutral pH initiation studies have been carried out from its early stage of recognition. The studies have investigated the effect of different mechanical,

metallurgical, and environmental factors on near-neutral pH SCC initiation. A review of the important findings in this regard is presented in the following subsections.

1.2.6.1. Effect of mechanical factors on near-neutral pH SCC initiation

a) Effect of loading condition

Parkins et al. [4] investigated the initiation of near-neutral pH SCC cracks in specimens subjected to cyclic loading and maximum stress approximating those of an operating pipe line. It was observed that the initiation of cracks was facilitated by the formation of corrosion pits at locations where localized environment were generated. By increasing the maximum applied stress in cyclic loading tests, a higher number of cracks were initiated.

Fang et al. [62] studied crack initiation in cyclic and constant loading tests. It was observed that the required time for crack initiation was considerably shortened in cyclic loading tests as compared to constant loading tests. This was explained by enhanced micro-deformation and crack tip strain rate due to cyclic loading.

Wang et al. [63] investigated the effect of cyclic loading prior to corrosion exposure under constant load, on near-neutral pH SCC initiation. It was found that at protected CP conditions, cyclic loading facilitates micro-crack initiation. The micro-cracks established sites for crack initiation, and facilitated the development of SCC cracks in subsequent SSR tests. No micro-cracks were observed at OCP condition, due to general corrosion occurring and covering the surface.

Despite some studies showing that near-neutral pH SCC crack could be initiated under sustained loading condition [62, 64], it has been suggested that near-neutral pH SCC is more a form of corrosion fatigue rather than SCC [29].

b) Effect of stress concentration

Regions of stress concentration could exist on the pipe body. They could be simulated in laboratories artificially (such as by forming scratches on a pipe surface), or naturally during long term laboratory tests (such as a result of formation of corrosion pits). Under this premise, Kushida et al. [65] and He et al. [66] indicated that scratches perpendicular to the loading direction facilitated near-neutral pH SCC crack initiation. Fang et al. [67] observed micro-cracks being initiated after long term cyclic loading tests from corrosion pits formed on the steel surface. While most researchers agree that stress concentration could facilitate the crack initiation, there are different explanations. Some explain that the increase in dislocation density at stressed concentrated regions could ease micro-crack formation [68]. Some explain stress concentration facilitates hydrogen ingress into steel microstructure, which could then facilitate the crack initiation [69, 70]. In addition to these explanations, there is evidence showing enhanced localized dissolution at highly deformed surfaces which contain stress concentrations [71, 72]. Despite the explanations, there is no solid understanding about the exact role of each factor on crack initiation.

c) Effect of residual stress

Boven et al. investigated the effect of residual stresses on near-neutral pH SCC initiation using long term cyclic loading tests [53]. The residual stresses were measured with the neutron diffraction method [73] at multiple points along the length and through the depth of the specimen. The formation of corrosion pits peaked at locations with the highest initial residual stresses. This suggested that areas with the highest residual stresses were anodic with respect to areas with lower residual stress levels. Micro-cracks were generally initiated from pits on the surface. However not all pits were associated with a micro-crack. Further investigations showed that locations with the highest initial residual stresses did not necessarily have the highest number of micro-cracks. Figure 1.9 shows the frequency of pitting and cracking as a function of residual stress. As can be seen from this figure, no micro-cracks have been initiated in regions with compressive

residual stresses or in the region with the highest tensile residual stress. This suggested the value of residual stresses measured prior to neutral pH SCC testing may not be the only factor controlling the SCC initiation [53].

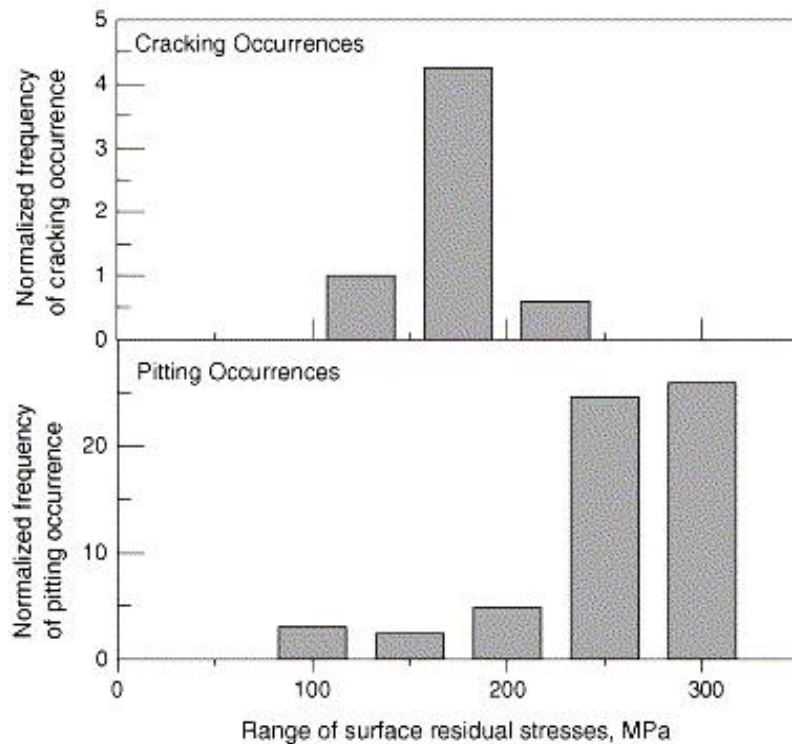


Figure 1.9: Surface residual stress versus normalized distribution of pitting and cracking after cyclic loading experiments [53].

Further investigations by Boven et al. showed cyclic loading could reduce both the maximum absolute residual stresses and the sharp variation of residual stresses (see Figure 1.10). The authors reported that in addition to variation of residual stresses in depth direction, this could be another reason explaining the different frequency of pitting and cracking on the specimen surface.

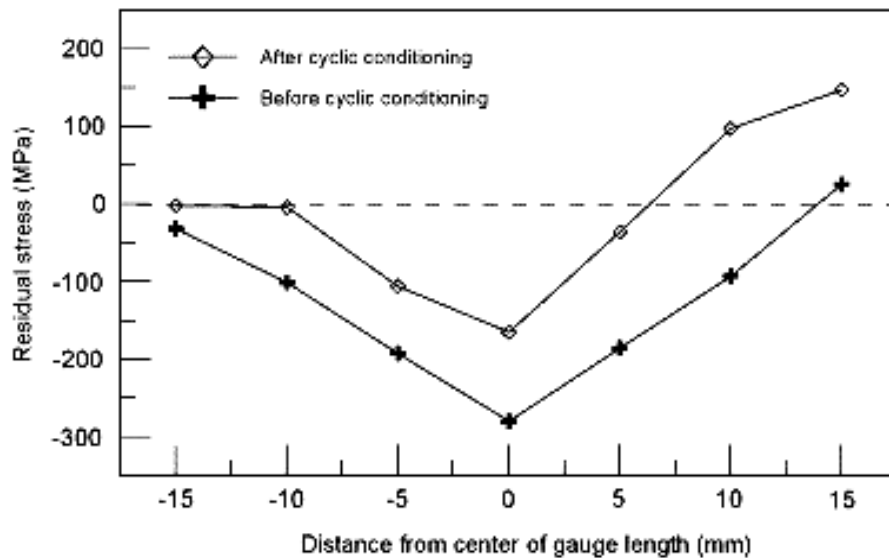


Figure 1.10: A comparison of axial residual stress along the gage length before and after cyclic loading in air [53].

1.2.6.2. Metallurgical and microstructural factors affecting near-neutral pH SCC initiation

a) Effect of steel microstructure and yield strength

Microstructure and yield strength are related to one another. Understanding the true effect of microstructure and yield strength on near-neutral pH SCC initiation is difficult and complicated. A review of important findings on this topic obtained from studies performed by SSR tests results is presented below:

Lu and Luo [21] investigated the effect of microstructure and yield strength on SCC resistance of different pipeline steels. Based on SSR test results, it was indicated that the relation between yield strength and SCC resistance is microstructural dependent. In this regard, pipeline steels with microstructures of fine grained bainite and ferrite had a better combination of strength and SCC resistance than those with ferrite and pearlite microstructures. A similar observation was reported by Bulger et al. [74]. For steels with similar microstructure, the SCC resistance dropped with increase in yield strength [21].

Looking into the microstructural effect using SSR tests, Liu et al. [75], investigated the effect of heat treatment on SCC susceptibility. A change in near-neutral pH SCC susceptibility determined by SSR tests was observed after heat treating the steel. In this regard, quenched X-70 pipeline steel with bainite microstructure was more susceptible to near-neutral pH SCC than the as-received X-70 pipe line steel with ferrite microstructure.

In relation with Liu et al. findings, [75], Torres-Islas and Gonzalez Rodriguez [76] investigations showed that quenched pipeline steels with martensite microstructures were more susceptible than the as-received pipeline steels which had ferrite-cementite microstructure. This observation was explained by the increased hydrogen uptake in the quenched steel than as in the as-received one.

Bulger and Luo [77], observed a direct relation between microstructure and SCC resistance of pipeline steel determined by the SSR test method. Annealed pipeline steels had better SCC and corrosion resistance than as-received or quenched ones. This was explained by the smaller grain size of the as-received and quenched steels, as compared to the annealed microstructures. Since the SCC resistance of the pipe steels was in direct relation with the corrosion rate of the pipeline steel, the authors suggested a dissolution based mechanism for the near-neutral pH SCC initiation.

Fang et al. [78] investigated the effect of the heat affected zone on near-neutral pH SCC susceptibility of pipeline steel using the SSR test method. An increase in SCC susceptibility was observed in the heat affected zone of the pipe steel, as compared to the base metal. This was explained by the coarser grain structure of the pipeline steel in the heat affected zone, as well as higher residual stress in this region.

Liu et al. [79] investigated the effect of inclusions on SCC initiation using the SSR test method. For the two types of inclusions identified on X-70 pipeline steel,

Al enriched inclusions (which were incoherent to the metal matrix and brittle) enhanced the SCC initiation; while the Si enriched inclusions (which were coherent to the metal matrix and soft) had no effect. Based on this observation, Liu et al. concluded that whether an inclusion affects the SCC initiation or not, depends on its composition and morphology.

As explained in section 1.2.5.1, SSR tests determine the susceptibility to crack initiation based on percent reduction of area (%RA) under aggressive loading conditions. The aggressive loading conditions used in these studies might have compromised the true role of the environment. Studies using cyclic loading tests might provide a more representative sample of the stress conditions responsible for near-neutral pH SCC initiation. In this regard:

Wang [55] observed that X-52 pipeline steel was more susceptible to near-neutral pH SCC than the X-65 pipeline steel. While one reason might be the difference between the percentages of inclusions for the two types of steels, other factors such as the difference in their yield strength, or the existence of micro-alloyed components in the more recent pipe grade might also be involved.

Kushida et al. [65] investigated the effect of pipeline strength and microstructure on near-neutral pH SCC susceptibility. They observed X-80 pipeline steel was more susceptible to near-neutral pH SCC compared to X-65 which had lower strength. This was then explained by the uniform microstructure of X-65 pipeline steel as opposed to the non-uniform microstructure of X-80 investigated in their study. It's worth mentioning that aggressive loading conditions and pre-notched specimens were used in the investigations, which might have compromised the results.

Fang et al. [67] investigated the effect of microstructure on near-neutral pH SCC initiation. Blunt cracks were initiated from corrosion pits. A higher number of cracks were initiated on the top surface of the specimen compared to the

transverse surface. The transverse surface represented mid-wall thickness of the pipeline, which contained more inclusions. Strong preferential dissolution from inclusions, in addition to enhanced anodic dissolution from the plastically deformed surface was identified as the main mechanisms for pitting corrosion.

Chu et al. [80] investigated the effect of microstructure on SCC initiation using cyclic loading tests. Wide transgranular micro-cracks were initiated at metallurgical discontinuities such as grain boundaries, pearlite colonies, and banded phase structures. No increase in SCC susceptibility was observed at physical discontinuities mechanically introduced on steel surface prior to the test, due to removal by general corrosion occurring on the surface during the tests.

Asahi et al. [81] investigated the effect of pipe steel microstructure on near-neutral pH SCC initiation using cyclic loading tests. Consistent with the Kushida et al. [65] findings, uniform microstructures were more resistant to SCC initiation as compared to mixed microstructures.

As determined by the two testing techniques (SSR test and cyclic loading tests), microstructural discontinuities increase the susceptibility to near-neutral pH SCC initiation. While SSR tests show steels with higher yield strength were more susceptible to crack initiation, there is no direct evidence about the effect of yield strength on near-neutral pH SCC using cyclic loading tests. The current understanding about the effect of microstructure and yield strength on near-neutral pH SCC initiation has been summarized in the chart below:

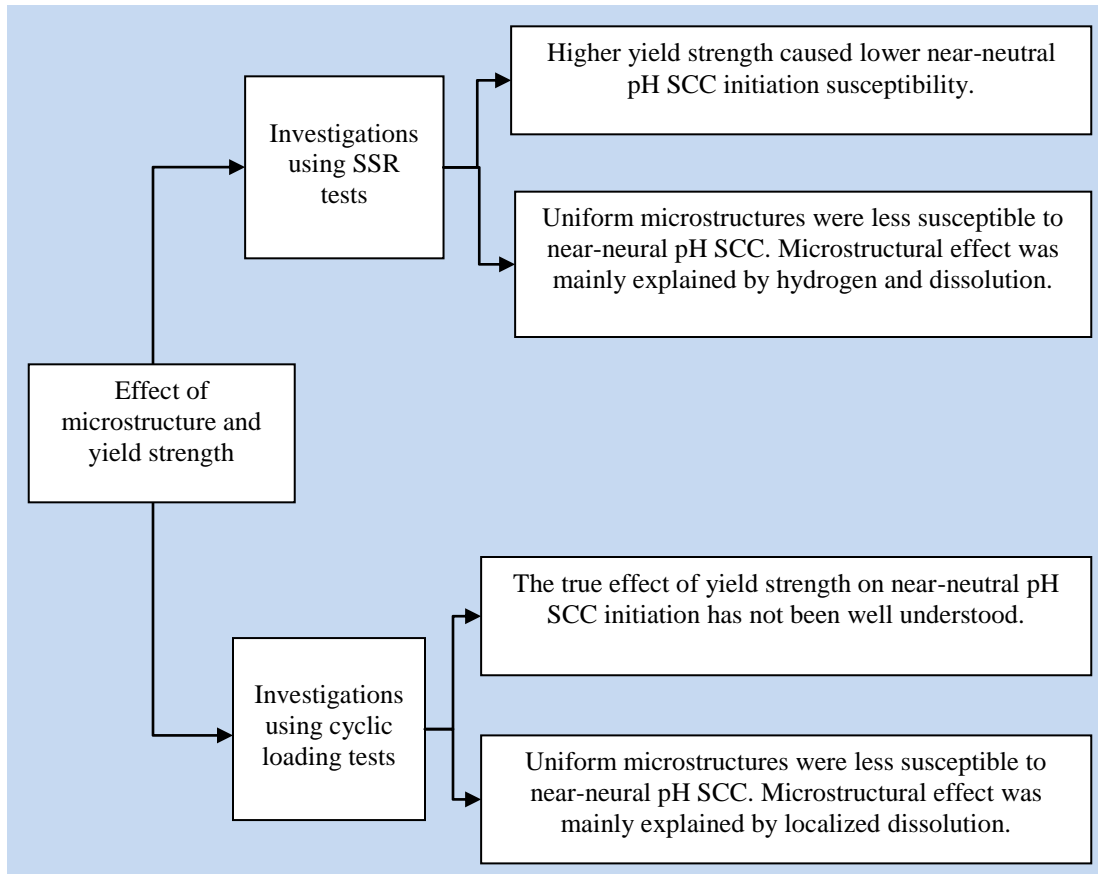


Figure 1.11: Summary graph showing effect of microstructure and yield strength on near-neutral pH SCC initiation, investigated by SSR tests and cyclic loading tests.

Despite the valuable results, the studies have not considered the combined effect of coating disbondment and CP in their investigations. To truly understand the role of microstructure and yield strength on near-neutral pH SCC initiation more realistic testing conditions might have to be considered.

b) Effect of steel surface condition

Researchers have observed correlations between steel surface condition and near-neutral pH SCC initiation. In this regard:

He et al. [66] investigated the effect of scratch orientation and surface roughness on near-neutral pH SCC initiation of X-65 pipeline steel using SSR tests. Results indicated that scratches perpendicular to the loading direction facilitated SCC

initiation, while those parallel to the loading direction had minor effect. Also, when the surface of the pipe steel was protected by CP, strong correlation between the surface roughness and SCC susceptibility was observed. The authors explained this behavior by different levels of hydrogen being generated.

Asahi et al. using cyclic loading tests showed that specimens with a mill scale surface had lower SCC resistance than specimens with a polished surface [81]. This was explained by the possible effect of a soft decarburized layer, containing coarser grain structure, existing under the mill scale surface. The authors proved this by work hardening the surface. Grit blasting increased the SCC resistance of the pipeline steel, by forming a hard deformed layer and introducing compressive residual stresses on the surface.

Again one should be cautious with the results obtained. The conclusions are based on tests performed under severe loading condition, and/or not considering the possible effect of coating disbondment and CP. Understanding the true effect of steel surface conditions on near-neutral pH SCC initiation could be complicated and requires further research.

1.2.6.3. Environmental factors affecting near-neutral pH SCC initiation

a) Effect of temperature

Studies using the SSR tests have shown that near-neutral pH SCC initiation is generally independent of temperature. In this regard, Parkins et al. [4] investigated the effect of temperature (in the range of 5°C – 45°C) using the SSR test technique. No significant change in the tendency of cracking was observed upon the temperature difference. This is different from what was observed for the high-pH SCC. The high-pH SCC occurs in limited range of pH and potential. The potential range is associated with the active-passive transition and moves towards the positive (noble) direction with a decrease in temperature [82].

Despite the obtained results by Parkins et al. [4], there is evidence showing enhanced corrosion rates with the increase in temperature in near-neutral pH environments. In this regard, Benmoussa et al. [61] observed increases in corrosion current density with increase in temperature in the range from (20-60) °C. If considering near-neutral pH SCC initiation is associated with anodic dissolution of pipeline steel (see section 1.2.7); increase in corrosion rate could mean increase in near-neutral pH SCC susceptibility. This contradicts with that determined by Parkins et al. [4].

In reality, the decrease in temperature would increase the solubility limit of CO₂ in ground water [1]. The increase in CO₂ content would increase the acidity of the ground water, which would then compensate the reduction in corrosion reaction kinetics caused by the temperature drop.

b) Effect of ground water chemistry

- **CO₂**

Investigations using SSR tests have shown increases in near-neutral pH SCC susceptibility by increasing CO₂ content of soil solutions [4, 48, 83, 84 and 85]. The increase in near-neutral pH SCC susceptibility was explained by the generation and penetration of more hydrogen into the steel microstructure. While this is true, for the susceptibility determined based on hydrogen effect determined by SSR tests, the situation might be different if considering near-neutral pH SCC initiation based on anodic dissolution mechanism (see section 1.2.7). In this regard, Zhang et al. [83] observed that with an increase in CO₂ partial pressure in the simulated soil solution (from 0 to 100%CO₂) the pH decreased, and the corrosion rate (anodic dissolution rate) of the pipeline steel increased.

As mentioned earlier in the field the situation is complicated, since CO₂ and temperature are related to one another.

- $\text{CO}_3^{2-}/\text{HCO}_3^-$

The dissolved CO_2 in ground water could form carbonic acid. Carbonic acid could then dissociate in ground water to form hydrogen ions (H^+), carbonate (CO_3^{2-}), and bicarbonate (HCO_3^-) ions. The concentration of CO_3^{2-} and HCO_3^- ions in the solution is in equilibrium with the pH of the solution (see Figure 1.12).

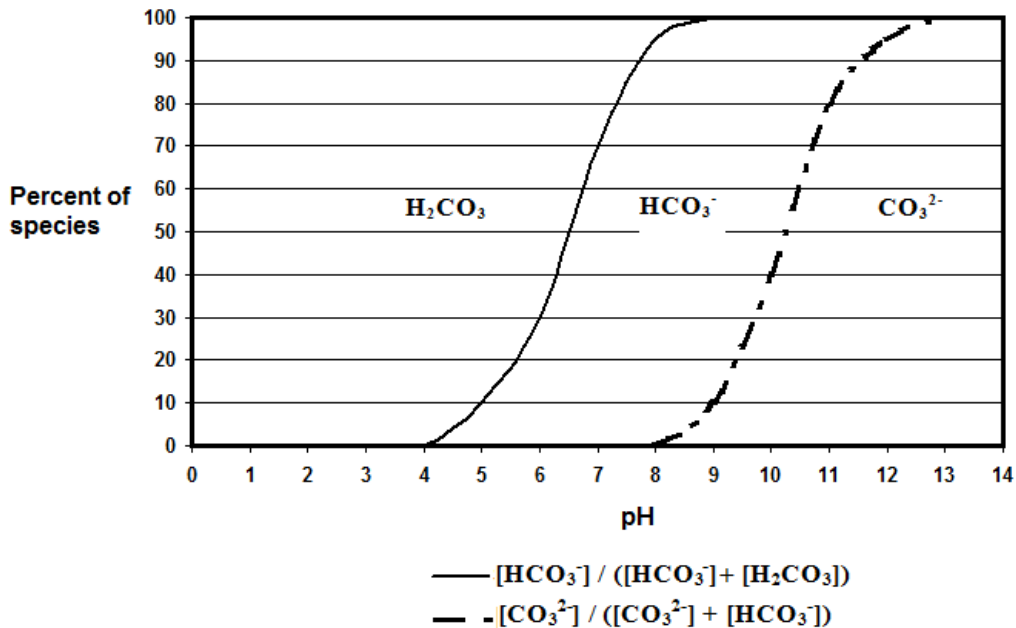


Figure 1.12: Relation between pH and percentage of $\text{CO}_3^{2-}/\text{HCO}_3^-$ species (figure reproduced from reference [86]).

Researchers have indicated, at concentrated levels of $\text{CO}_3^{2-}/\text{HCO}_3^-$ ions in soil environments with the pH in the range of 9.5-12.5 high-pH SCC could occur [87,88], while at dilute concentrations of $\text{CO}_3^{2-}/\text{HCO}_3^-$ in soil environments with the pH in range of 5.5 to 8.5 near-neutral pH SCC could occur [1, 30, 89].

The presence of CP could change the balance between the ions in electrolyte. In this regard, Asher et al. showed that the environmental conditions for transgranular and intergranular form of cracking are related to one another, and may change in the presence of CP [90].

- **Sulfides**

Sulfides are present either in the form of inclusions in steel microstructure, or in the bulk soil as a result of decomposition of sulfates by sulfate reducing bacteria (SRB) [33]. Sulfide could poison the steel surface, by preventing the recombination of hydrogen atoms to hydrogen molecules, and promoting hydrogen ingress into the steel microstructure [91]. In this regard, Cheng et al. [92] by performing hydrogen permeation tests in a simulated soil solution showed that the addition of 10 ppm of Na_2S increases the hydrogen permeation current considerably.

It is speculated that the increase in hydrogen ingress into the steel microstructure would weaken the pipe strength, and therefore facilitate crack initiation (see section 1.2.7). While this could be true, no long term near-neutral pH SCC initiation test (considering realistic testing conditions) has been conducted in this regard.

- **Oxygen**

Few researchers have investigated the effect of oxygen on near-neutral pH SCC initiation. In this regard:

Wang [55] investigated the effect of oxygen on near-neutral pH SCC initiation using long term cyclic loading tests. Large corrosion pits were formed in the presence of small amount of oxygen (1% O_2 with 5% CO_2/N_2) in the simulated soil solution environment. Smaller corrosion pits were formed in the absence of oxygen, or at higher concentration of oxygen (5% O_2 with 5% CO_2/N_2) in the soil solution environment. While the former was attributed to the less oxidizing condition of the solution in the absence of oxygen, the latter was explained by general corrosion covering the surface due to the high concentration of oxygen in the simulated soil solution.

Liu et al. [60] investigated the effect of dissolved oxygen on stress corrosion cracking of X-70 pipeline steel in a near-neutral pH solution using SSR tests. A decrease in SCC susceptibility was observed for an increase in oxygen concentration. This was explained by the consumption of hydrogen atoms in the presence of oxygen and the formation of an oxide layer which would limit the hydrogen entry into the steel microstructure. At concentrated dissolved oxygen levels, a stable oxide film was formed on the steel surface, which also reduced the anodic dissolution current. Niu and Cheng [93] obtained similar findings.

The studies on the effect of oxygen on near-neutral pH SCC initiation are not comprehensive in respect to considering the possible effects of CP and coating disbondments. Perhaps further research is required in this regard for clarification.

c) Effect of CP

Many researchers using SSR tests have investigated the effect of CP on near-neutral pH SCC initiation. In this regard:

Fang et al. [48] investigated the effect of cathodic potentials and soil solutions on near-neutral pH SCC initiation using SSR tests. Their investigation indicated increased SCC susceptibility at more negative CP potentials. Also, they observed higher SCC susceptibility in the soil solution extracted from real soils, when compared to the simulated NS4 solution. They suggested that the higher susceptibility to near-neutral pH SCC when using real soil extracts, as opposed to the simulated NS4 solution, might be due to higher level of CO₂ and/or microbial activities.

Gu et al. [84] investigated the effect of cathodic potential, hydrogen, and strain rate on near-neutral pH SCC initiation using SSR tests. They observed an increase in SCC susceptibility with increased CO₂ content, decreased strain rate, and decreased electro-chemical potentials towards more negative potentials.

Based on these results, they suggested that dissolution and hydrogen ingress are involved in the cracking process.

Liang et al. [94] investigated the effect of applied potential on SCC susceptibility of X-70 pipeline steel in near-neutral (pH= 8.9) solution. While no passive layer was formed in the simulated near-neutral pH solution, they observed increased SCC susceptibility at severe cathodic and anodic potentials. While the former was attributed to the role of anodic dissolution the latter was related to hydrogen induced cracking.

Bueno and Gomes [95] reported that hydrogen-embrittlement has an important role in the cracking process, as towards the more negative CP potential SCC susceptibility increased. Also, with a decrease in strain rate in SSR tests the SCC susceptibility increased. This was explained by the higher levels of hydrogen diffusion due to the longer exposure times with the decrease in strain rates.

Chen et al. [96] investigated the effect of soil chemistry and cathodic potential on near-neutral pH SCC initiation using the SSR testing method. For different soils the SCC susceptibility was found to be a function of soil pH in equilibrium with CO₂/N₂ gas mixture. The higher the pH (up to 7) of the simulated soils, the more conducive the soil was to near-neutral pH SCC. Also, Chen et al. observed increases in SCC susceptibility at more negative cathodic potentials. They explained this observation by the inhibition of general corrosion at more negative potentials (which otherwise could remove stress risers and defects from the specimen surface), and also by the increase of hydrogen content at more negative potentials (which could facilitate hydrogen-induced crack initiation).

The main conclusion from the studies performed by SSR tests is that the more negative the CP potentials the higher the susceptibility of the steel to near-neutral pH SCC. This higher susceptibility to near-neutral pH SCC was explained by the

higher levels of hydrogen, causing a lower percentage of reduction of area (%RA) in SSR tests.

Few studies have considered cyclic loading and CP in their investigations. In this regard, Wang et al. [63] observed that the presence of adequate CP would protect steel microstructural discontinuities from general corrosion. The surface discontinuities could then act as sites for crack initiation. From this study, it seems that the role of hydrogen on crack initiation is not critical as was observed from SSR tests. Perhaps, further research is required for clarification.

d) Effect of coating disbondment

As determined by field observations, section 1.2.3.1, near-neutral pH SCC is usually formed under PE tape coating disbondments in situations where CP is applied to protect the pipe surface from external corrosion and cracking. Despite this, most studies on near-neutral pH SCC initiation have ignored the combined effect of coating disbondments and CP in their investigations. The rationale behind this is that there would be no localized environments formed under coating disbondments due to the shielding effect of coating blocking the CP. However, some recent corrosion and electrochemical studies have shown in situations where adequate levels of CP are present, localized environments could be formed. This could be important in terms of understanding the possible conditions responsible for near-neutral pH SCC initiation. A review of important findings obtained from these studies is presented below:

Chen et al. [97] simulated coating disbondment on a pipe surface using a crevice with a gap distance of 0.9 mm. The local CP potential, pH, and oxygen concentration was then monitored as a function of distance from the holiday of the disbondment at different time intervals. It was observed that with the application of CP to the holiday of the disbondment the local pH increased from near-neutral to higher pH values. The more negative the CP potential; the higher the pH was inside the crevice. The local pH of the solution was less affected

toward the bottom of the crevice which had less CP protection. Also, oxygen concentration dropped from 8.3 mg/L at the crevice holiday to 1 mg/L at bottom of the crevice, no matter if CP was applied. Consistent with Song's et al. results [98], this showed that depletion of oxygen inside the crevice is independent from CP application. In fact, it was stated that geometry of the disbondment affects the diffusion of oxygen inside the crevice.

Chen et al. [99] investigated the effect of CP potentials on the local electrochemical condition formed under a simulated disbonded coating, using a rectangular crevice (gap distance was not reported). Similar to the Chen et al. finding [97], an increase in pH by applying CP potentials to the holiday of the simulated disbondment was observed. They explained the rise of pH as a result of reduction of water and dissolved O₂. However, when 5% CO₂ was continuously purged into the testing environment, it hydrated to a weak acid (H₂CO₃) and prevented the formation of an alkaline environment.

Yan et al. [100] also simulated coating disbondments using a narrow crevice with a gap distance of 0.5 mm. It was interesting to see that an alkaline environment was formed inside the crevice in the presence of CP even when it was continuously purged with 5% CO₂ (this was not seen in the simulated crevice with a larger gap distance [99]). The excess accumulation of hydroxide ions in the alkaline environment increased the conductivity of the solution by promoting more positive cations to migrate inside the disbondment. As a result of the high alkalinity of the solution inside the crevice, some sparingly soluble salts (Ca(OH)₂ and Mg(OH)₂) precipitated on the steel surface forming a layer on the steel surface. The increase in conductivity of the solution and the formation of sparingly soluble salts in the alkaline environment reduced the current requirement for polarizing the steel surface. Due to the restrained geometry of the crevice, the local alkaline environment was maintained for a relatively long time after CP was removed.

Perdomo and Song [101] indicated by performing studies in crevices with gap distances of 0.1 mm and 0.9 mm that crevices with smaller gap distances are more sensitive to environmental changes than larger ones due to the lower volume of solution in the smaller crevices.

Yan et al. [102] investigated the formation of local environments under a simulated disbonded coating and its relation to SCC susceptibility determined by SSR tests. Using a 0.5 mm gap distance crevice it was shown that CP interruptions could significantly affect the pH of the trapped solution inside a simulated crevice shifting the E-pH points into the susceptibility region of near-neutral pH SCC (the susceptibility region was determined based on SSR tests). At excessively negative CP potentials (overprotection), hydrogen bubbles were generated limiting the CP potential reaching deep inside the crevice.

The common conclusion from the studies is that localized environments could be formed under coating disbondments protected by CP. The missing part of the studies is that no loading was applied in the experiments. As explained in section 1.2.3, loading is a prerequisite for near-neutral pH SCC initiation (see Figure 1.5). Applying loading conditions matching to stress conditions on pipe surfaces, could clarify the role of the localized environments in near-neutral pH SCC initiation.

1.2.7. Current understanding of near-neutral pH SCC initiation mechanism

Since it is generally believed that no passive film/layer could be formed on a pipe steel surface in near-neutral pH soil environments, and also due to different morphology of the high-pH and near-neutral pH SCC cracks, researchers have suggested mechanisms different from the high-pH SCC. While several aspects of near-neutral pH SCC initiation are still under investigation, anodic dissolution and hydrogen based mechanisms are the most often suggested mechanisms among researchers.

For the anodic dissolution mechanism different scenarios such as the breakdown of passive films (similar to the breakdown observed for high-pH SCC [16]), anodic dissolution from inclusions, second phase microstructure, mill scale surface, and physical discontinuities [16, 67, 103, and 104] have been introduced. Since it is generally assumed that near-neutral pH SCC occurs in near-neutral pH soil environments with no passive films being formed, it has been suggested that the passive film breakdown is not correct [16]. Anodic dissolution from inclusions, second phase microstructures, and surface discontinuities are the most often accepted scenarios for the near-neutral pH environments. The preferential dissolution of the steel surface by the aforementioned mechanisms could cause formation of corrosion pits; which could then promote crack initiation due to stress concentration at these locations [105]. Evidence showing enhanced anodic dissolution in the stressed concentrated regions further supports this mechanism [67].

Hydrogen based mechanisms are explained by atomic hydrogen being generated at or close to the pipe surface, entering into the steel microstructure and weakening the atomic bonding, and therefore facilitating crack initiation [79]. The most likely source of hydrogen in near-neutral pH environments is carbonic acid formed by the dissolution of CO₂ in the groundwater [106]. Another source of hydrogen could be water dissociation due to presence of adequate CP on pipe surface [46]. Decohesion and internal pressure theories are the two common theories which explain the embrittlement caused by hydrogen in steel microstructure [107, 108]. According to the decohesion theory atomic hydrogen could enter the metal structure, be trapped in lattice defects and reduce the toughness and ductility of the material by reducing the bond strength between the metal atoms as a result of penetrating in the interstitial sites in the lattice. The internal pressure theory is based on hydrogen accumulating in the voids and the lattice defect of the microstructure, forming hydrogen gas until a equilibrium pressure is obtained. The gas expansion could cause internal pressures close to

yield strength of the metal, facilitating crack initiation. Recently, some molecular dynamic simulation has been carried out by Liu et al. [109] relevant to the subject.

As observed in previous sections, the hydrogen based mechanisms are mainly supported by near-neutral pH SCC studies performed by the SSR tests, and could not explain how crack are initiated in the first place. Therefore some researchers have suggested mechanisms which consider combinations of hydrogen and anodic (preferential) dissolution [29, 30, 60, 75, 84, 89, 110, and 111]. The suggested mechanisms, despite being valuable in terms of explaining different aspects of near-neutral pH SCC initiation, could still not give definitive answers to some important questions raised from field observations, such as:

- Why near-neutral pH SCC could be found at certain locations under disbonded coatings?
- Why corrosion and cracking could be observed close to one another under the same coating disbondment?
- Why intergranular cracks are occasionally observed close to transgranular cracks?
- How would the combination of CP and coating disbondment affect near-neutral pH SCC initiation?

1.3. Research objective and thesis structure

The objective of this thesis study is to investigate and understand the exact mechanism of near-neutral pH SCC initiation, and the true effect of some environmental and pipeline operational factors on this form of cracking. In this regard the following goals were introduced:

- Design of a comprehensive test setup better capable of simulating actual field conditions responsible for near-neutral pH SCC initiation, as opposed to the traditional test setups used for near-neutral pH SCC investigations.

- Investigate the true effect of some pipeline operational factors, such as maximum operating pressure and pressure fluctuations on near-neutral pH SCC initiation.
- Investigate the effect of some environmental factors believed to affect near-neutral pH SCC initiation.
- Determine the role of CP and coating on near-neutral pH SCC initiation.
- Determine the exact mechanism(s) responsible for near-neutral pH SCC initiation.

The structure of this dissertation which is meant to cover the mentioned objectives is as follows:

- Chapter 2 introduces a comprehensive test setup best capable of simulating field conditions responsible for near-neutral pH SCC.
- Chapter 3 will report a study of a near-neutral pH SCC initiation under a simulated coating disbondment using the novel test setup, and report an investigation of the effect of time and maximum stress on near-neutral pH SCC initiation.
- Chapter 4 will investigate the effect of stress fluctuations (R-ratio) and CO₂ on near-neutral pH SCC initiation under the simulated coating disbondment. In this chapter new insights about near-neutral pH SCC initiation mechanisms are provided.
- Chapter 5 will investigate the effect of oxygen on near-neutral pH SCC initiation under the simulated coating disbondment. This chapter will provide new insight about the role of oxygen on near-neutral pH SCC initiation.
- Chapter 6 will investigate corrosion of pipeline steel under the simulated coating disbondment. While the localized corrosion of the pipe steel was investigated in the previous chapters, this chapter will focus more on the general corrosion of pipeline steel. New findings about the corrosion rate of pipeline steels under coating disbondments are presented in this chapter,

which could assist near-neutral pH SCC initiation and crack growth modeling.

- Chapter 7 will investigate the effect of CO₂, CP, exposed pipe surface area, coating disbondment gap size, and coating material on the electrochemical conditions under disbonded coatings of pipeline steel using the novel test setup. Understanding the effect of these parameters on the electrochemical conditions under coating disbondments is important since, as it is indicated in previous chapters, it could significantly affect corrosion and near-neutral pH SCC initiation.

1.4. References

[1] National Energy Board (NEB), Report of the Inquiry-Stress Corrosion Cracking on Canadian Oil and Gas Pipelines, 1996.

[2] B.S. Delanty, J. O'Beirne, Major Field Study Compares Pipeline SCC with Coatings, Oil & Gas Journal, 15 (1992) 39-44.

[3] A. Eslami, T. Place, Landscape investigation on corrosion and SCC of a Tape Coated pipeline, International Pipeline Conference 2012, Calgary, Canada.

[4] R.N. Parkins, W.K. Blanchard Jr., B.S. Delanty, Transgranular Stress Corrosion Cracking of High-Pressure Pipelines in Contact with Solutions of Near Neutral pH, Corrosion Engineering, 50 (1994) 394-408.

[5] J.A. Beavers, C.L.Durr, S.S. Shademan, L. Collins, Materials for Resource Recovery and Transport, The Metallurgical Society of CIM, Canada, (1998) 51-69

[6] R.N. Parkins, A Review of Stress Corrosion Cracking of High Pressure Gas Pipelines, In Proceeding of Corrosion 2000, Orlando, Florida, USA, 2000.

[7] B.Y. Fang, A. Atrens, J.Q. Wang, E.H. Han, Z.Y. Zhu, W. Ke, Review of Stress Corrosion Cracking of Pipelines Steels in “Low” and “High” pH Solutions, Journal of Materials Science, 38 (2003) 127-132.

[8] M. Baker Jr. Inc., Stress Corrosion Cracking Study- Final Report, Department of Transportation Research and Special Programs Administration Office of Pipeline Safety- Integrity management program delivery order DTRS56-02-D-70036, 2005.

[9] http://www.nts.gov/investigations/reports_pipeline.html.

[10] F. Jeglic. Analysis of Ruptures and Trends on Major Canadian Pipeline Systems. National Energy Board, Calgary, Canada, 2004.

[11] P.J. Kentish, Gas Pipeline Failures - Australian Experience, British Corrosion Journal, 20 (1985) 139-146.

- [12] R.L. Wenk, Field Investigations of Stress Corrosion Cracking, 5th Symposium on Line Pipe Research, American Gas Association, 1974.
- [13] Catastrophic Ruptures of a Pipeline as a Result of SCC, Dec. 13, 2003. <http://www.corrosion-doctors.org/Pipeline/Williams-explosion.htm>.
- [14] R.N. Parkins, Controlling Parameters in Stress Corrosion Cracking, 5th Symposium Line Pipe Research, American Gas Association, Arlington VA USA, 1974.
- [15] Y. Wang, R. Revie, R. Parkins, Mechanistic Aspect of Stress Corrosion Cracking and Early Propagation, In Proceeding of Corrosion 1999, San Antonio, Texas, USA, 1999.
- [16] J.A. Beavers, B.A. Harle, Mechanisms of High-pH and Near-neutral-pH SCC of Underground Pipelines, In Proceeding of International Pipeline Conference IPC1996, Calgary, Canada, 1996.
- [17] F. King, T.R. Jack, M. Kolar, R. Worthingham, A Permeable Coating Model for Predicting the Environment at the Pipe Surface under CP-Compatible Coatings, Corrosion 2004, New Orleans, USA, 2004.
- [18] F. Song, D.W. Kirk, J.W. Graydon, D.E. Cormack, D. Wong, Corrosion under Disbonded Coatings Having Cathodic Protection, Materials Performance, 42 (2003) 24-26.
- [19] A.C. Toncre, On Achieving Polarization Beneath Unbonded Pipe Coatings, Material Performance, 23 (1984) 22-27.
- [20] API Specification 5L, Specification for Line pipe, Forty-Third Addition, March 2004.
- [21] B.T. Lu, J.L. Luo, Relationship Between Yield Strength and Near-neutral pH Stress Corrosion Cracking Resistance of Pipeline Steels- An Effect of Microstructure, Corrosion, 62-2 (2006) 129-140.
- [22] J.A. Beavers, B.A. Harle, Mechanisms of High-pH and Near-neutral-pH SCC of Underground Pipelines, Journal of Offshore Mechanics and Arctic Engineering, 123 (2001) 147-151.
- [23] R. Sutherby, T. Jack, G. Van Boven, M. Wilmott, CEPA Study on Characterization of Pipeline Pressure Fluctuations in Terms of Relevant to Stress Corrosion Cracking, In Proceeding of International Pipeline Conference IPC2000, Calgary, Alberta, Canada.
- [24] R.N. Parkins, Stress Corrosion in Buried Pipelines, TCPL, 1990.
- [25] J. Been, H. Lu, R. Eadie, G. Shen, R. Sutherby, The Role of Stress Intensifiers in Near-neutral pH Corrosion Fatigue of Line Pipe, In Proceeding of Corrosion 2004, New Orleans, Louisiana, USA, 2004.
- [26] B.A. Harle, J.A. Beavers, C.E. Jaske, Mechanical and Metallurgical Effects on Low-pH Stress Corrosion Cracking of Natural Gas Pipelines, In Proceeding of Corrosion 95, Huston, Texas, USA, 1995.
- [27] J.A. Beavers, C.E. Jaske, Near-neutral pH SCC in Pipelines: Effect of Pressure Fluctuations on Crack Propagation, In Proceeding of Corrosion 1998, San Diego, California, USA, 1998.
- [28] J.A. Beavers, C.L. Durr, B.S. Delanty, D.M. Owen, R.L. Sutherby, Near-neutral pH SCC: Crack Propagation in Susceptible Soil Environments, In Proceeding of Corrosion 2001, Huston-Texas, USA, 2001.

- [29] W. Chen, R. Kania, R. Wothingham, G.V. Boven, Transgranular Crack Growth in Pipeline Steels Exposed to Near-neutral pH Soil Solutions: The Role of Hydrogen, *Acta Materialia*, 57 (2009) 6200-6214.
- [30] W. Chen, F. King, E. Vokes, Characteristics of Near-neutral-pH Stress Corrosion Cracks in an X-65 Pipeline, *Corrosion*, 58-3 (2002) 267-275.
- [31] J. Been, R.L. Sutherby, Effects of Loading Frequency on Near-neutral pH Crack Growth on Operating Pipelines, In proceeding of NACE Northern Area Conference, Calgary, Canada, 2006.
- [32] J.T. Johnson, C.L. Durr, J.A. Beavers, B.S. Delanty, Effects of O₂ and CO₂ on Near-neutral-pH Stress Corrosion Crack Propagation, In Proceeding of Corrosion 2000, Orlando, Florida, USA.
- [33] R.L. Eadie, K.E. Sklarz, R.L. Sutherby, Corrosion Fatigue and Near-neutral pH Stress Corrosion Cracking of Pipeline Steel and Effect of Hydrogen Sulfide, *Corrosion*, 61 (2005) 167-173.
- [34] B. Fang, R.L. Eadie, W. Chen, M. Elboujdaini, Electrochemical Method Pits Generation and its Application in Crack Initiation in Pipeline Steel in Near-neutral pH Environment, In Proceeding of NACE Northern Area Western Conference, Edmonton, Alberta, Canada, 2008.
- [35] M.H. El Haddad, T.H. Topper, K.N. Smith, Prediction of Non Propagating Cracks, *Engineering Fracture Mechanics*, 11(1979) 573-584.
- [36] W. Chen, R.L. Sutherby, Crack Growth Behavior of Pipeline Steel in Near-neutral pH Soil Environments, *Metallurgical and Materials Transaction A*, 38 A (2007) 1260-1268.
- [37] M.H. Marvasti, Crack Growth Behavior of Pipeline Steels in Near neutral pH Environment, M.Sc. Thesis, University of Alberta, 2010.
- [38] J.A. Beavers, Near-neutral pH SCC: Dormancy and Re-initiation of Stress Corrosion Cracks, CC Technologies Report, 2004.
- [39] A. Plumtree, B.W. Williams, S.B. Lambert, R. Sutherby, SCC Growth in Pipeline Steel, In Proceedings of Conference of Environmental-Induced Cracking of Materials, Volume 2: Prediction, Industrial Developments and Evaluation, Banff, Alberta, Canada, 2008.
- [40] W. Zheng, W. Revie, F.A. Macleod, O. Dinardo, Low pH SCC: Environmental Effects on Crack Propagation, Pipeline Research Council International, Category No. L51791E, Houston, Texas, USA.
- [41] P. Paris and F. Erdogan, A Critical Analysis of Crack Propagation Laws, *Journal of Basic Engineering*, Transactions of the American Society of Mechanical Engineers, 85 (1963) 528-534.
- [42] X.Y. Zhang, S.B. Lambert, R. Sutherby, A. Plumtree, Transgranular Stress Corrosion Cracking of X-60 Pipeline Steel in Simulated Ground Water, *Corrosion*, 55-3 (1999) 297-305.
- [43] S.B. Lambert, R. Sutherby, Fracture Mechanics Modeling of Stress Corrosion Crack Colonies, International Conference of Pipeline Reliability, Montreal, Canada, 1998.
- [44] S.B. Lambert, J.A. Beavers, B. Delanty, R. Sutherby, A. Plumtree, Mechanical Factors Affecting Stress Corrosion Crack Growth Rates in Buried Pipelines, In Proceeding of International Pipeline Conference IPC2000, Calgary, Alberta, Canada.

- [45] S.B. Lambert, A. Plumtree, R. Sutherby, Modeling of Environmental Crack Growth in Pipeline Steel, In Proceeding of Corrosion 2000, Orlando, Florida, 2000.
- [46] A.T. Egbewande, A. Eslami, W. Chen, R. Worthingham, R. Kania, G.V. Boven, Growth of Surface-type Stress Corrosion Cracks in Near-neutral pH Environments under Disbonded Coatings, In Proceedings of the 8th International Pipeline Conference IPC2010, Calgary, Alberta, Canada, 2010.
- [47] W. Chen, RL. Eaide, RL. Sutherby, Environmental Effects of Near-neutral pH Stress Corrosion Cracking in Pipelines. In: Second International Conference on Environmental Induced Cracking of Metals. Banff, Alberta, Canada, 2004.
- [48] B. Fang, E.H. Han, J. Wang, W. Ke, Mechanical and Environmental Influences of Stress Corrosion Cracking of an X-70 Pipeline Steel in Dilute Near-neutral pH solutions, *Corrosion*, 63-5 (2007) 419-432.
- [49] W. Chen, S. Wang, R. Chu, F. King, T.R. Jack, R.R. Fessler, Effect of Precyclic Loading on Stress-Corrosion-Cracking Initiation in an X-65 Pipeline steel Exposed to Near-neutral pH Soil Environment, *Metallurgical and Materials Transaction A*, 34A (2003) 2601-2608.
- [50] J. Been, R. Eadie, R. Sutherby, Predictions of Environmentally Assisted Cracking on Gas and Liquid Pipelines, In Proceedings of the 6th International Pipeline Conference IPC2006, Calgary, Alberta, Canada, 2006.
- [51] X. Liu, and X. Mao, Electrochemical Polarization and Stress Corrosion Cracking Behaviours of a Pipeline Steel in Dilute Bicarbonate Solution with Chloride Ion, *Scripta Metallurgica Materialia*, 33 (1995) 145-150.
- [52] Standard Practice for Slow Strain Rate Testing to Evaluate the Susceptibility of Metallic Materials to Environmentally Assisted Cracking, ASTM G 129-95, 1995.
- [53] G. Van Boven, W. Chen, R. Rogge, The Role of Residual Stress in Neutral pH Stress Corrosion Cracking of Pipeline Steels. Part 1: Pitting and Cracking Occurrence, *Acta Material*, 55 (2007) 29-42.
- [54] R.P. Gangloff, Environmental Cracking-Corrosion Fatigue, In: *Corrosion Tests and Standards: Application and Interpretation* (2nd Edition), R. Baboian, ASTM International, 302-321, 2005.
- [55] H. Wang, Effect of the Environment on Near-neutral pH Stress Corrosion Cracking of X-52 Pipeline Steel, M.Sc. Thesis, University of Alberta, 2009.
- [56] D.X. He, W. Chen, J.L. Luo, Effect of Cathodic Potential on Hydrogen Content in a Pipeline Steel Exposed to NS4 near-neutral pH Soil Solution, *Corrosion*, 60 (2004) 778-786.
- [57] D. A. Jones, *Principle and Prevention of Corrosion*, Second Edition, 1996.
- [58] Z. Devanathan, Z. Stachurski, The Adsorption and Diffusion of Electrolytic Hydrogen in Palladium, *Proceedings of the Royal Society of London Series A-Mathematical and Physical Sciences*, 270 (1962) 90-102.
- [59] M.C. Li, Y.F. Cheng, Mechanistic Investigation of Hydrogen-Enhanced Anodic Dissolution of X-70 Pipe Steel and its Implication on Near-neutral pH SCC of Pipelines, *Electrochimica Acta*, 52 (2007) 8111-8117.
- [60] Z.Y. Liu, X.G. Du, L.X. Wang, Y.Z. Huang, Effect of Dissolved Oxygen on Stress Corrosion Cracking of X70 Pipeline Steel in Near-neutral pH Solution, *Corrosion*, 66- 1 (2010) 150011–150016.

- [61] A. Benmoussa, M. Hadjel, M. Traisnel, Corrosion Behavior of API 5L X-60 Pipeline Steel Exposed to Near-neutral pH Soil Simulating Solution, *Materials and Corrosion*, 57-10 (2006) 771-777.
- [62] B.Y. Fang, E.H. Han, J.Q. Wang, W. Ke, Stress Corrosion Cracking of X-70 Pipeline Steel in Near Neutral pH Solution Subjected to Constant Load and Cyclic Load Testing, *Corrosion Engineering, Science and Technology*, 42-2 (2007) 123-129.
- [63] S.H. Wang, W. Chen, F. King, T.R. Jack, R.R. Fessler, Precyclic-Loading-Induced Stress Corrosion Cracking of Pipeline Steels in a Near-neutral-pH Soil Environment, *Corrosion*, 58 (2002) 526-535.
- [64] B.W. Pan, X. Peng, W.Y. Chu, Y.J. Su, L.J. Qiao, Stress Corrosion Cracking of API X-60 Pipeline in a Soil Containing Water, *Materials Science and Engineering A*, 434 (2006) 76-81.
- [65] T. Kushida, K. Nose, H. Asahi, M. Kimura, Y. Yamane, S. Endo, H. Kawano, Effects of Metallurgical Factors and Test Conditions on Near-neutral pH SCC of Pipeline Steels, In *Proceeding of Corrosion 2001*, Houston, Texas, USA.
- [66] D. He, W. Chen, J. Luo, F. King, T. Jack, K. Krist, Effect of Surface Scratch Roughness and Orientation on the Development of SCC of Line Pipe Steel in Neutral pH Environment, In *Proceeding of International Pipeline Conference IPC2000*, Calgary, Alberta, Canada, 2000.
- [67] B. Fang, R. Eadie, W. Chen, M. Elboudjaini, The Effect of Microstructure on Pit-to-Crack Transition and Crack Growth in an X-52 Pipeline Steel in Near-neutral pH Environment, In *Proceeding of International Pipeline Conference IPC 2008*, Calgary-Alberta, Canada, 2008.
- [68] B. Fang, R. Eadie, W. Chen, M. Elboudjaini, Pit to Crack Transition in X-52 Pipeline Steel in Near-neutral pH Environment; Part 1- Formation of Blunt Cracks from Pits under Cyclic Loading, *Corrosion Engineering Science and Technology*, 45 (2010) 302-312.
- [69] J. Been, J., H. Lu, F. King, T. Jack, R. Sutherby, The Role of Hydrogen in EAC of Pipeline Steels in Near-neutral pH Environments, *Proc. Environmentally Assisted Cracking of Materials*, 2 (2008) 255-266.
- [70] S.L. Asher, P.M. Singh, Role of Stress in Transgranular Stress Corrosion Cracking of Transmission Pipelines in Near-neutral pH Environments, *Corrosion*, 62 (2009) 79-87.
- [71] Y.F. Cheng, Thermodynamically Modeling the Interaction of Hydrogen Stress, and Anodic Dissolution at the Crack Tip During Near-neutral pH SCC in Pipelines, *Journal of Materials Science*, 42 (2007) 2701-2705.
- [72] F. King, T. Jack, W. Chen, M. Wilmott, R.R. Fessler, K. Krist, Mechanistic Studies of Initiation and Early Stages Crack Growth for NNpHSCC on Pipelines, *Corrosion 2000*, Houston-Texas, USA, 2001.
- [73] T.M. Holden, G. Roy, The Application of Neutron Diffraction to the Measurement of Residual Stress and Strain, *Handbook of Measurement of Residual Stress*, Society for Experimental Mechanics, Fairmont Press, 1996.
- [74] J.T. Bulger, B.T. Lu, J.L. Luo, Microstructural Effect on Near-neutral pH Stress Corrosion Cracking Resistance of Pipeline Steels, *Journal of Materials Science*, 41 (2006) 5001-5005.
- [75] Z.Y. Liu, X.G. Li, C.W. Du, G.L. Zhai, Y.F. Cheng, Stress Corrosion Cracking Behavior of X-70 Pipe Steel in an Acidic Soil Environment, *Corrosion Science*, 50 (2008) 2251-2257.

- [76] A. Torres-Islas, J.G. Gonzalez-Rodriguez, Effect of Electrochemical Potential and Solution Concentration on the SCC Behaviour of X-70 Pipeline Steel in NaHCO₃, *International Journal of Electrochemistry*, 4 (2009) 640-652.
- [77] J. Bulger, J. Luo, Effect of Microstructure on Near-neutral pH SCC, In *Proceeding of International Pipeline Conference IPC2000*, Calgary, Alberta, Canada, 2000.
- [78] B. Fang, E-H Han, J. Wang, W. Ke, R. Eadie, M. Elboujdaini, W. Zheng, R. Revie, The Influence of Weld Heat-affected Zone on Stress Corrosion Cracking of Pipeline Steels in Near-neutral pH Environment, *Corrosion 2008 Conference and Exposition*, New Orleans, Los Angeles, USA, 2008.
- [79] Z.Y. Liu, X.G. Li, C.W. Du, L. Lu, Y.R. Zhang, Y.F. Cheng, Effect of Inclusions on Initiation of Stress Corrosion Cracks in X70 Pipeline Steel in an Acidic soil Environment, *Corrosion Science*, 51 (895-900) 2009.
- [80] R. Chu, W. Chen, S.-H Wang, F. King, T.R. Jack, R.R. Fessler, Microstructure Dependence of Stress Corrosion Cracking Initiation in X-65 Pipeline Steel Exposed to Near-neutral pH Soil Environment, *Corrosion*, 6-3 (2004) 275-283.
- [81] H. Asahi, T. Kushida, M. Kimura, H. Fukai, S. Okano, Role of Microstructure on Stress Corrosion Cracking of Pipeline Steels in Carbonate-Bicarbonate Solution, *Corrosion*, 55-7 (1999) 644-652.
- [82] G.H. Koch, J.A. Beavers, W.E. Berry, Effect of Temperature on Stress-Corrosion Cracking of Pre-cracked Pipeline Steels, NG-18 Report No. 148, American Gas Association, Catalog No. L51491, Arlington, Virginia, USA.
- [83] L. Zhang, X.G. Li, C.W. Du, Y.G. Cheng, Corrosion and Stress Corrosion Cracking of X70 Pipeline Steel in a CO₂-containing Solution, *Journal of Materials Engineering and Performance*, 18-3 (2009) 319-323.
- [84] B. Gu, W.Z. Yu, J.L. Luo, and X. Mao, Transgranular Stress Corrosion Cracking of X-80 and X-52 Pipeline Steels in Dilute Aqueous Solution with Near-neutral pH, *Corrosion*, 55-3 (1999) 312-318.
- [85] M. Wu, X. Chen, C. He, J. XIAO, Effect of CO₂ Partial Pressure on SCC Behavior of Welded X80 Pipeline in Simulated Soil Solution, *ACTA Metallurgica SINICA (English Letters)*, 24-1 (2011) 65-74.
- [86] R. N. Parkins, Stress Corrosion Cracking In Pipelines, in: *Proc. NACE Canadian Western Regional Conference.*, Calgary, Canada, 1994.
- [87] N. Leis, R.N. Parkins, Mechanics and Material Aspects in Predicting Serviceability Limited by Stress-Corrosion Cracking, *Fatigue and Fracture of Engineering Materials and Structures*, 21 (1998) 583-601.
- [88] J. Sutcliffe, W. Boyd, R. Fessler, R. Parkins, Stress-Corrosion Cracking of Carbon-Steel in Carbonate Solution, *Corrosion*, 28 (1972) 313-320.
- [89] B. Gu, J. Luo, X. Mao, Hydrogen-facilitated Anodic Dissolution-Type Stress Corrosion Cracking of Pipeline Steels in Near-neutral pH Solution, *Corrosion*, 55 (1999) 96-109.
- [90] S.L. Asher, B. Leis, J. Colwell, and P.M. Singh, Investigating a Mechanism for Transgranular Stress Corrosion Cracking on Buried Pipelines in Near-neutral pH Environments, *Corrosion*, 63-10 (2007) 932-939.

- [91] R.N. Parkins, The Influence of Hydrogen on Crack Growth in Pipelines, *Materials for Resource Recovery and Transport*. L. Collins (Ed.), The Metallurgical Society of CIM, (1998) 35-49.
- [92] Y.F. Cheng, Analysis of Electrochemical Hydrogen Permeation through X-65 Pipeline Steel and its Implications on Pipeline Stress Corrosion Cracking, *International Journal of Hydrogen Energy*, 32 (2007) 1269-1276.
- [93] L. Niu, Y.F. Cheng, Corrosion Behavior of X-70 Pipe Steel in Near-Neutral pH Solution, *Applied Surface Science*, 253 (2007) 8626-8631.
- [94] Z. Liang, L. Xiaogang, D. Cuiwei, H. Yizhong, Effect of Applied Potentials on Stress Corrosion Cracking of X70 Pipeline Steel in Alkali Solution, *Materials and Design*, 30 (2009) 2259-2263.
- [95] A.H.S Bueno, J.A.C.P. Gomes, Environmentally Induced Cracking of API Grade Steel in Near-neutral pH Soil, *Journal of the Brazilian Society of Mechanical Science & Engineering*, 31-2 (2009) 97-104.
- [96] W. Chen, F. King, T.R. Jack, and M.J. Wilmot, Environmental Aspects of Near-neutral pH Stress Corrosion Cracking of Pipeline Steel, *Metallurgical and Materials Transactions*, 33A (2002) 1429-1436.
- [97] X. Chen, X.G. Li, C.W. Du, Y.F. Cheng, Effect of Cathodic Protection on Corrosion of Pipeline Steel under Disbonded Coating, *Corrosion science*, 52 (2009) 2242-2245.
- [98] F.M. Song, N. Sridhar, Modeling Pipeline Crevice Corrosion under a Disbonded Coating with or without Cathodic Protection under Transient and Steady State Conditions, *Corrosion Science*, 50 (2008) 70-83.
- [99] X. Chen, C. Du, X. Li, Y. Huang, Effect of Cathodic Potential on the Local Electrochemical Environment under a Disbonded Coating, *Journal of Applied Electrochemistry*, 39 (2009) 697-704.
- [100] M.C. Yan, J.Q. Wang, E.H. Han, W. Ke, Electrochemical Measurements Using Combination Micro-Electrodes in Crevice Simulating Disbonded of Pipeline Coatings under Cathodic Protection, *Corrosion Engineering Science and Technology*, 42-1 (2007) 42-49.
- [101] J.J Perdomo, I. Song, Chemical and Electrochemical Conditions on Steel under Disbonded Coatings: The Effect of Applied Potential, Solution Resistivity, Crevice Thickness, and Holiday Size, *Corrosion Science*, 42 (2000) 1389-1415.
- [102] M. Yan, J. Wang, E. Han, W. Ke, Local Environment under Simulated Disbonded Coating on Steel Pipelines in Soil Solution, *Corrosion Science*, 50 (2008) 1331-1339.
- [103] D. He, TR. Jack, F. King, W. Chen, Effect of Surface Scratch Roughness and Orientation on SCC of Line Pipe Steel in Near-neutral pH Environment, In 2000 International Pipeline Conference, Calgary, Alberta, Canada, 2000.
- [104] M. Elboujdaini, YZ. Wang, RW. Revie, RN. Parkins, MT. Shehata, Stress Corrosion Crack Initiation Processes: Pitting and Microcrack Coalescence, In Proceeding of Corrosion 2000, Houston, Texas, USA, 2000.
- [105] Y. Kondo, Prediction of Fatigue Crack Initiation Life Based on Pit Growth, *Corrosion*, 45 (1989) 7-11.

- [106] G. Schmidt, Fundamental Aspects of CO₂ Corrosion, In Proceeding of Corrosion 83, Texas, 1983.
- [107] A.R. Troiano, The Role of Hydrogen and Other Interstitials in the Mechanical Behavior of Metals, Transactions of the Metallurgical Society of AIME, 52 (1960) 54-80.
- [108] C.A. Zapffe, C.E. Sims, Hydrogen Embrittlement Internal Stress and Defects in Steels, Transactions. American Institute of Mining, Metallurgical and Petroleum Engineers, 145, (1941) 225-259.
- [109] X. Y. Liu, W. B. Xie, W. X. Chen, H. Zhang, Effects of Grain Boundary and Boundary Inclination on Hydrogen Diffusion in Alpha-Iron, Journal of Materials Research, 26 (2011) 2735-2743.
- [110] R.N. Parkins, Environment Sensitive Cracking of High-pressure Pipelines in Contact with Carbon Dioxide-containing Solution, AGA N-18 Report Number 205, 1992.
- [111] S.L. Asher, Investigating the Mechanism of Transgranular Stress Corrosion Cracking in Near-neutral pH Environments on Buried Fuel Transmission Pipelines, PhD Thesis, Georgia Institute of Technology, 2007.

**Chapter 2: Design of a Comprehensive Test Setup for Simulating
Field Conditions Responsible for Near-neutral pH SCC**

2.1. Introduction

As shown in the previous chapter there is inconsistency between laboratory, and field conditions responsible for near-neutral pH SCC. Coating disbondment, CP, and realistic loading conditions are the main elements which have been ignored in most of the laboratory experiments. Table 2.1 summarizes some of the inconsistencies between laboratory testing conditions and field conditions causing near-neutral pH SCC.

Table 2.1: Comparison between field conditions responsible for near-neutral pH SCC and laboratory test conditions.

Field condition	Laboratory tests
<p>Loading:</p> <ul style="list-style-type: none"> • Near-static, low frequency cyclic loading. 	<p>Loading:</p> <ul style="list-style-type: none"> • Aggressive loading condition, not representing the actual pipe stress condition, has been used in most laboratory simulations.
<p>Environment:</p> <ul style="list-style-type: none"> • Localized under coating disbondments. • Seasonal fluctuations, anaerobic/aerobic conditions could exist. 	<p>Environment:</p> <ul style="list-style-type: none"> • Coating disbondment and environmental changes have not been considered in most laboratory simulation.
<p>Cathodic protection:</p> <ul style="list-style-type: none"> • Is applied to all pipes. 	<p>Cathodic protection:</p> <ul style="list-style-type: none"> • Has not been considered in most laboratory simulations.

It is believed that the key to better understanding near-neutral pH SCC is using a test setup capable of simulating the true field conditions responsible for near-neutral pH SCC.

2.2. Design of a comprehensive test setup for simulating near-neutral pH SCC

Considering field conditions, a schematic showing a coating disbondment on a pipe section was sketched (See Figure 2.1). Based on the schematic, a comprehensive test setup was designed and built. The main components of the test setup are the corrosion cell and the specimen. Each is briefly explained in the following subsections.

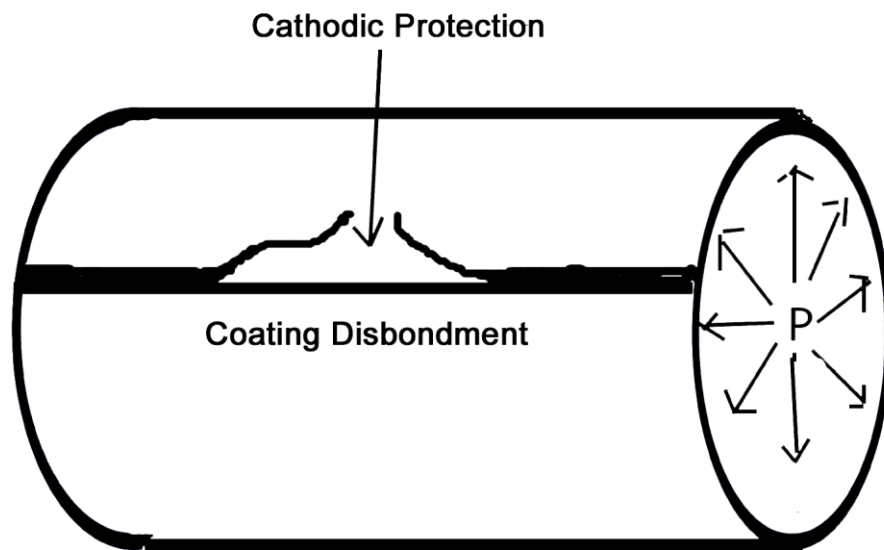


Figure 2.1: Schematic showing coating disbondment on a pipe section.

2.2.1. The Corrosion cell

Figure 2.2 shows a schematic of the designed corrosion cell. The application of loading, coating disbondment, and CP have been considered in the designed corrosion cell.

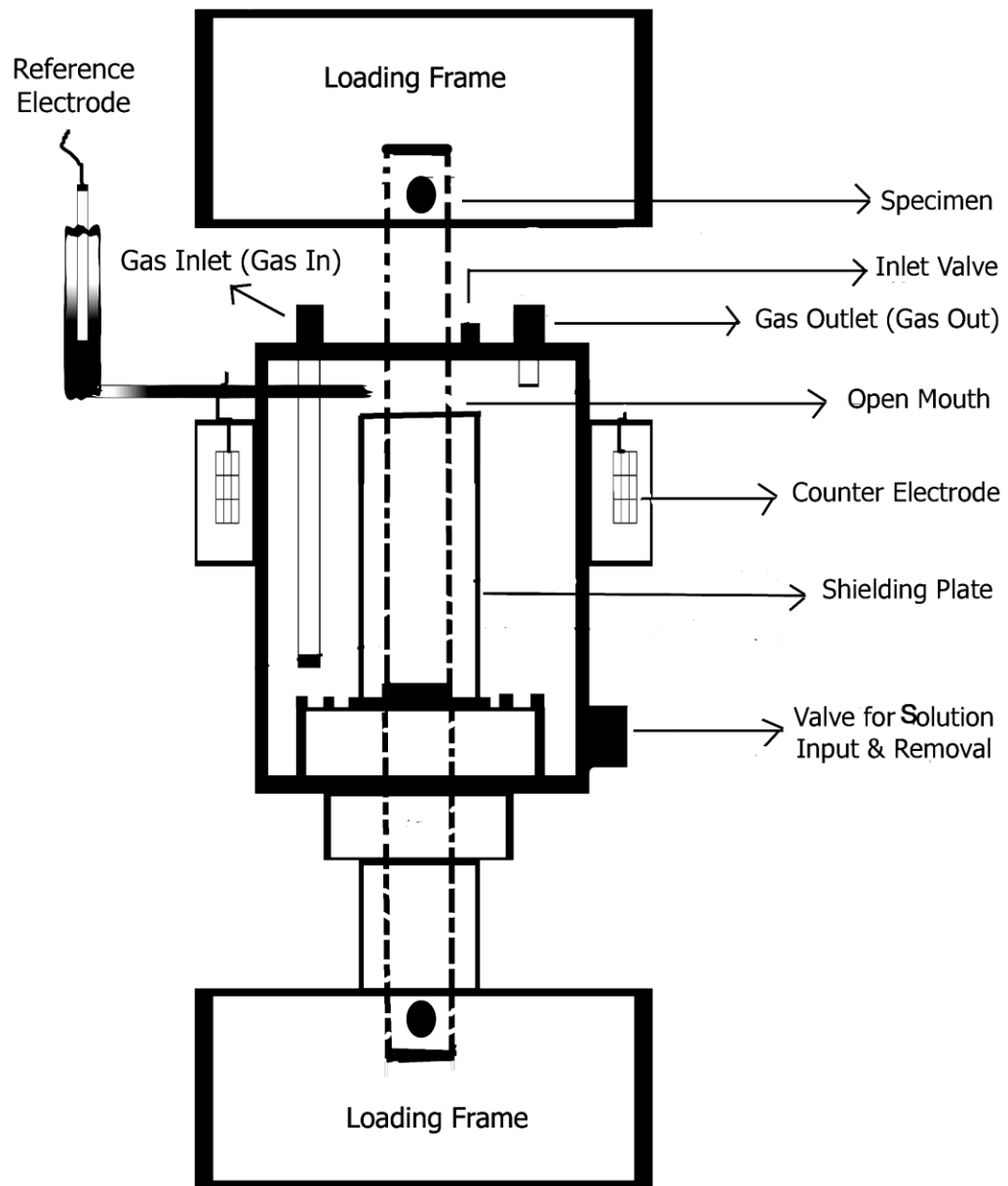


Figure 2.2: Schematic of the corrosion cell designed for simulating near-neutral pH SCC.

Coating disbondment was simulated by using a shielding plate which is attached to the bottom of the corrosion cell (see Figure 2.2). Only the top of the shielding plate is open to the surrounding environment which was termed the Open Mouth (OM). The OM simulates the open mouth of a coating disbondment (see Figure 2.1). The corrosion cell was designed in a way that the shielding plate could be replaced with other shielding plates, simulating coating disbondments made from different materials and/or geometries.

Different levels of CP could be applied to the OM of the simulated coating disbondment, using a three electrode system. In this system the specimen is the working electrode, two platinum gauzes are used as counter electrodes, and a standard saturated calomel electrode (SCE) is used as the reference electrode (see Figure 2.2). To minimize contamination of solution by oxygen produced on the counter electrodes, the platinum gauzes are separated from the main chamber of the corrosion cell. A salt bridge containing saturated Potassium Chloride (KCl) mixed with Agar-agar is used to apply the CP potential to the portion of the specimen located at the OM. While the level of CP potential could be determined at the OM of the simulated coating disbondment using the potentiostat, it is also important to know the level of CP potential deep inside the coating disbondment. In this regard, a long portable reference electrode was designed and built. The portable reference electrode could be placed inside the simulated coating disbondment from the inlet valve located at top of the corrosion cell (shown in Figure 2.2), and could measure the CP potential of the front of the specimen surface inside the coating disbondment at the desired depth. Also, the pH value of the solution inside the coating disbondment may be determined using small commercial microelectrodes, which they could also be placed inside the corrosion cell from the inlet valve. The micro-electrodes should be carefully calibrated in buffer solutions with pH values of 4, 7, 10, and 12 before each use.

Tensile specimen made from the pipe material may be sandwiched inside the simulated coating disbondment. The tensile specimen when exiting the corrosion

cell is pin holed to a jaw at the bottom of the corrosion cell. The jaw is fixed to a loading frame where cyclic loading could be applied. Depending on the capability of the loading machine, different loading cycles and frequencies could be applied in order to simulate the stress fluctuations on the pipe surface. The specimen is mechanically sealed (using O-rings) inside the corrosion cell, therefore no leaks are likely when applying the cyclic loading.

Inlet and outlet gas tubes were also considered in the corrosion cell design. To simulate variation in ground water level, a valve is placed at the bottom of the corrosion cell (see Figure 2.2). Using this valve the level of solution outside the disbondment could be adjusted or the soil solution could be refreshed.

The corrosion cell was designed in a way which could be easily assembled before and dissembled after each experiment. In order to perform tests in controlled environments, all joints were O-ring fitted. While this would minimize the penetration of air from outside environment into the corrosion cell, it also removes the need for using chemical sealants when assembling the corrosion cell. Overall this design means that the corrosion cell could be filled with simulated ground water, CP could be applied, and the specimen could undergo different loading cycles all at the same time.

2.2.2. Specimen

The length of the specimen was designed in such a way as to simulate a wide variety of corrosion conditions when sandwiched inside the simulated coating disbondment. In this regard, flat tensile specimens with a gage length, width and thickness of 145, 12 and 10 mm respectively could be made from pipeline steel, and sandwiched inside the simulated coating disbondment inside the corrosion cell.

2.2.3. Other considerations

Near-neutral pH SCC is closely related to corrosion of the pipeline steel. Knowing the corrosion rate of the pipeline steel at different locations inside the coating disbondments in different environmental conditions could assist with a better understanding of near-neutral pH SCC initiation mechanisms. Therefore in order to be able to determine the corrosion rate of the pipeline steel at different positions from the OM inside the simulated coating disbondment a coupon holder was also designed and made¹. Similar to the tensile specimen the coupon holder could be sandwiched inside the simulated coating disbondment in the corrosion cell. A total number of 7 coupons made from the pipeline steel with the dimensions of (2×2×0.5) cm may be placed in the coupon holder. The coupons inside the coupon holder could be electrically connected to one another, while only their front surface would be exposed to soil solution when placed inside the corrosion cell. This would make determining the weight loss of the metal when there is a gradient of CP under the coating disbondment possible. Figure 2.3 shows a schematic of the designed tensile specimen and coupon holder.

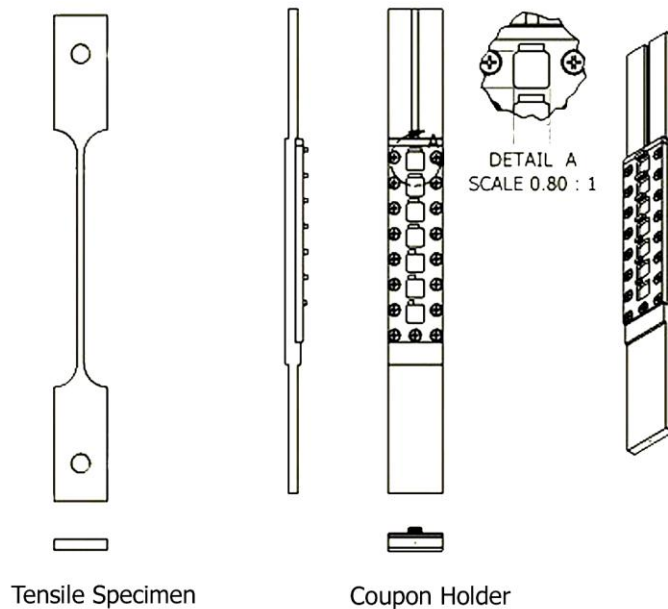


Figure 2.3: Schematic of the tensile specimen and coupon holder.

¹ The coupon holder could be used in corrosion tests with similar environmental conditions as the SCC tests, where no loading is applied.

2.3. Summary

Using the novel test setup the synergistic effects of coating disbondment, CP and cyclic loading can be investigated. Also, using the comprehensive test setup the effect of different levels of CP, loading cycles, coating materials, disbondment geometries, soil chemistry etc. in controlled environments may be investigated. A summary of capabilities of the novel test setup in simulating field conditions responsible for near-neutral pH SCC is presented in Table 2.2.

Table 2.2: Novel test setup capabilities in simulating field conditions responsible for near-neutral pH SCC.

Field conditions	The novel test setup
Loading: <ul style="list-style-type: none"> • Low frequency cyclic loading 	Loading: <ul style="list-style-type: none"> • Depending on the capability of the loading frame, different loading cycles may be applied.
Environment: <ul style="list-style-type: none"> • Localized under coating disbondments. • Anaerobic environment with certain amount of dissolved gases. • Variable environment with fluctuations in ground water level. 	Environment: <ul style="list-style-type: none"> • Effect of coating disbondments may be considered. • Controlled environment may be applied.
Cathodic protection: <ul style="list-style-type: none"> • Might have an effect. • Different levels of CP exist on pipe surface. 	Cathodic protection: <ul style="list-style-type: none"> • Different levels of cathodic protection may be applied.

**Chapter 3: Near-neutral pH Stress Corrosion Crack Initiation
under a Simulated Coating Disbondment: Effect of Time and
Maximum Stress¹**

¹ A version of this chapter has been published: A. Eslami, B. Fang, R. Kania, B. Worthingham, J. Been, R. Eadie, W. Chen, Stress Corrosion Cracking Initiation under the Disbonded Coating of Pipeline Steel in Near-neutral pH Environment, **Corrosion Science**, 52 (2010) 3750-3756.

3.1. Introduction

Near-neutral pH stress corrosion cracking has been an integrity risk for oil and gas pipelines for more than two decades. It was first reported by Delanty in 1985 [1]. Extensive field investigations have shown that near-neutral pH SCC is characterized by wide transgranular cracks [1, 2], and usually occurs in dilute near-neutral pH environments with a pH around 6.5 [3, 4, 5]. The cracking is particularly severe in polyethylene (PE) tape coated pipelines, where the disbonded coatings form long wrinkles that fill with ground water. Disbondments also form at tented regions along some types of seam welds (e.g. double submerged arc welds). Despite extensive research in this field, the mechanism(s) of near-neutral pH SCC initiation remains undetermined.

Many researchers [2, 4, and 6] have tried to reproduce near-neutral pH SCC in the laboratory. A number of factors affecting crack initiation have been identified from laboratory simulations including the effect of cyclic loading [7], surface discontinuities, microstructures, [8] and residual stresses [9, 10]. Most of these simulations were carried out using steel specimens directly immersed in a sealed corrosion cell containing near-neutral pH soil solutions under a free corrosion condition. The rationale of such an experimental setup is that near-neutral pH SCC occurs underneath a disbonded coating where cathodic protection (CP) is severely diminished or absent due to shielding by the coating and the high resistivity of the groundwater.

It is believed that the free corrosion experimental setup neglects an important contributor to corrosion: the concentration cell, which could be formed because of the effect of the shielding near the open mouth and the reactions from gradients in cathodic protection at the mouth of the disbondment that may alter the chemistry of the trapped soil solution.

There have been a few laboratory simulations [11, 12, 13, and 14] of the electrochemical conditions underneath disbonded coatings on pipeline steel when

CP is applied. However, it is believed that these simulations are imprecise in at least one of the following aspects: 1) the disbanded gap was designed to be only 0.2 mm to 1.5 mm [11, 13, and 14] which appears to be inconsistent with field observations of large disbondments; 2) cyclic loadings that better represent field conditions were not applied, since most of the tests were conducted using slow strain rate (SSR) tests [15, 16, and 17].

The aim of the current study is to provide a better understanding of near-neutral pH SCC initiation mechanism(s) by using more realistic test conditions.

3.2. Experimental

3.2.1. Specimen, solution and corrosion cell

The chemical composition of the X-65 pipeline steel used in this study is shown in Table 3.1. The X-65 pipeline steel had a yield strength and tensile strength of 522.8 and 607.8 MPa, respectively. This steel was characterized as being susceptible to near-neutral pH SCC [9, 18, and 19]. The specimens were selected from intact sections of an underground pipe with around 15 years of service from a joint where SCC cracks were detected. This was to ensure that the material to be tested was susceptible to near-neutral pH SCC. The section selected for the specimens in this investigation was free of SCC cracks because the coating had remained intact. The section was also free of other mechanical damage. The specimens were machined and ground to 180 grit. We believe that such used pipe is more appropriate than new pipe for near-neutral pH SCC initiation simulation. Pipeline steels become susceptible to near-neutral pH SCC only when coatings on pipeline steels are damaged. This usually happens after 5 to 10 years of operation. During this 5-10 year period, the pipeline steels have been mechanically conditioned by the stress variations in the pipe, which we believe can be a key factor to the cracking after the coating is damaged. More details about stress conditioning can be found in a study performed by Chen et al. [19].

Flat tensile specimens with gage length, width and thickness of 145, 12 and 10 mm respectively were machined from the selected section. Only the front surfaces of the gage length were exposed to the corrosion environment, while the sides were coated with 100% silicone sealer prior to corrosion exposure.

Table 3.1: Chemical composition of the X-65 pipeline steel used in this study, API specification for X-65 is also given.

Element	X-65 Steel (Wt %)	API X-65 Steel (Wt %)
Aluminum	0.029	-
Boron	<0.0005	-
Calcium	0.0012	-
Carbon	0.12	0.26*
Chromium	0.065	-
Cobalt	0.004	-
Copper	0.014	-
Manganese	1.5	1.45*
Molybdenum	<0.03	-
Nickel	<0.02	-
Niobium	0.049	-
Phosphorus	0.017	0.03*
Silicon	0.26	-
Sulfur	0.0046	0.03*
Tin	0.0016	-
Titanium	<0.005	-
Vanadium	<0.01	-
Zirconium	<0.002	-
Iron	Balance	Balance

* Maximum

The test environment in this study was a simulated soil solution using C2 solution, with the chemistry shown in Table 3.2. When the simulated soil solution was purged with 5% CO₂/N₂ for 48 hours prior to testing it reached a stable pH of 6.29.

Table 3.2: C2 solution chemistry [20].

Component	Concentration (g/L)
MgSO ₄ .7H ₂ O	0.0274
CaCl ₂	0.0255
KCl	0.0035
NaHCO ₃	0.0195
CaCO ₃	0.0606

The tensile specimen and soil solution were placed inside the corrosion cell schematically shown in Figure 2.2. The shielding material used in the corrosion cell was made from PMMA¹, which has lower gas permeability rate compared to the PE tape coatings commonly used for pipelines [21, 22]. Using PMMA shielding with a large gap represents the condition where gas mainly enters the disbondment through the OM, not through the coating. Thus the gas condition is correct, but it is not achieved by permeation. The distance between the shielding and the specimen surface was fixed to 10 mm. The upper ends of the shielding were 45 mm away the top lid of the corrosion cell. The level of solution was kept above the upper end of the shielding during the test. A potentiostat, model EG&G 363, was used to apply a CP potential of to the portion of the tensile specimen just above the OM of the shielding (see Figure 2.2).

3.2.2. Stress corrosion cracking initiation tests

Two long term stress corrosion cracking initiation tests were designed and performed. They were named Test A and Test B. The conditions for both tests are shown in Table 3.3. As can be seen from this table, Test B was a longer test with more aggressive loading conditions. During both tests a CP potential of -1.2 V_{SCE} was applied to the portion of the specimen at the OM, and the soil solution was continuously purged with 5%CO₂/N₂. The reason that a high potential of -1.2 V_{SCE} was selected, was to see the effect of potential gradient on the formation of different corrosion products.

Table 3.3: Near-neutral pH SCC initiation tests.

Test	Maximum Stress (SMYS)*	Frequency (Hz)	Amplitude (R-Ratio)	Duration (day)
Test A	100 %	0.0001	0.8	90
Test B	107 %	0.0001	0.8	180

* Specified Minimum Yield Strength

¹ Poly(methyl methacrylate)

3.2.3. Characterization

During the tests, commercial combination micro-electrodes were used to record the pH at different locations from the OM. The micro-electrodes had a diameter less than 1.6 mm and were carefully calibrated in buffer solutions of pH 4, 7, 10 and 12 at different time intervals. The micro-electrodes had a response time of less than 10 seconds and a stability of around 0.05 pH units per day. The level of actual CP potential at different positions from OM was monitored using a portable standard reference calomel electrode. The reference electrode was moved to the desired location, and the potential between the specimen surface and the reference electrode was recorded by using a voltmeter. Monitoring of pH and potential was done at different time intervals for the entire 90 days of testing.

After the tests, the tensile specimen was removed from the corrosion cells, dried and cleaned immediately using acetone/ethanol. Then the gauge length of the tensile specimen was sectioned into smaller parts which were placed in a rust removing solution for about 2 minutes (the chemical composition of the rust remover solution is shown in Table 3.4). The surface and cross sections of the specimens were analyzed using Optical Microscope, and Scanning Electron Microscope (SEM) equipped with an Energy Dispersive X-ray analyzer (EDX). In some cases, the sample was plated with nickel prior to cross sectioning, to preserve the surface characteristics and obtain better quality imaging.

Table 3.4: Chemical composition of the rust remover solution.

Component	Volume (ml)
H ₂ O	100
Cis-2-Butene-1, 4-Diol	4
HCl	3

3.3. Results and discussion

3.3.1. C2 solution

The pH of C2 solution before purging with 5%CO₂/N₂ was 6.7. After 2 days of purging the pH dropped to 6.29 and then remained stable. The new pH was a result of the following steps:

- 1) After purging the solution with 5%CO₂/N₂, the dissolved CO₂ was hydrated to carbonic acid.
- 2) Then, the following reactions occurred between the species in C2 solution containing carbonic acid:



A new balance between solution species shown in Equations 3-1- 3-5 caused a pH of 6.29.

3.3.2. Potential distribution

The initial potential of the specimen at different locations from OM in C2 solution prior to applying CP is shown in Figure 3.1. This potential is referred to as the initial open circuit potential (OCP). When a CP of -1.2 V_{SCE} was applied to the OM the initial OCP changed at different locations from OM, and then remained almost stable for the entire 90 days of monitoring (Figure 3.1). As can be seen from Figure 3.1 the further from the OM, the more the potential has increased from the -1.2 V_{SCE} applied at the OM. At locations beyond 12 cm from the OM, the potential was close to OCP whether there was CP applied or not. The potential drop in the shielding can be modeled as a transmission line equivalent circuit. In this type of model, the potential is determined based on the

polarization resistance, the solution resistance the applied current, and the disbondment dimensions. At locations beyond 12 cm from the OM the potential had dropped to values close to OCP mainly due to the polarization resistance and the solution resistance inside the shielding.

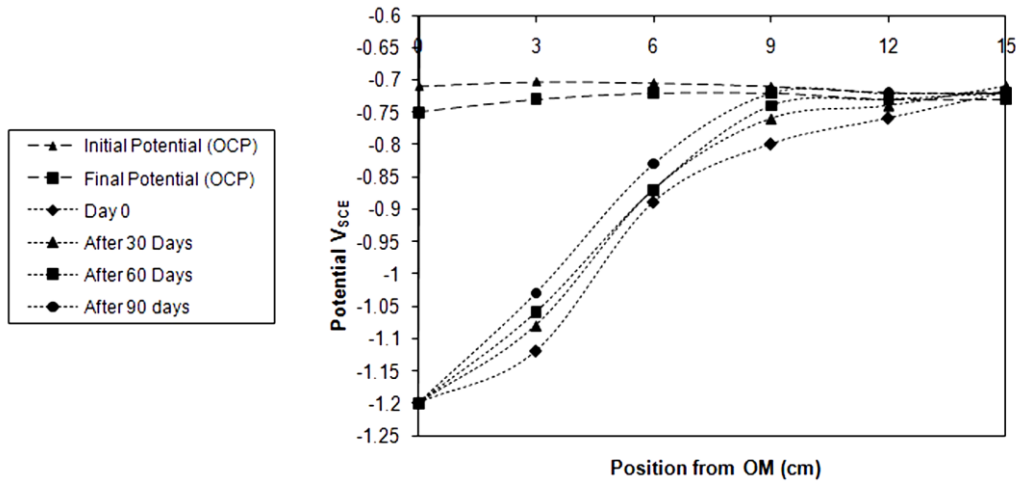


Figure 3.1: Cathodic protection levels at different positions from OM, at different time intervals.

3.3.3. pH distribution

The pH at different positions from the OM when continuously purged with 5%CO₂/N₂ prior to applying CP is shown in Figure 3.2. As can be seen from this figure, when CP of -1.2 V_{SCE} was applied at the beginning of the test to the OM, the pH increased at all locations from its initial value of 6.29 depending on the position from the OM. The pH remained near-neutral for the entire 90 days of monitoring. The increase in pH is related to the consumption of H⁺ or generation of OH⁻ from the reduction reactions.

Despite a significant potential difference at various positions from OM, section 3.3.2, only minor pH differences were observed. This can be explained by the mixing of the solution by the flowing gas 5%CO₂/N₂.

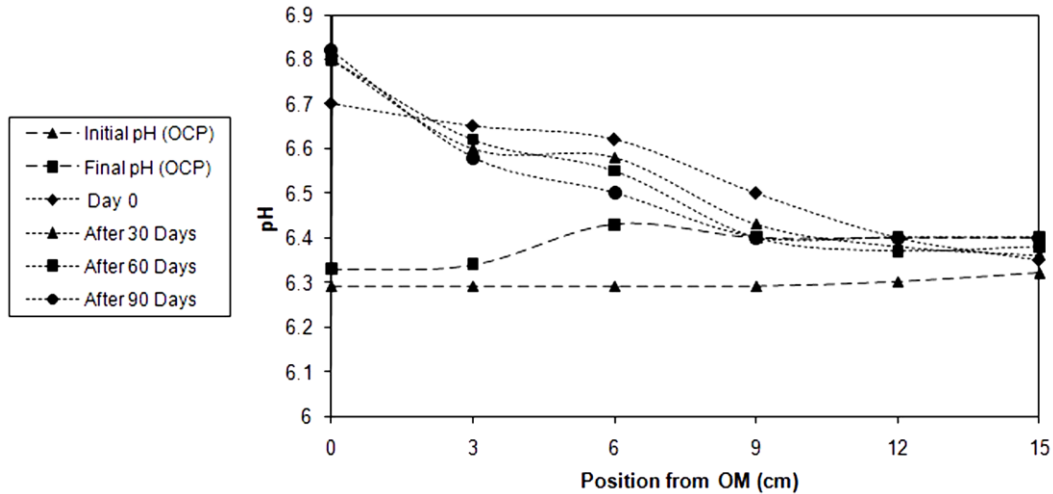
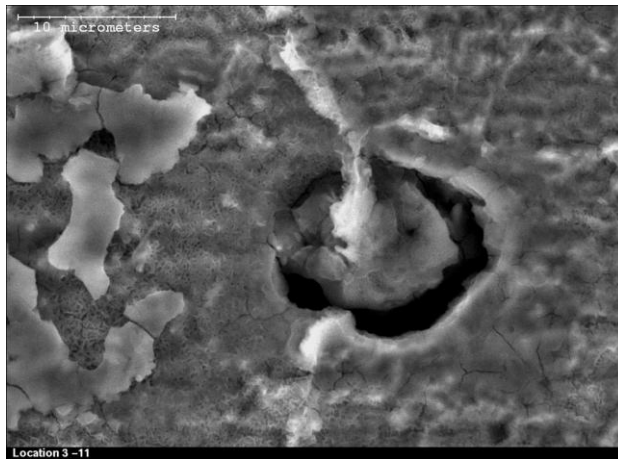


Figure 3.2: pH distribution of the soil solution inside the shielding at different positions from OM, at different time intervals.

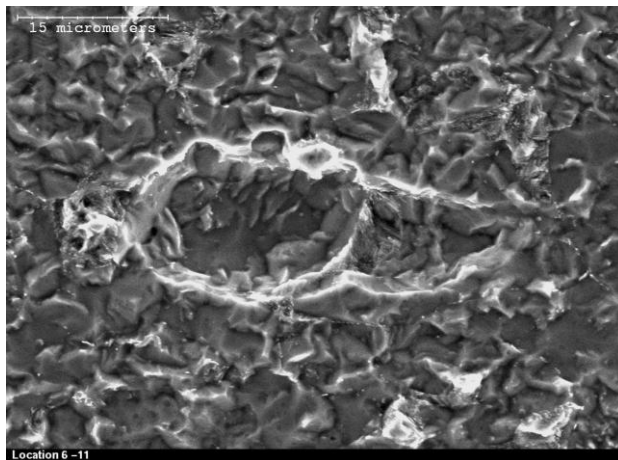
3.3.4. Stress corrosion cracking initiation in Test A

a) Surface characterization

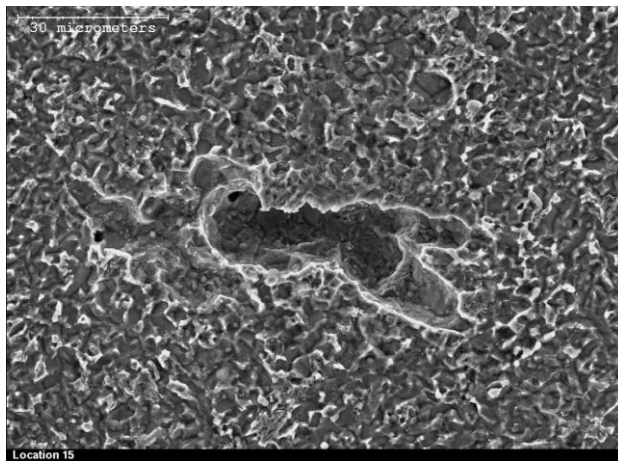
Typical surface morphologies of the specimen at different positions from the OM after Test A are shown in Figure 3.3. As can be seen from these photographs, rather than SCC cracks, only pits with different morphologies have been formed. At locations close to OM (up to 3 cm from the OM) small circular pits were formed. This was a region with sufficient CP potential (see Figure 3.1). At locations far away from OM (beyond 12 cm from the OM) larger pits with irregular shapes were formed. General corrosion had partially covered the boundaries of these irregular pits. General corrosion at the far end away from the OM was related to the lack of CP potential in this region (see Figure 3.1).



(a)



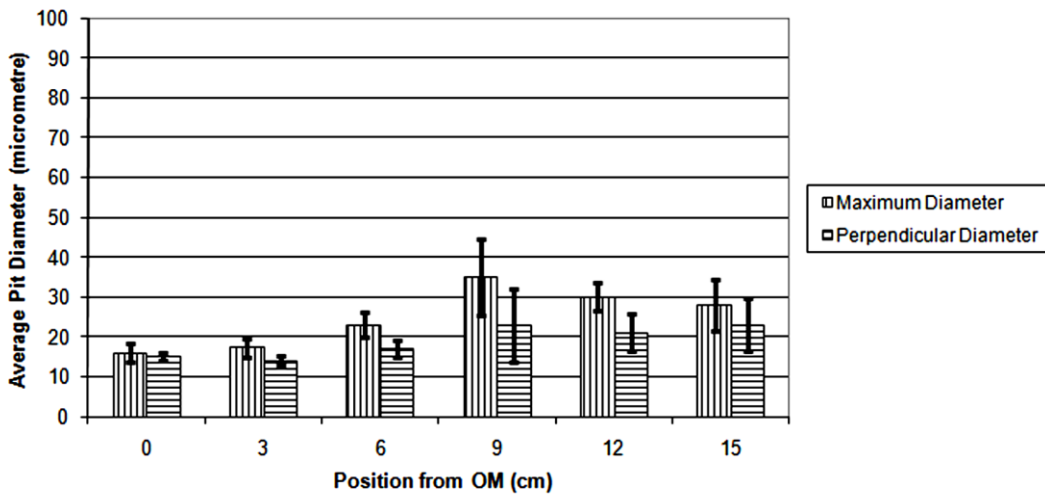
(b)



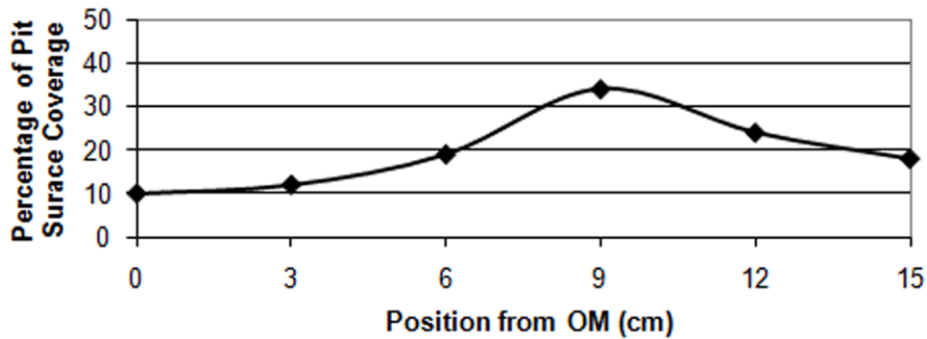
(c)

Figure 3.3: Typical surface morphologies of the tensile specimen after Test A, at locations: (a) close to OM, (b) between OM and the far end, (c) remote from the OM.

Average pit diameter and percentage of pit surface coverage based on their position from the OM are shown in Figure 3.4. The largest of the pits with the highest percentage of surface coverage were formed at 9 cm from the OM. This region received some CP during the test with electrochemical potentials from about 100 to 50 mV_{SCE} below OCP. By comparing Figures 3.1, 3.3 and 3.4 one can say that a decrease in CP level resulted in the formation of bigger pits, as long as pit formation was not limited by rapid general corrosion, which would occur in the regions at voltages near OCP remote from the OM.



(a)



(b)

Figure 3.4: (a) Average pit diameter based on position from OM in Test A, (b) percent pit surface coverage based on position from OM in Test A.

Non-metallic inclusions containing Mn, Mg, Ca, Al, S and O were detected at the surface of some pitted areas. These inclusions were found mainly in regions with sufficient CP, *i.e.* with electrochemical potentials more than 100 mV_{SCE} below OCP. A micrograph showing an inclusion inside a pitting site at 3 cm from the OM can be seen in Figure 3.3a. The EDX analysis presented in Figure 3.5 shows the inclusion is particularly rich in Mn, Ca, O and S. Pit formation at these locations may have been enhanced by galvanic coupling between inclusions and the base metal, and/or the dissolution of the inclusions by the surrounding environment.

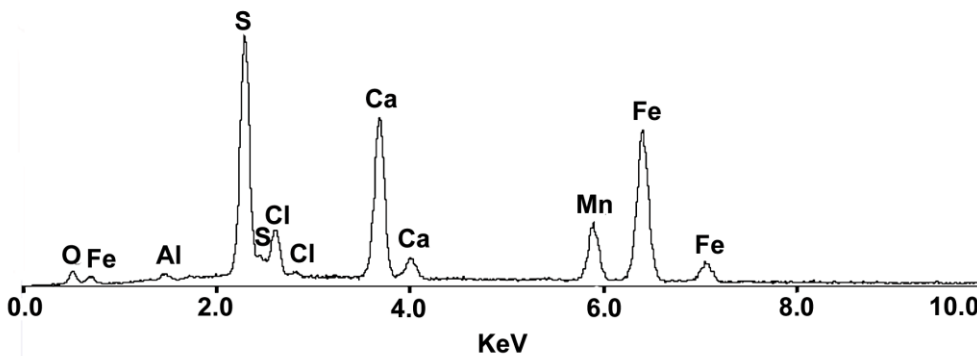


Figure 3.5: EDX spectra showing the composition of the non-metallic inclusion.

b) Cross section characterization

Cross sections of the specimen after Test A were prepared to see if any cracks had initiated from the bottom of pits. No cracks were observed, although pits with different depths were formed.

The lack of cracks in Test A might be due to insufficient test time and/or stress. In the field, it might take up to several years for well defined cracks to initiate. Also, the stress level might exceed the maximum allowable stress for the operating pipelines. This could be caused by different sources of additional stress such as residual stresses from manufacturing, welding, or bending. Therefore, a longer experiment with more aggressive loading conditions was designed and performed (Test B).

3.3.5. Stress corrosion cracking initiation in Test B

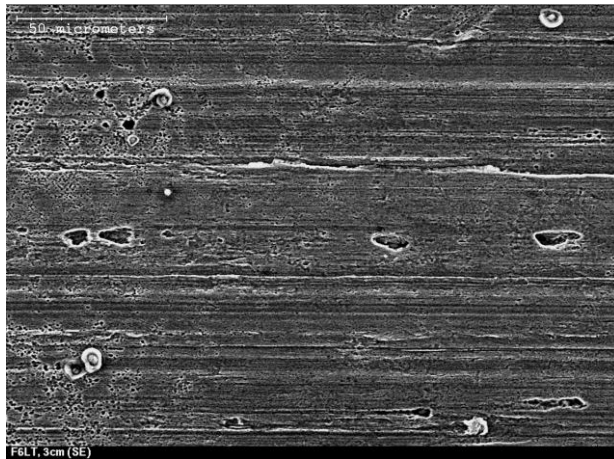
a) Surface characterization

Typical surface morphologies of the specimen after Test B are shown in Figure 3.6. The same trend in pitting as in Test A was observed. Close to the OM, small pits were formed while far from the OM, general corrosion had partially covered the pitted boundaries. Average pit diameter and percentage of pit surface coverage based on their position from OM is shown in Figure 3.7. The highest percentage of pit coverage was observed at 9 cm from OM, while the largest of pits were found at 12 cm from the OM. Again both locations had minor CP with electrochemical potentials between about 50 and 100 mV_{SCE} below OCP. Pit coverage was reduced when electrochemical potentials were close to OCP remote from the applied CP.

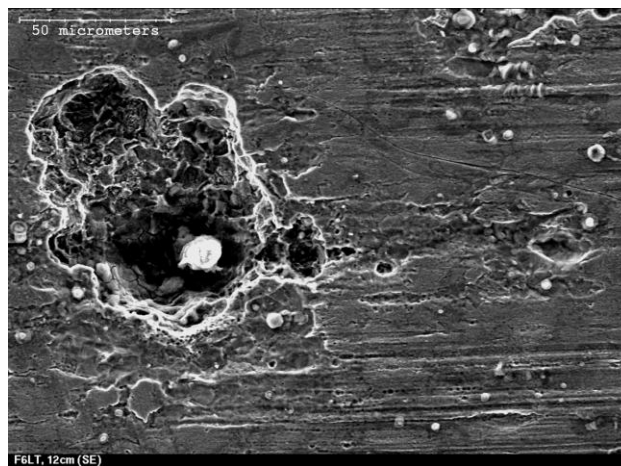
Comparing Test A and Test B from Figures 3.4 and 3.7, one can say that by increasing the test time and maximum level of stress, the pitting size and percentage of surface area covered by them increased considerably in regions with insufficient CP. Pitting in these regions was not mitigated by sufficient CP which existed close to the OM, and/or general corrosion which existed at the far end, which was remote from the OM. The increase in pitting size could raise the stress concentration at pit boundaries, and eventually lead to crack initiation. This has been shown by Hoepfner^[24] (Equation 3-6). For a semielliptical surface flaw Hoepfner calculated the stress intensity factor as follow:

$$K_{sf} = 1.1S \sqrt{\pi \frac{a}{Q}} \quad (3-6)$$

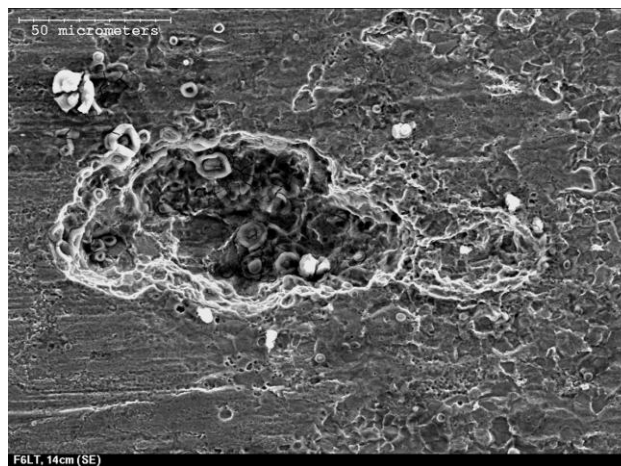
Where “ K_{sf} ” is the stress intensity factor corresponding to a surface flaw, “ S ” is the applied stress, “ a ” is the size of flaw, and “ Q ” is the shape factor. An example of a large pit in which a micro-crack appears to have initiated, can be seen in Figure 3.6b.



(a)

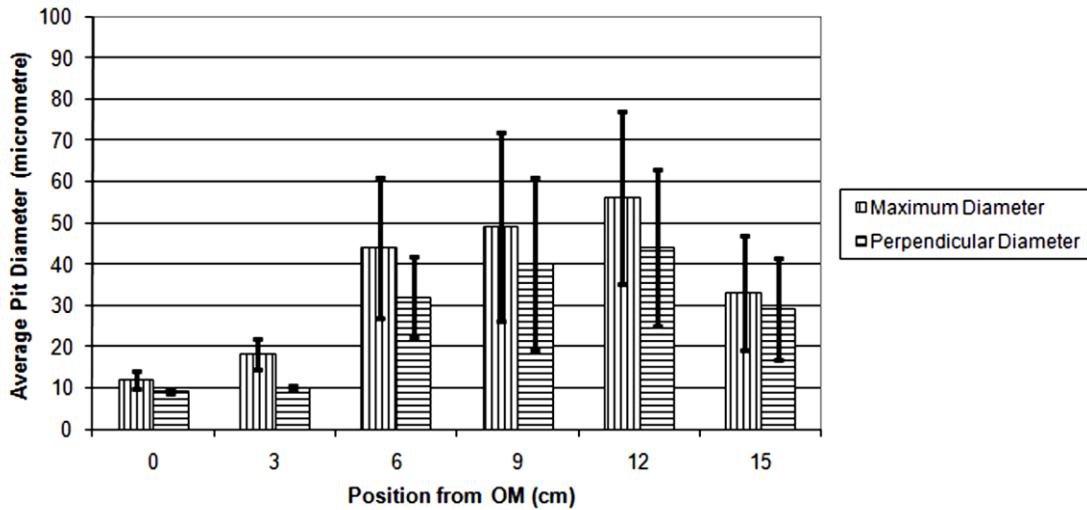


(b)

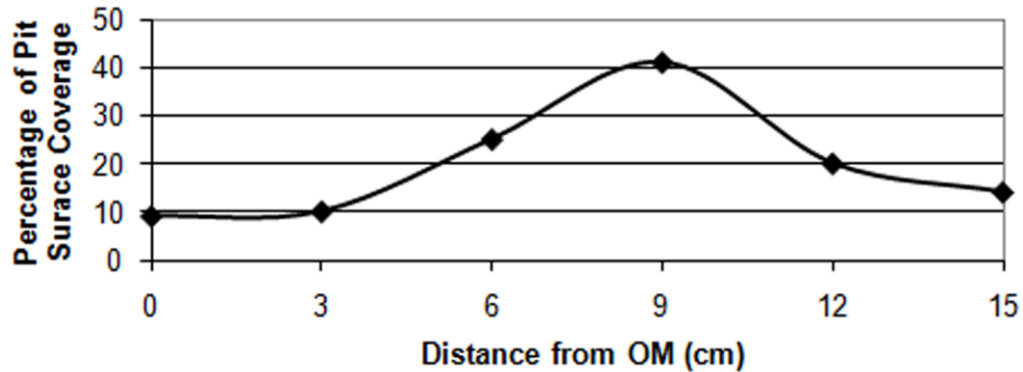


(c)

Figure 3.6: Typical surface morphologies of the tensile specimen after Test B at locations: (a) close to OM, (b) between the OM and the far end, (c) remote from the OM.



(a)



(b)

Figure 3.7: (a) Average pit diameter based on position from OM in Test B, (b) percent pit surface coverage based on positions from OM in Test B.

b) Cross section characterization

Cross sections of the sample in Test B were prepared to see if any cracks initiated, and to characterize the pitting depth.

The average pit depth relative to position from the OM, for both Test A and Test B are shown in Figure 3.8. As can be seen from the figure, pitting depth is minor for both Tests A and B at locations close to the OM, while it increased considerably at locations far from the OM. Comparing Figures 3.1 and 3.8 it can be stated that, at locations close (within 6 cm) to the OM, CP effectively mitigated

any increase in pitting depth. An increase in depth was observed beyond 6 cm and that increase was enhanced by increased test time or test stress.

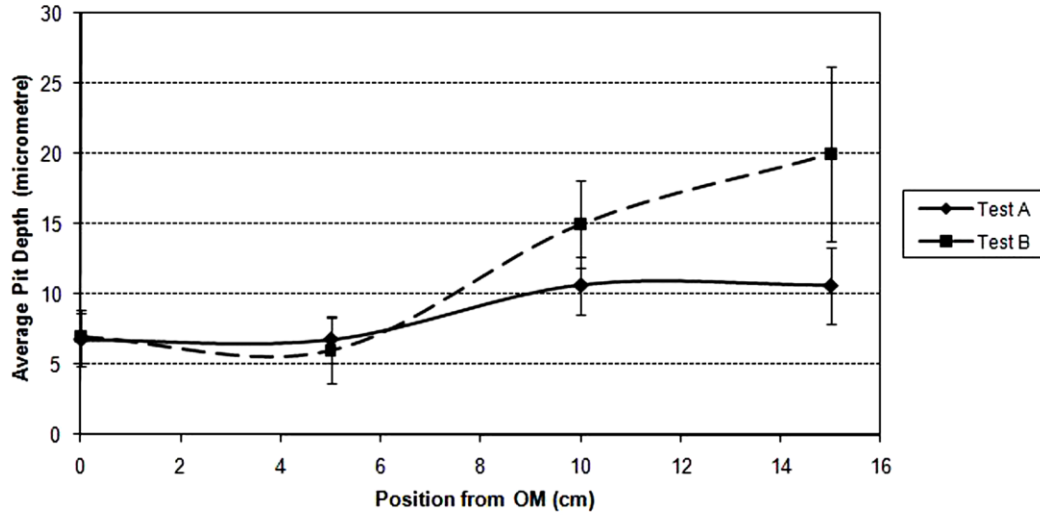


Figure 3.8: Average pit depth as a function of position from OM in Test A and Test B.

When several cross sections of Test B sample were prepared, a few micro-cracks that had initiated at the bottom of pits were observed. They were located in the region with insufficient CP potential (close to 10 cm from the OM). An example of a micro-crack initiating at the bottom of a pit is shown in Figure 3.9. In this figure, the sample was plated with nickel prior to cross sectioning to preserve the surface shapes. As can be seen from this figure, nickel diffused inside the metal gap created by the pit and the micro-crack. Initiation of micro-cracks from the bottom of pits correlates well with field observations [25]. The reason that they can initiate at the bottom of pits is due to the high stress concentration that can exist at the bottom of a pit. This was well shown by a corrosion fatigue model developed by Kondo [26]:

$$\Delta K = 2.24\sigma_a \sqrt{\pi c \frac{\alpha}{Q}} \quad (3-7)$$

Where “ σ_a ” is stress amplitude, “ a ” is the pit depth, “ α ” is “ a/c ”, “ $2c$ ” is the flaw size, and “ Q ” is the shape factor. This formula shows that the stress concentration factor range can increase significantly with pitting depth. The pitting depth in Test B increased considerably, comparing to Test A (Figure 3.8), which led to crack initiation.

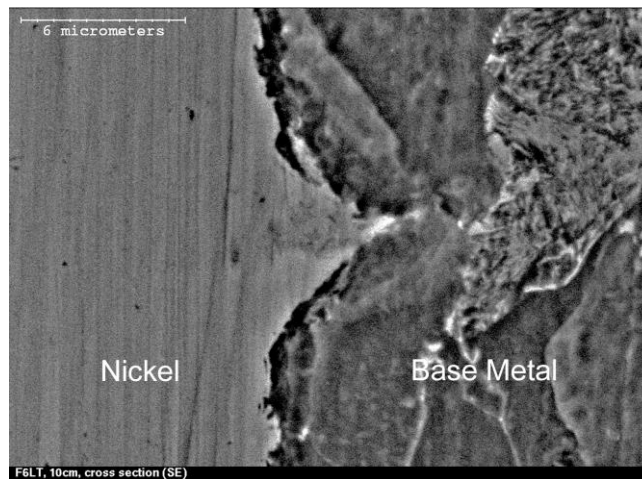


Figure 3.9: Secondary Scanning Electron Microscope (SEM) image showing the cross section of the sample after Test B, at 10 cm from the OM.

Increase in pitting depth was not the only factor causing the crack initiation. As the Kondo formula shows (Equation 3-7), the shape factor is another important factor. Our study showed that, although some pits were deeper than others, no crack was initiated from these pits. This can be explained by their different morphology ending in different stress concentration. The sharper a pit, the bigger its shape factor would be ending in higher stress concentration. The morphology of some deep pits in our experiment was semi circular at the bottom, which could not generate high stress concentration compared to those with sharper tips. An example of this can be seen when comparing Figures 3.9 and 3.10.

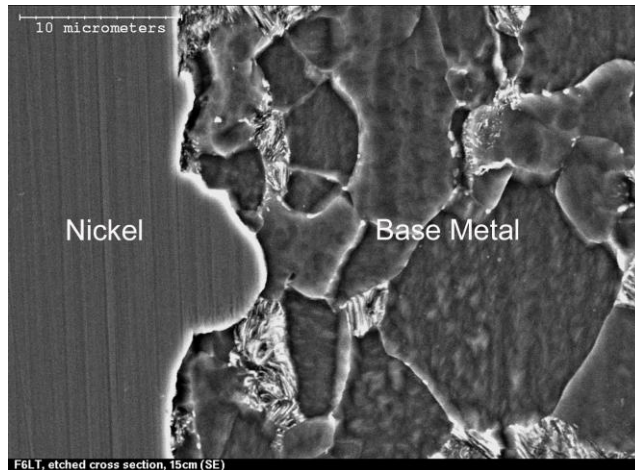


Figure 3.10: Secondary Scanning Electron Microscope (SEM) image showing the cross section of the sample after Test B, at 15 cm from the OM.

3.3.6. SCC initiation mechanism

The current research has shown that cracks can initiate in a near-neutral pH environment with the right combination of cyclic loading, environment, and material under the disbonded coatings of pipeline steel. In this regard pits were first generated by localized anodic dissolution. Then with time, the pits grew in both the surface and depth directions, which caused an increase in stress concentration at the pit. Cyclic loading, when combined with localized anodic dissolution facilitated the pit-to-crack transition in regions with the highest stress concentration. This ended in crack initiation from both the bottom and surface of pits. A schematic diagram showing a summary of the SCC initiation mechanism is shown in Figure 3.11. It's worth mentioning that if longer testing time was given, the initiated micro-cracks could eventually turn into well defined SCC cracks. Under field conditions it might take up to several years for well defined SCC cracks to be observed [27].

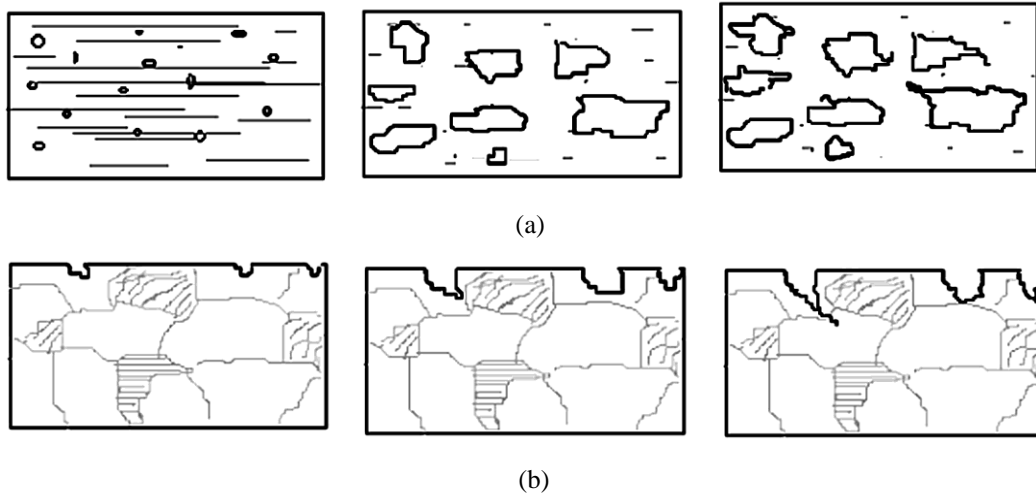


Figure 3.11: Schematic showing SCC initiation mechanism from: (a) surface of pits (surface view), (b) Bottom of pits (cross section view).

3.4. Conclusions

Based on the current research the following conclusions can be obtained:

1. CP works effectively in mitigating the pitting corrosion at locations with sufficient CP potential.
2. Pitting corrosion in terms of size and percentage of surface coverage was most severe at regions with insufficient CP potential; not regions completely free from CP as previously believed. Locations with minimum CP had the deepest pits. Deep pits were not necessarily at high risk of crack initiation. Only those with a high stress concentration were most prone to crack initiation.
3. Micro-cracks were initiated both from the surface and bottom of pits.
4. Stress, time, and the level of CP were the three important factors in increasing the possibility of crack initiation. Therefore locations with high levels of stress fluctuation such as old pipes and insufficient CP (but not totally lacking) are more prone to SCC initiation.

3.5. References

- [1] B.S. Delanty, J. O'Beirne, Major Field Study Compares Pipeline SCC with Coatings, *Oil & Gas Journal*, 15 (1992) 39-44.
- [2] R.N. Parkins, W.K. Blanchard, B.S. Delanty, Transgranular Stress Corrosion Cracking of High-Pressure Pipelines in Contact with Solutions of Near Neutral PH, *Corrosion*, 50 (1994) 394-408.
- [3] J.A. Beavers, C.L. Durr, S.S. Shademan, L. Collins, Materials for Resource Recovery and Transport, in: *Inter. Sym. on Mater. for Resource Recovery and Transport*, CIM, Calgary, Canada, 1998.
- [4] R.N. Parkins, A Review of Stress Corrosion Cracking of High Pressure Gas Pipelines, in: *Proc. Corrosion/2000*, TX: NACE International, Huston, USA, 2000.
- [5] B. Fang, A. Atrens, J. Wang, E. Z. Han Zhu, W. Ke, Review of Stress Corrosion Cracking of Pipeline Steels in "Low" and "High" pH Solutions, *Journal of Material Science*, 38 (2003) 127-132.
- [6] J.A. Beavers, C.L. Durr, B.S. Delanty, D.M. Owen, R.L. Sutherby, Near-Neutral pH SCC: Crack Propagation in Susceptible Soil Environments, in: *Proc. Corrosion/2001*, TX: NACE International, Huston, USA, 2001
- [7] S. Wang, W. Chen, F. King, Precyclic-loading-Induced Stress Corrosion Cracking of Pipeline Steels in a Near-Neutral-pH Soil Environment, *Corrosion*, 58 (2002) 526-534.
- [8] R. Chu, W. Chen, S.H. Wang, F. King, T.R. Jack, R.R. Fessler, Microstructure Dependence of Stress Corrosion Cracking Initiation in X-65 Pipeline Steel Exposed to a Near-Neutral pH Soil Environment, *Corrosion*, 60 (2004) 275-283.
- [9] G.V. Boven, W. Chen, R. Rogge, The Role of Residual Stress in Neutral pH Stress Corrosion Cracking of Pipeline Steels, Part 1: Pitting and Cracking Occurrence, *Acta Materialia*, 55 (2007) 29-42.
- [10] W. Chen, G.V. Bovan, R. Rogge, The Role of Residual Stress in Neutral pH Stress Corrosion Cracking of Pipeline Steels-Part II: Crack Dormancy, *Acta Materialia*, 55 (2007) 45-43.
- [11] M.C. Yan, J.Q. Wang, E.H. Han, W. Ke, Electrochemical Measurements Using Combination Microelectrode in Crevice Simulating Disbonded of Pipeline Coatings under Cathodic Protection, *Corrosion Engineering Science & Technology*, 42 (2007) 42-49.
- [12] R. Brousseau, S. Qian, Distribution of Steady-State Cathodic Currents Underneath a Disbonded Coating, *Corrosion*, 50 (1994) 907-911.
- [13] Z. Li, F. Gan, X. Mao, A Study on Cathodic Protection against Crevice Corrosion in Dilute NaCl Solutions, *Corrosion Science*, 44 (2002) 689-701.
- [14] F. Gan, Z.W. Sun, G. Sabde, D.T. Chin, Cathodic Protection to Mitigate External Corrosion of Underground Steel Pipe Beneath Disbonded Coating, *Corrosion*, 55 (1994) 804-816.
- [15] L. Zang, X.G. Li, C.W. Du, Y.F. Cheng, Corrosion and Stress Corrosion Cracking of X70 Pipeline Steel in a CO₂ Containing Solution, *Journal of Materials Engineering and Performance*, 18 (2009) 319-323.

- [16] Z.Y. Liu, X.G. Li, C.W. Du, L. Lu, Y. R. Zhang, Y. F. Cheng, Effect of Inclusions on Initiation of Stress Corrosion Cracks in X70 Pipeline Steel in an Acidic Soil Environment, *Corrosion Science*, 51 (2009) 895-900.
- [17] P. Liang, X.G. Li, C.W. Du, X. Chen, Stress Corrosion Cracking of X-80 Pipeline Steel in Simulated Alkaline Soil Solution, *Materials & Design*, 30 (2009) 1712-1717.
- [18] Y.Z. Wang, R.W. Revie, M.R. Shehata, R.N. Parkins, K. Krist, Initiation of Environment Induced Cracking in Pipeline Steel: Microstructural Correlations, in: *Proc. IPC/98*, Calgary, Canada, 1998.
- [19] W. Chen, S.H. Wang, R. Chu, F. King, T.R. Jack, R.R. Fessler, Effect of Precyclic Loading on Stress-Corrosion-Cracking Initiation in an X-65 Pipeline Steel Exposed to Near-Neutral pH Soil Environment, *Metallurgical and Materials Transaction A*, 34A (2003) 2601-2608.
- [20] W. Chen, RL. Eaide, RL. Sutherby, Environmental Effects of Near-neutral pH Stress Corrosion Cracking in Pipelines. In: *Second International Conference on Environmental Induced Cracking of Metals*. Banff, Alberta, Canada: The Banff Center; 2004.
- [21] S. Pauly, Permeability and diffusion data, in: J. Brandrup and E.H. Immergut (Eds.), *Polymer Handbook*, 3rd Edition., John Wiley & Sons, New York, NY, 1989.
- [22] T.A. Osswald, G. Menges, *Materials Science of Polymers for Engineers*, 2nd Edition, Hanser Gardeners Publications Inc., 2003.
- [23] B. Gu, W.Z. Yu, J.L. Luo, X. Mao, Transgranular Stress Corrosion Cracking of X-80 and X-52 Pipeline Steels in Dilute Aqueous Solution with Near-Neutral pH, *Corrosion*, 55 (1999) 312-318.
- [24] D. W. Hoepfner, Model for Prediction of Fatigue Life Based Upon a Pitting Corrosion Fatigue Process, *Fatigue Mechanisms*, ASTM STP 675 (1979) 841-870.
- [25] R. N. Parkins, Stress Corrosion Cracking In Pipelines, in: *Proc. NACE Canadian Western Regional Conf.*, Calgary, Canada, 1994.
- [26] Y. Kondo, Prediction of Fatigue Crack Initiation Life Based on Pit Growth, *Corrosion*, 45 (1989) 7-11.
- [27] National Energy Board (NEB), Report of the Inquiry - Stress Corrosion Cracking on Canadian Oil and Gas Pipelines, 1996.

**Chapter 4: Near-neutral pH Stress Corrosion Crack Initiation
under the Simulated Coating Disbondment: Effect of CO₂ and
R-ratio¹**

¹ A version of this chapter has been published: A. Eslami, R. Kania, B. Worthingham, G.V. Boven, R. Eadie, W. Chen, Effect of CO₂ and R-Ratio on Near-neutral pH Stress Corrosion Cracking Initiation Under a Disbonded Coating of Pipeline Steel, **Corrosion Science**, 53 (2011) 2318-2327.

4.1. Introduction

Near-neutral pH stress corrosion cracking (Near-neutral pH SCC) has been an integrity risk for oil and gas pipeline for more than two decades. The first failure of this type was reported by Delanty in 1985 [1]. Since then tens of major failures have been identified in the pipeline system in Canada alone [2]. Although this situation has been improved by considerable mitigating actions, near-neutral pH SCC still remains a major concern for oil and gas industry.

Near-neutral pH SCC is a trans-granular form of cracking, which is often found under polyethylene tape coated pipes at locations where the coating gets disbonded and/or damaged [1, 2]. Disbondments are usually formed at tented regions along some type of seam weld. A digital camera image showing a typical polyethylene coating disbondment on a pipe surface is shown in Figure 4.1. This form of cracking can not be found in situations where the coating is perfectly attached to the pipe surface, since the coating acts as a barrier between the solution and the pipe surface, or in situations where the coating is badly damaged, since cathodic protection (CP) can easily reach the pipe surface and protect the steel.

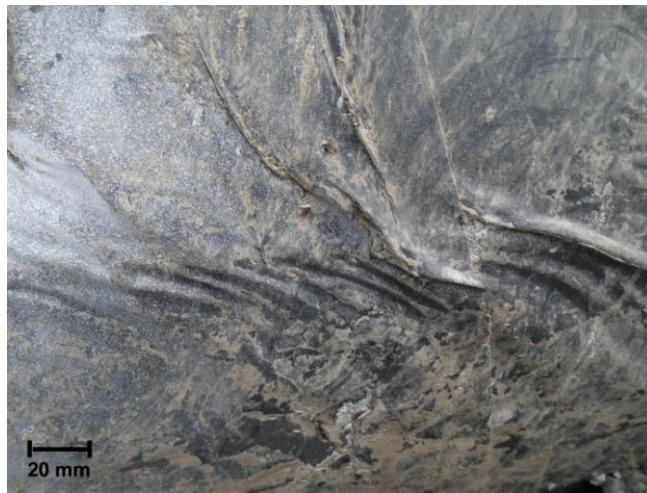


Figure 4.1: Digital camera image showing a polyethylene tape coating disbondment on pipe surface.

Many researchers have tried to initiate near-neutral pH SCC in laboratories, but have been stymied from using unrealistic stress conditions [3-13]. Although there have been some improvements in the understanding of near-neutral pH SCC, several aspects of this form of cracking still remain contentious. Concepts like its initiation mechanism(s) and others, such as why near-neutral pH SCC initiates in certain regions under disbonded coatings and why pitting, general corrosion and near-neutral pH SCC can occasionally be seen under the same disbondment and close to one another are examples of this lack of understanding.

Simplifications of the complicated field conditions in laboratories may be the reason for the aforementioned difficulties. The authors believe that a comprehensive test set up which could produce conditions closer to the actual field environment could be beneficial in obtaining better understanding of near-neutral pH SCC initiation: therefore, a novel test set up which can simulate the synergistic effects of cyclic loading, cathodic protection, and coating disbondment was designed and constructed.

In our previous studies, using this setup, we showed that there could be a wide range of corrosion features including pitting, cracking, and general corrosion on the steel surface up the gradient of CP in an environment with continuous supply of CO₂ [14]. This study further investigates the role of variable environments at two different R-ratios on near-neutral pH SCC initiation. It is anticipated that the results of this study will provide a more insightful understanding of the initiation mechanism(s) of near-neutral pH SCC.

4.2. Experimental

4.2.1. Specimen, solution and corrosion cell

The specimens, solution, and corrosion cell used for this study was same to that explained in section 3.2.1.

4.2.2. Stress corrosion cracking initiation tests

4.2.2.1. CO₂ variation in the tests

Field investigations have shown that there could be a significant variation in the level of the CO₂ in soil environments surrounding buried pipes [1, 2]. In order to investigate the role of CO₂ fluctuations on near-neutral pH SCC initiation, long term 3 month¹ tests with different levels of CO₂ supply were designed. The tests were named as Test A, Test B, Test C, and consisted of continuous, cyclic and limited purging of the simulated soil solution with 5%CO₂/N₂ respectively. In the continuous purging test the soil solution was continuously purged with 5%CO₂/N₂ for the entire 3 month of the test. In the cyclic purging test the soil solution was purged with 5%CO₂/N₂ for the first 2 days of each month during the 3 month test. In the limited purging test the soil solution was only purged with 5%CO₂/N₂ for the first 2 days of the 3 month test.

4.2.2.2. R-ratio

In oil and gas pipelines R-ratio (R=minimum stress/maximum stress) could be significantly affected by the operating condition as well as the nature of the transport material (whether it is liquid or gas). A study on actual oil and gas line pressure variation by CEPA² showed that liquid pipelines average 2500 low R-cycles (R less than 0.5) annually, while gas pipelines undergo fewer than 10 of these large amplitude cycles per year [15]. Therefore the effect of R-ratio on the most susceptible environments on crack initiation was investigated in this study. R-ratio was changed from 0.8 to 0.4 in this regard. The detail of each testing condition is presented in Table 4.1.

¹ A month was defined as 30 days.

² Canadian Energy Pipeline Association

Table 4.1: Near-neutral pH SCC initiation tests.

Test	Maximum Stress (SMYS)*	Frequency (Hz)	R-ratio (R)	Time (day)	Environment
Test A	100 %	0.0001	0.8	90	Continuous purging
Test B	100 %	0.0001	0.8	90	Cyclic purging
Test C	100 %	0.0001	0.8	90	Limited purging
Test D	100 %	0.0001	0.4	90	Continuous purging
Test E	100 %	0.0001	0.4	90	Limited purging

* Specified Minimum Yield Strength (for the X-65 pipeline steel used in this study the 100% SMYS was 448 MPa. The X-65 pipeline steel had a yield strength and tensile strength of 522.8 and 607.8 MPa, respectively).

4.2.2.3. Characterization

The characterization process was similar to that explained in section 3.2.3.

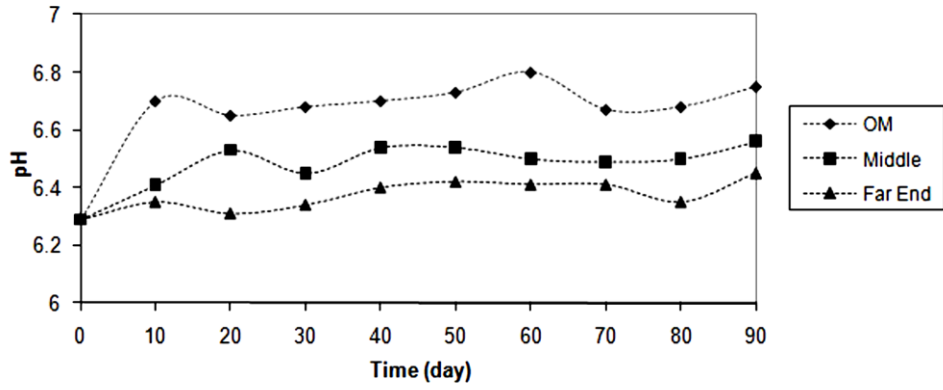
4.3. Results and discussion

4.3.1. pH and potential distribution

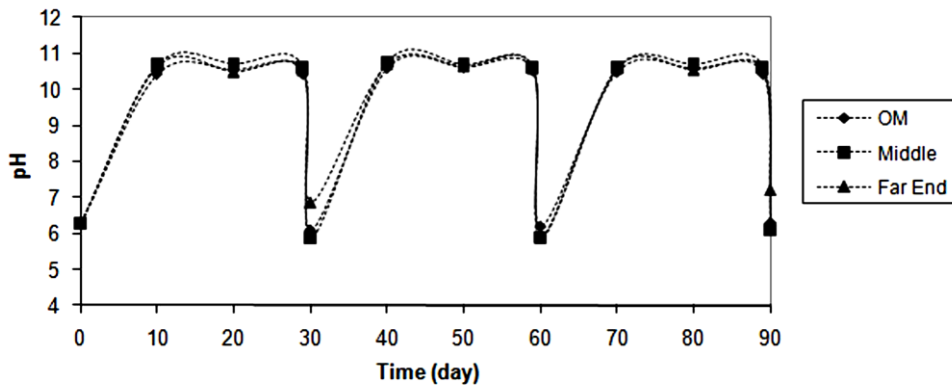
pH variation by time at different positions from the OM in Test A, Test B, and Test C is shown in Figure 4.2. As can be seen from this figure in Test A, the test with continuous purging of 5%CO₂/N₂, the pH stayed close to near-neutral at all positions with respect to the OM¹ (Figure 4.2a). In Test B, the test with cyclic purging of 5%CO₂/N₂, and in Test C, the test with limited purging of 5%CO₂/N₂, the pH increased to high values above 10 at times when there was no supply of 5%CO₂/N₂ (Figure 4.2b and Figure 4.2c). In Test B the pH dropped from high values above 10 to near-neutral pH values when the solution was purged with 5%CO₂/N₂ (Figure 4.2b). Generation of hydrogen ions, as a result of formation and dissociation of carbonic acid in the presence of 5%CO₂/N₂, and generation of hydroxide ions, due to water dissociation at times when there was no supply of 5%CO₂/N₂, are the main reasons for the significant pH variations inside the

¹There is a slight difference in the reported pH values for Test A to that reported in our previous study [10]. This could be due to the differences in the steel surface area used in parallel tests for monitoring the pH or changes in the gas flow. Experiencing this, in the current study the gas flow was fixed and samples with the exact same surface area as the loaded test were used in the parallel tests.

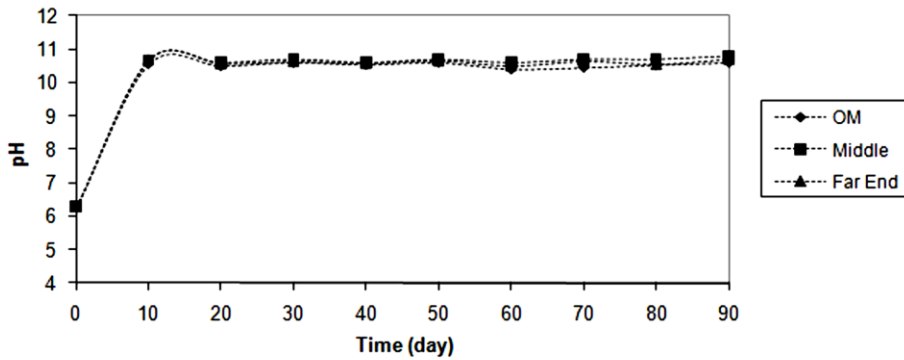
shielding. More details in regard to this in addition to the detailed reactions could be found in other papers [14, 16, and 17].



(a)



(b)



(c)

Figure 4.2: pH variation inside the shielding at different positions from the OM in: (a) Test A, (b) Test B, and (c) Test C.

The initial potential of the specimen at different positions from the OM in C2 solution prior to applying CP is shown in Figure 4.3. This potential is referred to as the initial open circuit potential (OCP). When a CP of $-1.2 \text{ V}_{\text{SCE}}$ was applied to the OM in the near-neutral pH solution, the CP decreased from $-1.2 \text{ V}_{\text{SCE}}$ at the OM to values close to OCP at the far end from the OM as shown in Figure 4.3. The CP distribution in the localized high-pH solution is different from that in the near-neutral pH solution (Figure 4.3). There was less CP drop in the localized high-pH environment compared to that in the near-neutral pH solution. This is related to the lower resistivity of the localized high-pH solution when compared to the near-neutral pH solution [17].

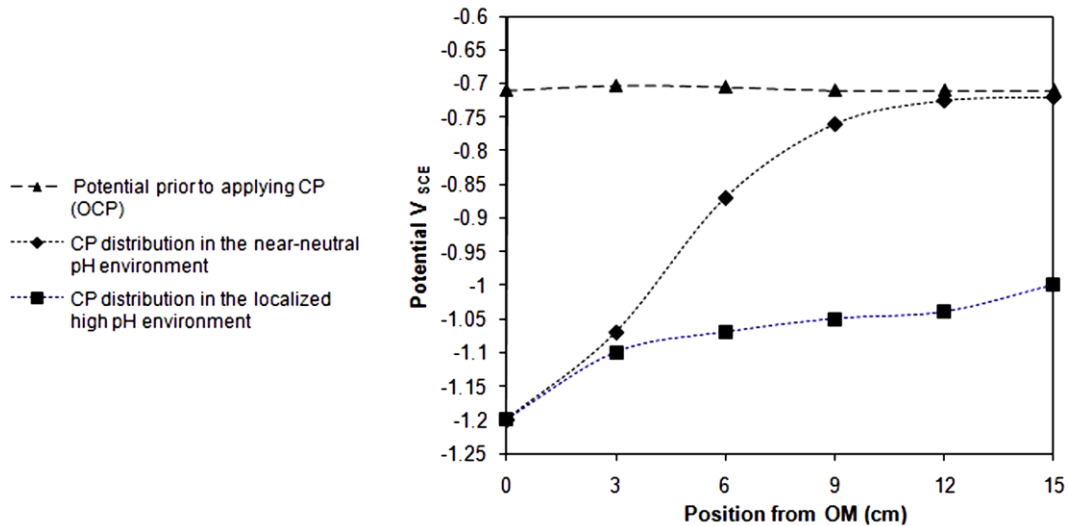


Figure 4.3: Potential distribution prior and after applying CP at different positions from the OM (cm).

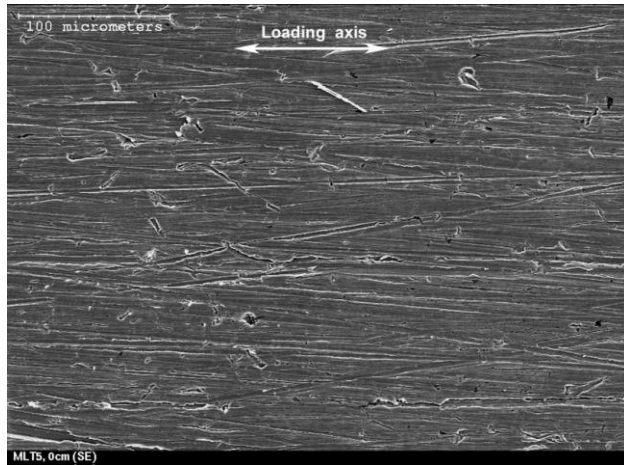
4.3.2. Stress corrosion cracking initiation tests

When stress corrosion cracking initiation tests were conducted under cyclic loading, depending on the pH of the localized environments, different SCC initiation mechanisms were involved on the steel surface up the gradient of CP.

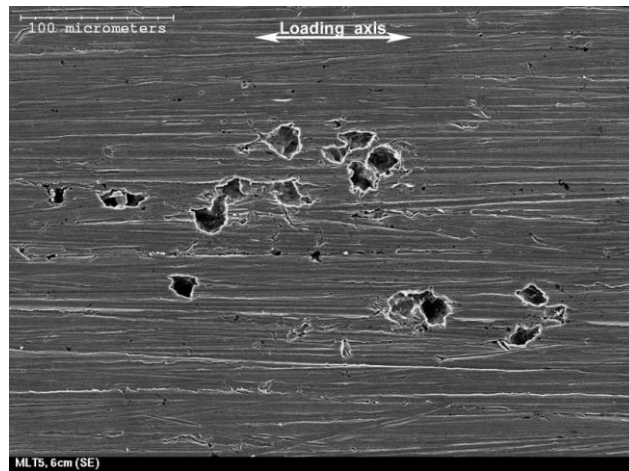
a) Test A (continuous supply of 5%CO₂/N₂)

This scenario was completely investigated in our previous study [14]. As shown in that study, after the 3 month test, no cracks were initiated. Pitting and general corrosion were the main features formed at different locations from the OM (Figure 4.4). Pitting corrosion in terms of size and percentage of surface coverage was most severe at locations with insufficient CP potential (the region between the OM and the far end from the OM); not regions completely free from CP as previously believed (at the far end from the OM which had OCP condition) [14]. However, at locations free of CP the deepest pits were formed, while general corrosion had also occurred [14]. Figure 4.5 shows a semi-quantitative distribution of the number of corrosion pits¹ at different locations from the OM.

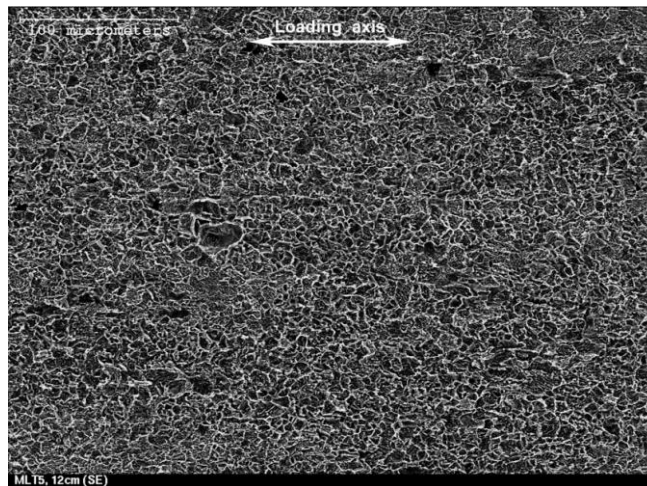
¹ For simplification only corrosion pits with a minimum diameter of 20µm have been considered. Our previous study showed that these pits were more prone to crack initiation [14].



(a)



(b)



(c)

Figure 4.4: Typical surface morphologies of the tensile specimen after Test A, at: (a) close to OM, (b) between OM and the far end, (c) remote from the OM.

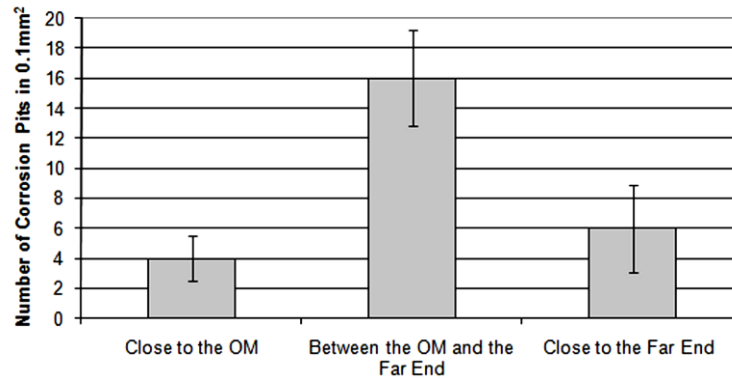


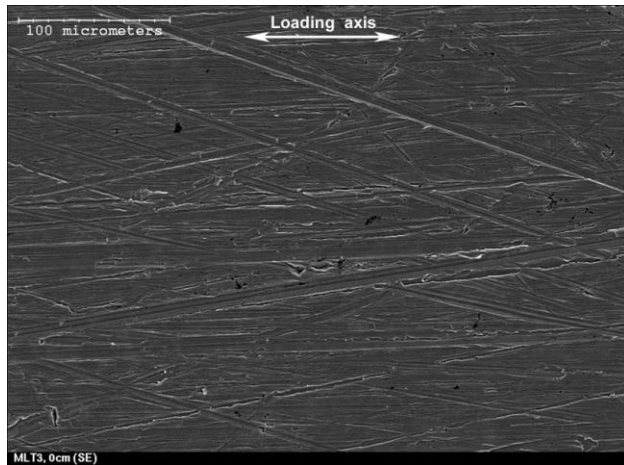
Figure 4.5: A semi-quantitative distribution of the number of corrosion pits at different positions from the OM after Test A.

b) Test B (cyclic supply of 5% CO₂/N₂)

This was a test condition in which the pH inside the simulated disbondment increased to high values above 10 at times when there was no CO₂ supply (Figure 4.2b). Less corrosion and pitting had occurred at all locations from the OM when compared to the test in near-neutral pH environment, Test A (see Figures 4.4 and 4.6). This is due to the lower corrosion rates (see Table 4.2), and better CP protection (see Figure 4.3) in the localized high-pH environment formed during the test. The localized high-pH environment contains lower concentrations of hydrogen ions, compared to the near-neutral pH environment, reducing the corrosion rate of X-65 pipeline steel [17].

While corrosion and pitting were minor, a few surface micro-cracks were observed on the steel surface especially in the mid region between the OM and the far end. The micro-cracks were shallow (less than a grain size in depth direction), and were mainly inclined 45° to the loading direction (Figure 4.7a). Some were also formed along the scratch lines produced on the pipe surface during sample preparation (Figure 4.7b). The formation of micro-cracks was less at locations close to OM where the surface was well protected by CP, or at the far end from the OM where slight corrosion had occurred. Figure 4.8 shows a semi-quantitative distribution of the number of the surface micro-cracks¹ and corrosion pits¹ which were formed at different locations from the OM during this test.

¹ For simplification only the micro-cracks with a minimum length of 10µm have been considered.



(a)



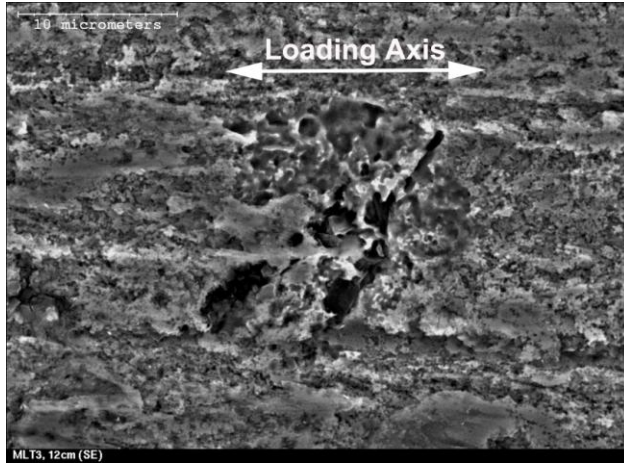
(b)



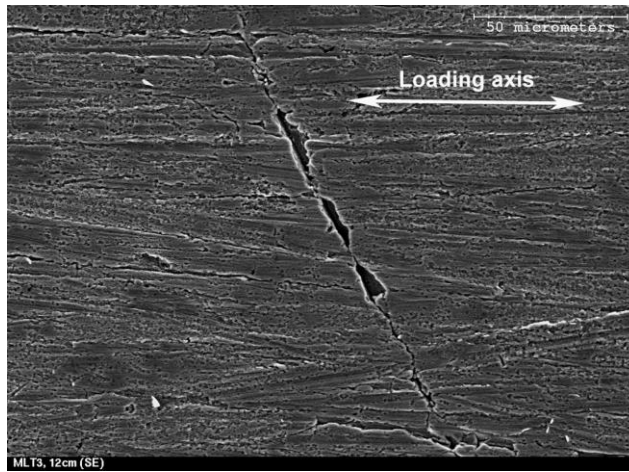
(c)

Figure 4.6: Typical surface morphologies of the tensile specimen after Test B at: (a) close to OM, (b) between the OM and the far end, (c) remote from the OM.

¹ For simplification only corrosion pits with a minimum diameter of 20 μ m have been considered.



(a)



(b)

Figure 4.7: (a) Typical image showing surface micro-cracks formed after Test B inclined 45° inclined to the loading direction (b) a surface micro-crack formed along a scratch line.

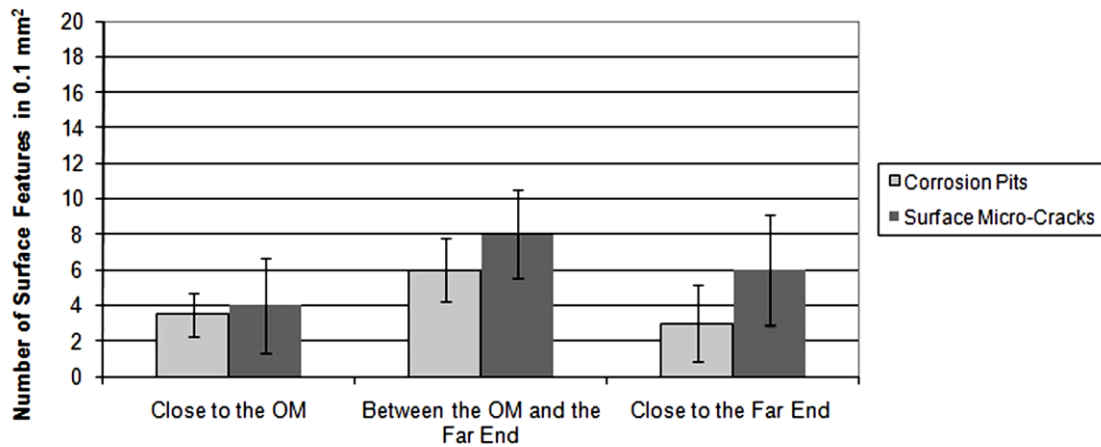


Figure 4.8: A semi-quantitative distribution of the number of corrosion pits and surface micro-cracks at different positions from the OM after Test B.

Table 4.2: Corrosion Rate of X-65 pipeline steel in simulated soil solution at different pH values [17].

pH	Corrosion Rate (mm/sec)
6.29	1.21E10-8
8.3	2.2E-09
10.3	1.47E-09

Similar features to the micro-cracks were observed by Wang et al. on the steel surface after cyclic loading tests were performed (in a simulated soil solution where the sample was protected by CP) [8]. Wang et al. indicated that the initiation of these features could be related to the formation of localized deformed surfaces. The localized deformed surface could be caused by the formation of persistent slip bands, or could exist at the bottom of the deep scratch-lines. Wang et al. indicated that preferential dissolution from the localized deformed surfaces could lead to the formation of the shallow surface micro-cracks [8].

c) Test C (limited supply of 5%CO₂/N₂)

This was a test condition in which a dominant high-pH environment was formed inside the simulated coating disbondment (see Figure 4.2c). Several micro-cracks in addition to a few pits were the main features observed on the steel surface (especially in the mid region between the OM and the far end from the OM) after this test (Figure 4.9). The micro-cracks were shallow (few micrometer in depth direction), and were mainly inclined 45° to the loading direction. Some were also formed along the scratch lines as in the previous scenario. A semi-quantitative distribution of the number of the surface micro-cracks¹ and corrosion pits² formed at different locations from the OM after this test has been shown in Figure 4.10. As can be seen from this figure, the region between the OM and the far end away from the OM has the highest number of the surface micro-cracks. Sufficient CP close to the OM, or slight corrosion at the far end from the OM had mitigated the formation of the micro-cracks.

¹ For simplification only the micro-cracks with a minimum length of 10µm have been considered.

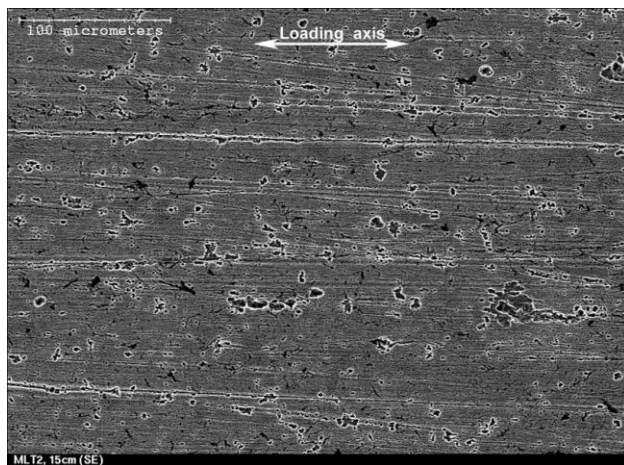
² For simplification only corrosion pits with a minimum diameter of 20µm have been considered.



(a)



(b)



(c)

Figure 4.9: Typical surface morphologies of the tensile specimen after Test C at: (a) close to OM, (b) between the OM and the far end, (c) remote from the OM.

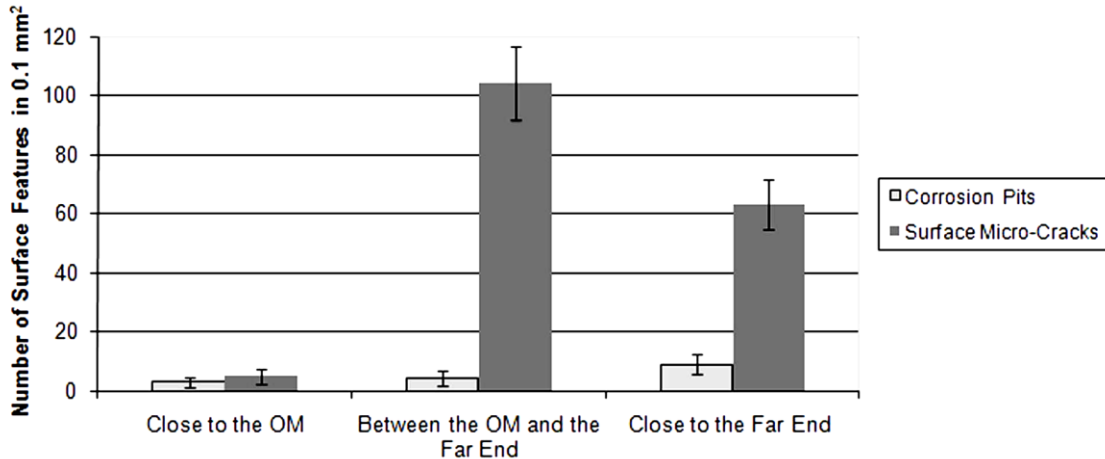


Figure 4.10: A semi-quantitative distribution of the number of corrosion pits and surface micro-cracks at different positions from the OM after Test C.

Since the loading condition was similar to the previous scenario, a different crack initiation mechanism would have been responsible for the formation of the high number of micro-cracks in this test when compared to the previous scenario (compare Figure 4.8 and Figure 4.10). Higher magnification SEM images from the micro-cracks revealed some interesting findings in this regard. Several sub-micrometer pits were observed in and around the micro-cracks as typically shown in Figure 4.11. The authors believe that this is the key for the crack initiation mechanism in this scenario. It is well known that the existence of surface discontinuities such as the sub-micrometer pits could enhance the crack initiation during fatigue cycles in the direction of maximum shear stress [18]. The maximum shear stress in unidirectional loading occurs at 45° direction relative to the loading axis. This could initiate branched micro-cracks from the localized deformed surfaces (by dislocation glide) in those grains having slip systems close to the maximum shear stress direction.

Further studies on the formation of the sub-micrometer pits showed that these features were formed in the early stages of corrosion in the near-neutral pH environment by preferential dissolution of sub-micrometer constituents in the steel microstructure. It was indicated that longer exposure to the near-neutral pH environment could polish away these features. Since Test C was exposed to the

near-neutral pH environment for only 2 days during the 3 month test, the sub-micrometer pits should have been formed during this period and been maintained in the localized high-pH environment where the corrosion rate is significantly lower (see Table 4.2) with a possibility of a surface passivation [17]. Longer exposure times of the sub-micrometer pits to the near-neutral pH environment in Test A and Test B, should have removed these features.



Figure 4.11: High magnification image showing the formation of several sub-micrometer pits in and around the surface micro-cracks after Test C.

4.3.3. Effect of R-ratio

a) Test D (continuous supply of 5% CO₂/N₂ and reduced R-ratio)

Reducing the cyclic stress R-ratio could increase the stress range and subsequently the stress intensity range at the pit boundaries as shown by the following formula (Equation 3-1) obtained from the Hoepfner^[19] Equation,

$$\Delta K_{sf} = 1.1\Delta S \sqrt{\pi \frac{a}{Q}} \quad (4-1)$$

where ΔK_{sf} is the difference between the maximum and minimum stress intensity factor corresponding to a surface flaw when the cyclic loading is applied, ΔS is the difference between the maximum and minimum applied stress in the cyclic loading, a is the size of flaw, and Q is a shape factor.

When Test D was performed, which had the same testing condition as Test A except that the R-ratio was reduced, a few micro-cracks were initiated at and branched out from the mouth of large pits. A typical image showing this is shown in Figure 4.12. As can be seen from this figure the branching has occurred in direction close to 45° of the loading direction, which is the direction of maximum shear stress under unidirectional loading. Cracks could be initiated at the mouth of the large pits with high stress concentration, and then branched in the direction of maximum shear stress. The reason that cracks could be initiated at the mouth of the large pits can be explained by Equation 4.1. As can be seen from this equation, for a specific amount of applied cyclic load (ΔS), the larger a pit (the parameter) the greater the stress intensity at its boundaries causing the crack initiation.

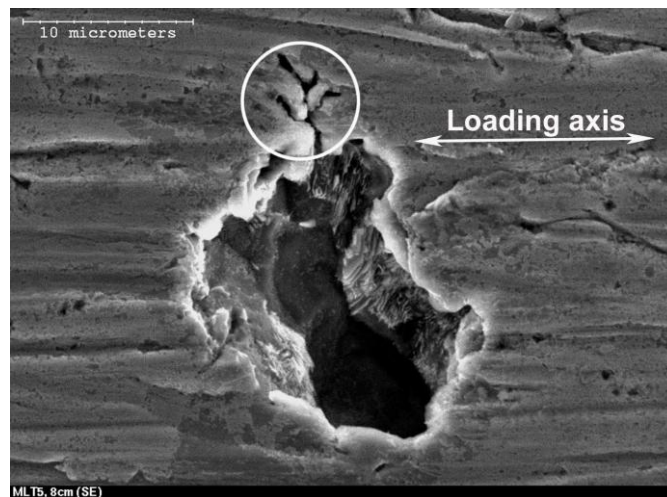


Figure 4.12: Typical image showing branched micro-cracks initiated at the mouth of a large pit after Test D. Circle shows branched micro-cracks which were initiated at and branched out from the mouth the pit during the test.

Although pits with sharper tips were observed in the cross section view when the R-ratio was reduced (see Figure 4.13), no cracks were initiated from bottom of the pits. The pitting depth was not considerably affected by reducing the R-ratio (Figure 4.14). Perhaps if longer testing time or more aggressive loading condition were given, pit to crack transition could have occurred from the bottom of the pits [14, 20].

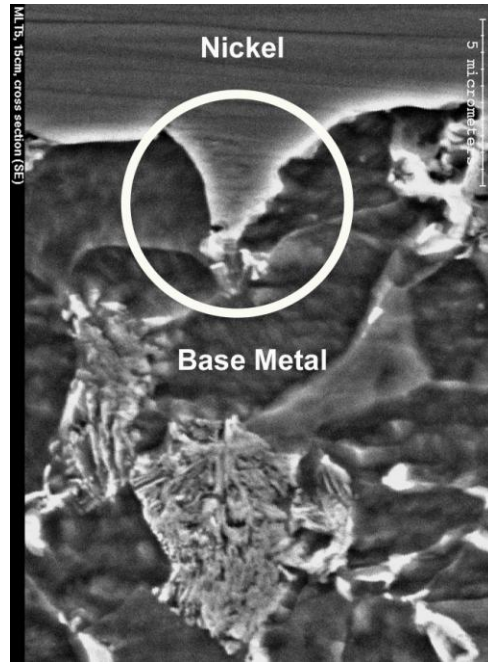


Figure 4.13: Typical image showing the cross section of the sample after Test D. Circle shows the cross section of a pit with a sharp tip formed during the test.

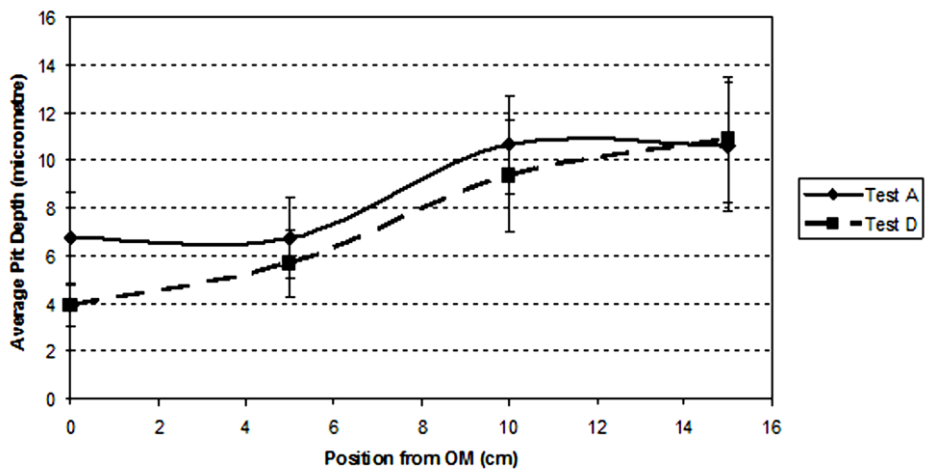


Figure 4.14: Average pit depth as a function of position from the OM in Test A and Test D.

b) Test E (limited supply of 5% CO₂/N₂ and reduced R-ratio)

When Test E was performed with the same environmental conditions as Test C, the same shallow micro-cracks seen in Test C were observed. Reducing the R-ratio did not cause any significant difference in the size and distribution of the surface micro-cracks. As mentioned in Section 4.3.2 (C) the micro-cracks were

initiated from several sub-micrometer pits which could act as stress concentration sites on the steel surface.

Perhaps, since the sub-micrometer pits were too small, reducing the stress ratio (R) was not sufficient to raise the stress intensity value high enough to cause significant change in initiation (see Equation 4-1). The effect of reduced R-ratio might be more significant at the later stages of crack growth.

4.3.4. The role of anodic dissolution, CP, and hydrogen in crack initiation mechanisms

It's believed that the crack initiation mechanisms are more a function of anodic dissolution, CP and hydrogen concentration. This study showed that localized corrosion, due to anodic dissolution, could cause different pitting mechanisms which could lead to crack initiation. While complete CP protection could prevent the SCC crack initiation, its incomplete protection could enhance the crack initiation mechanisms by:

- 1- Partially protecting the regions around the localized corroded surfaces where cracks could be initiated.
- 2- Generating hydrogen at the partially protected surfaces [21]. The generated hydrogen could potentially facilitate the crack initiation mechanisms, while having some effect on the anodic dissolution rate [5, 22, and 23]. Understanding the exact role of hydrogen on crack initiation requires further investigation, as being different from its role on crack growth [24, 25].

4.4. Conclusions

1. The current study showed that near-neutral pH SCC initiation is a complex process that is a function of environment, stress, and the level of CP under the disbonded coating.

2. Depending on CO₂ concentration and the level of CP, different localized environments were formed under the disbonded coating of pipeline steel. A near-neutral pH environment was formed when there was continuous supply of CO₂, while the high-pH environments were formed when there was limited supply of CO₂.
3. Depending on the pH of the localized environments under the disbonded coating, different SCC initiation mechanisms were involved. Crack initiation from the mouth of large pits, crack initiation due to formation of persistent slip bands, crack initiation at the bottom of deep scratch lines, and crack initiation as a result of linkage of several sub-micrometer pits were some of the mechanisms identified in this study.
4. Reducing the R-ratio (increasing the stress change) from R=0.8 to R=0.4 initiated branched micro-cracks from the mouth of large pits in the near-neutral pH environment. Reducing the R-ratio did not significantly affect the initiation of surface micro-cracks formed in the localized high-pH dominant environment.

4.5. References

- [1] B.S. Delanty, J. O'Beirne, Major Field Study Compares Pipeline SCC with Coatings, Oil & Gas Journal, 15 (1992) 39-44.
- [2] National Energy Board (NEB), Report of the Inquiry - Stress Corrosion Cracking on Canadian Oil and Gas Pipelines, 1996.
- [3] R.N. Parkins, W.K. Blanchard, B.S. Delanty, Transgranular Stress Corrosion Cracking of High-Pressure Pipelines in Contact with Solutions of Near Neutral PH, Corrosion, 50 (1994) 394-408.
- [4] Y.Z. Wang, R.W. Revie, M.R. Shehata, R.N. Parkins, K. Krist, Initiation of Environment Induced Cracking in Pipeline Steel: Microstructural Correlations, in: Proc. IPC/98, Calgary, Canada, 1998.
- [5] B. Gu, W.Z. Yu, J.L. Luo, X. Mao, Transgranular Stress Corrosion Cracking of X-80 and X-52 Pipeline Steels in Dilute Aqueous Solution with Near-Neutral pH, Corrosion, 55-3 (1999) 312-318.
- [6] M. Elboudjaini, Y.Z. Wang, R.W. Revie, Initiation of Stress Corrosion Cracking on X-65 Line-pipe Steels in Near-Neutral pH Environment, Proc. IPC/2000, Calgary, Canada, 2000.

- [7] J.A. Beavers, C.L. Durr, B.S. Delanty, D.M. Owen, R.L. Sutherby, Near-Neutral pH SCC: Crack Propagation in Susceptible Soil Environments, in Proceeding of Corrosion 2001, Huston, Texas, USA, 2001.
- [8] S. Wang, W. Chen, F. King, Precyclic-loading-Induced Stress Corrosion Cracking of Pipeline Steels in a Near-Neutral-pH Soil Environment, *Corrosion*, 58 (2002) 526-534.
- [9] W. Chen, S.H. Wang, R. Chu, F. King, T.R. Jack, R.R. Fessler, Effect of Precyclic Loading on Stress-Corrosion-Cracking Initiation in an X-65 Pipeline Steel Exposed to Near-Neutral pH Soil Environment, *Metallurgical and Materials Transaction A*, 34A (2003) 2601-2608.
- [10] G. VanBoven, W. Chen, R. Rogge, The Role of Residual Stress in Neutral pH Stress Corrosion Cracking of Pipeline Steels, Part 1: Pitting and Cracking Occurrence, *Acta Materialia*, 55 (2007) 29-42.
- [11] A. Torres-Islas, J.G. Gonzales-Rodriquez, J. Uruchurtu, S. Serna, Stress Corrosion Cracking Study of Microalloyed Pipeline Steel in Dilute NaHCO₃ Solutions, *Corrosion Science*, 50 (2008) 2831-2839.
- [12] Z.Y. Liu, X.G. Li, C.W. Du, L. Lu, Y.R. Zhang, Y.F. Cheng, Effect of Inclusions on Initiation of Stress Corrosion Cracks in X70 Pipeline Steel in an Acidic Soil Environment, *Corrosion Science*, 51 (2009) 895-900.
- [13] P. Liang, X. Li, C. Du, X. Chen, Stress Corrosion Cracking of X80 Pipeline Steel in Simulated Alkaline Soil Solution, *Materials & Design*, 30 (2009) 1712-1717.
- [14] A. Eslami, B. Fang, R. Kania, B. Worthingham, J. Been, R. Eadie, W. Chen, Stress Corrosion Cracking Initiation under the Disbonded Coating of Pipeline Steel in Near-neutral pH Environment, *Corrosion Science*, 52 (2010) 3750- 3756.
- [15] R. Sutherby, T. Jack, G. Van Boven, M. Wilmott, CEPA Study on Characterization of Pipeline Pressure Fluctuations in Terms Relevant to Stress Corrosion Cracking, in: *Proc. IPC/2000*, Calgary, Canada, 2000.
- [16] B. Fang, A. Eslami, R. Kania, R. Worthingham, J. Been, W. Chen, Stress Corrosion Crack Initiation in X-65 Pipeline Steel under Disbonded Coating with Cathodic Protection, in: *Proc. IPC/2008*, Calgary, Canada, 2008.
- [17] A. Eslami, W.Chen, R. Eadie, Corrosion of X-65 Pipeline Steel under a Disbonded Coating in Simulated Near-neutral pH Soil Environment, Submitted to *Corrosion*, 2012.
- [18] D. William, Ir. Callister, *Materials Science and Engineering an Introduction*, Seventh Edition, 2007.
- [19] D. W. Hoepfner, Model for Prediction of Fatigue Lives Based Upon a Pitting Corrosion Fatigue Process, *Fatigue Mechanisms*, ASTM STP 675 (1979) 841-870.
- [20] B. Fang, R. Eadie, W. Chen, M. Elboujdaini, Pit to Crack Transition in X-52 Pipeline Steel in Near-neutral pH Environment; Part 1- Formation of Blunt Cracks from Pits under Cyclic Loading, *Corrosion Engineering Science and Technology*, 45 (2010) 302-312.
- [21] D.X. He, W. Chen, J.L. Luo, Effect of Cathodic Potential on Hydrogen Content in a Pipeline Steel Exposed to NS4 Near-neutral pH Solution, *Corrosion*, 60 (2004) 778-786.
- [22] B.T. Lu, J.L. Luo, P.R. Norton, Environmentally Assisted Cracking Mechanism of Pipeline Steel in Near-neutral pH Groundwater, *Corrosion Science*, 52 (2010) 1787-1795.

[23] M.C. Li, Y.F. Cheng, Mechanistic Investigation of Hydrogen-Enhanced Anodic Dissolution of X-70 Pipe Steel and its Implication on Near-neutral pH SCC of Pipelines, *Electrochimica Acta*, 52 (2007) 8111-8117.

[24] W. Chen, R. Kania, R. Worthingham and G.V. Boven, Transgranular Crack Growth in the Pipeline Steels Exposed to Near-neutral pH Soil Aqueous Solutions: The Role of Hydrogen, *Acta Materialia*, 57 (2009) 6200–6214.

[25] Y.W. Kan, W. Chen, R. Kania, G. VanBoven, R. Worthingham, Simulation of Crack Growth During Hydrostatic Testing of Pipeline Steel in Near-neutral pH Environment, *Corrosion Science*, 53 (2011) 968-975.

**Chapter 5: Near-neutral pH Stress Corrosion Crack Initiation
under the Simulated Coating Disbondment: Effect of Oxygen¹**

¹ A version of this chapter has been submitted to the journal of **Corrosion Science** for publication.

5.1. Introduction

Near-neutral pH stress corrosion cracking (SCC) was first detected in Canada on a TransCanada pipeline in the mid-1980s [1]. Since then it has been responsible for several pipeline ruptures and leaks in the United States, Canada, and Russia [2]. This form of cracking usually occurs close to the seam weld of tape coated pipes at locations where the coating is disbonded and damaged, and where a wrinkle filled with ground water could form. Due to the high resistivity of the ground water, cathodic protection (CP) could not completely penetrate inside the coating wrinkle and a suitable environment for corrosion and/or crack initiation could be formed.

Although a much better understanding of corrosion and near-neutral pH SCC initiation under disbonded coatings has been obtained [3-5], uncertainties about the role of environmental factors on this form of cracking still remain. One of these environmental factors is oxygen. Some studies have been carried out in this regard. A comprehensive field investigation by Delanty et al. in 1985 showed that depending on seasonal fluctuations the level of oxygen in the underground environment surrounding buried pipes could vary between 1-5 % [6]. While Wang et al. [7] determined that larger pits could be formed on pipeline surface in the presence of 1 % oxygen as compared to 5% oxygen, Liu et al. using Slow Strain Rate (SSR) tests showed that SCC susceptibility is inversely proportional to the dissolved oxygen level [8]. Ahmad et al. determined that the presence of oxygen may facilitate the anodic dissolution that has been observed on the crack faces of field failures [9]. Despite these studies, the exact role of oxygen on near-neutral pH SCC initiation under disbonded coatings has not been thoroughly understood. This might be due to the aggressive loading conditions used in the studies (such as those used in SSR tests), or from ignoring the effect of coating disbondment and CP.

This study investigates the effect of oxygen on neutral pH SCC initiation under a disbonded coating of pipeline steel, by considering the synergistic effects of

cyclic loading, coating disbondment, and CP. It is anticipated that the results of this study will further improve the current understanding about the role of oxygen on near-neutral pH SCC initiation.

5.2. Experimental

5.2.1. Specimen, solution and corrosion cell

The specimens, solution, and corrosion cell used for this study are same to that explained in section 3.2.1.

5.2.2. Stress corrosion cracking initiation tests

To investigate the effect of oxygen on near-neutral pH SCC initiation, two long term 90 day tests were performed: a Reference Test (Test A) with no oxygen in the testing environment, and a test with 1% oxygen (Test B). During each test a CP potential of $-1.2 V_{SCE}$ was applied to the specimen surface located just above the OM of the simulated disbondment¹. The specimen was subjected to low frequency cyclic loading during each test. The detailed condition of each test is presented in Table 5.1.

Table 5.1: SCC initiation tests performed in this study.

Test	Environmental Condition	Loading Condition	Duration
Test A (Reference Test)	Continuously purging C2 solution with 5%CO ₂ /N ₂	100%SMYS R=0.4 F=0.0001 Hz	90 days
Test B (Test with the effect of 1% oxygen)	Continuously purging C2 solution (5%CO ₂ +1%O ₂)/N ₂	100%SMYS R=0.4 F=0.0001 Hz	90 days

* Specified Minimum Yield Strength (for the X-65 pipeline steel specimen used in this study the 100% SMYS was 448 MPa. The X-65 pipeline steel had a yield strength and tensile strength of 522.8 and 607.8 MPa, respectively).

¹ The detailed procedure of applying the CP can be found in section 2.2.1.

5.2.3. Electrochemical test

The potentiodynamic polarization method was used to determine the corrosion rate of X-65 pipeline steel in the two environments. A Gamry PC4/300 potentiostat was used for this purpose. A piece of X-65 pipeline steel with a surface area of 1 cm^2 was used as the working electrode. The working electrode was ground to 600 grit and cleaned in acetone prior to the corrosion measurements. A standard saturated calomel electrode was used for the reference electrode, while two platinum meshes with dimension of $5 \times 5 \text{ cm}$ were used as counter electrodes for the electrochemical testing. The scanning rate for the potentiodynamic polarization test was set at 0.5 mV/s . A digital camera image of the test setup used for the electrochemical polarization tests is shown in Figure 5.1.



Figure 5.1: Digital camera image of the test setup used of electrochemical polarization tests.

5.2.4. Characterization

The characterization process was similar to that explained in section 3.2.3.

5.3. Results and Discussion

5.3.1. The Reference Test (Test A)

As mentioned earlier, the Reference Test was a 90 day test with no oxygen in the testing environment. It is presented in the current study for comparison purposes¹.

5.3.1.1. CP and pH distribution

When a CP potential of $-1.2 V_{SCE}$ was applied to the OM of the simulated disbondment, in the near-neutral pH environment the CP dropped from full protection at close to the OM to values close to Open Circuit Potential (OCP) at around 12 cm from the OM (Figure 5.2). The drop in CP potential is due to both solution resistance and polarization resistance. The following reactions could occur inside the solution with the presence of CP:



¹ Parts of the results and discussions for Test A have been presented in the previous chapter.

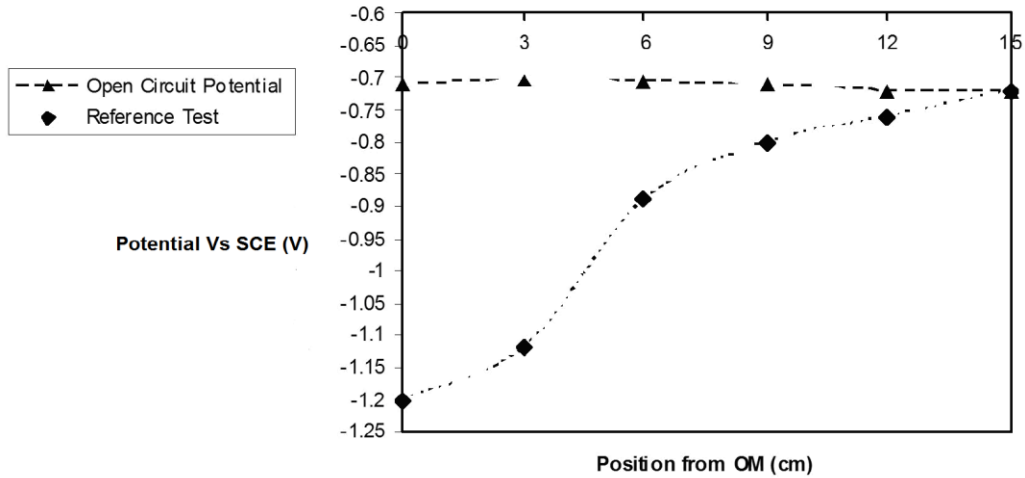


Figure 5.2: Open Circuit Potential (OCP) and CP potential distribution at different positions from the OM and at the beginning of Test A (the Reference Test).

Although CP could raise the pH of trapped soil solutions inside disbondments [4, 10-13]; the pH stayed near-neutral for the entire test (Figure 5.3). This was due to the continuous supply of the 5%CO₂/N₂ during the test, which prevented the rise in pH [4].

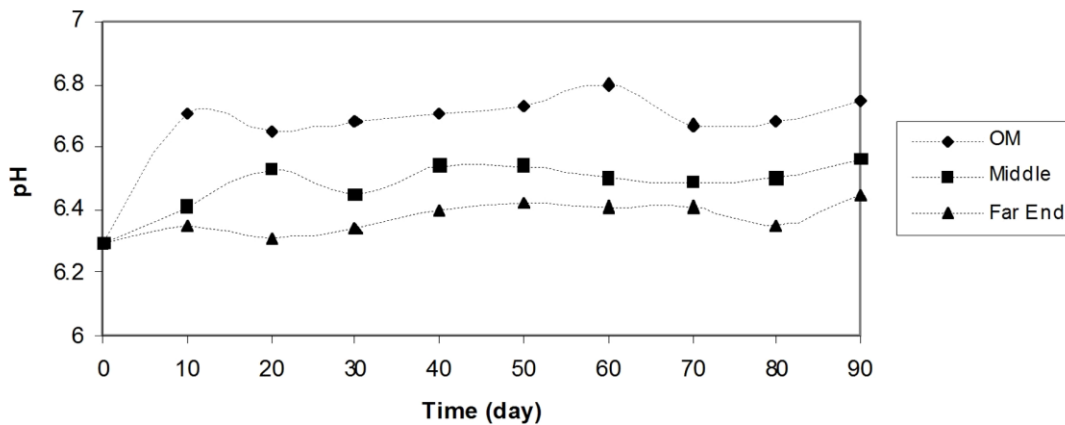


Figure 5.3: pH variation at different positions from the OM in Test A (the Reference Test).

5.3.1.2. General observation

Figure 5.4 shows a digital camera image of the specimen inside the corrosion cell at the end of Test A (the Reference Test). As can be seen from this figure, considerable amounts of surface deposits have been formed close to the OM.

XRD analysis showed that the surface deposits mainly consisted of CaCO_3 with small quantities of FeOOH .

Under cathodic conditions, Ca^{2+} from the solution could electro-migrate to the cathodic protected surface, increasing the concentration of Ca^{2+} and making the deposition of CaCO_3 possible. It was reported by He et al. that CaCO_3 can be deposited when a cathodic potential of $-950 \text{ mV}_{\text{SCE}}$ is applied [14]. Since the region close to the OM had lower CP potential, it is reasonable to see more CaCO_3 deposits at this location.

FeOOH could be formed as a result of the following reactions:



Since the solution in the Reference Test was free of oxygen, the formation of FeOOH should have occurred when the sample was removed from the corrosion cell, and was exposed to the air environment.

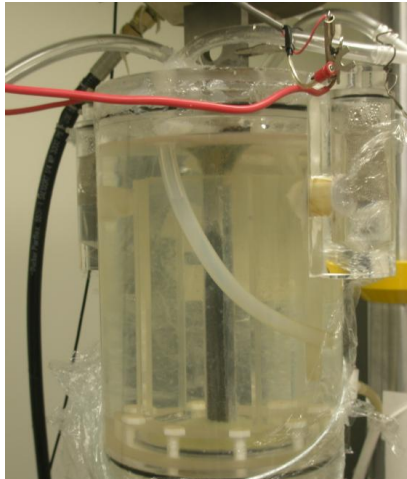


Figure 5.4: Digital camera image of the specimen inside the corrosion cell at the end of Test A (the Reference Test).

5.3.1.3. Stress corrosion cracking initiation

When the surface of the specimen was characterized by Scanning Electron Microscope (SEM), depending on the position from the OM, corrosion features had formed on the steel surface. Pitting corrosion in terms of size and percentage of surface coverage was most severe at locations with insufficient CP (between the OM and the far end), not locations completely free from CP (at the far end from the OM) as previously believed. A few micro-cracks were initiated from the mouth of the large pits located between the OM and the far end, caused by the high stress concentration at these locations (see Chapter 4, Test D) [4].

When the cross section of the specimen was characterized to see whether any cracks had been initiated from the bottom of the pits, no cracks were observed. Only deep pits with sharp tips in the cross sectional view were observed. The pits with the sharp tips were not necessarily the deepest ones. General corrosion had removed the sharp tips of some deeper pits, making them less susceptible to crack initiation [5].

5.3.2. Effect of oxygen on near-neutral pH SCC Initiation (Test B)

Based on a previous study by Wang [7], and since larger pits are more susceptible to crack initiation [15], the effect of oxygen on near-neutral pH SCC initiation under the disbonded coating was investigated by adding 1% oxygen to the testing environment.

5.3.2.1. CP and pH distribution

CP potential distribution at different positions from the OM is shown in Figure 5.5. As can be seen from this figure, the presence of 1% oxygen in the testing environment has caused a more rapid CP drop compared to the Reference Test. The larger CP drop is due to the increased oxidizing condition of the solution caused by the presence of oxygen. In the presence of oxygen, in addition to the

reactions shown in Equations 5-1 - 5-4, the following reactions could occur, causing an increased oxidizing condition:

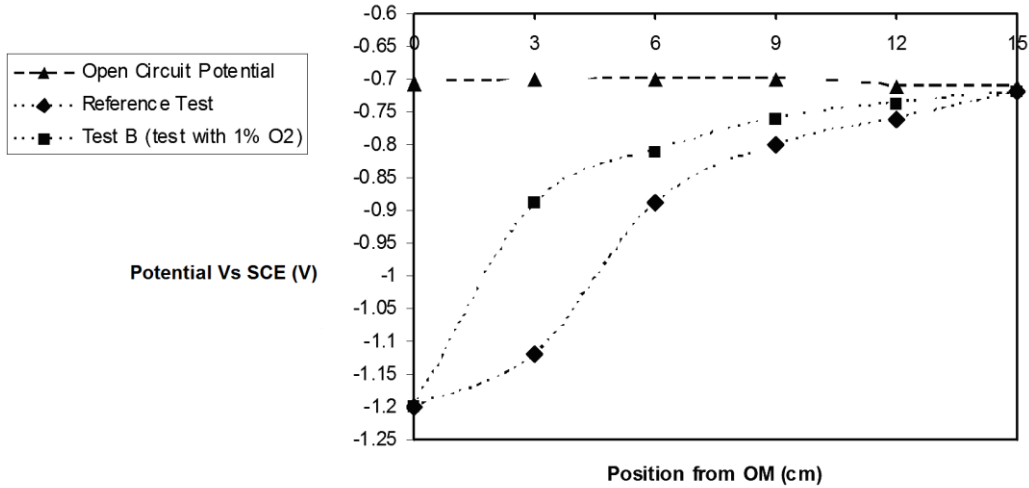
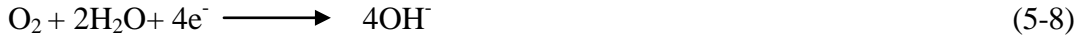
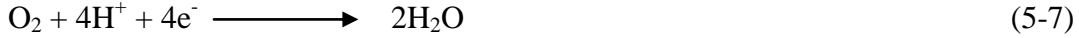


Figure 5.5: Open Circuit Potential and CP potential distribution at different positions from the OM, at the beginning of Reference Test and Test B (the test with 1% oxygen).

The pH inside the simulated disbondment did not change significantly despite the presence of CP and oxygen. This could be due to the low level of oxygen (only 1%), in addition to the reaction of the generated hydroxide with the free CO₂ in the solution [16].

5.3.2.2. General observations

Figure 5.6 shows a digital camera image of the specimen inside the corrosion cell after Test B. As can be seen from this figure the solution inside the corrosion cell has a yellowish color compared to the relatively clear solution in the Reference Test (see Figure 5.4). The yellowish color of the solution in Test B should be due to formation of considerable amount of FeOOH during the test¹ (Equation 5-5 –

¹ FeOOH has a yellowish color [17].

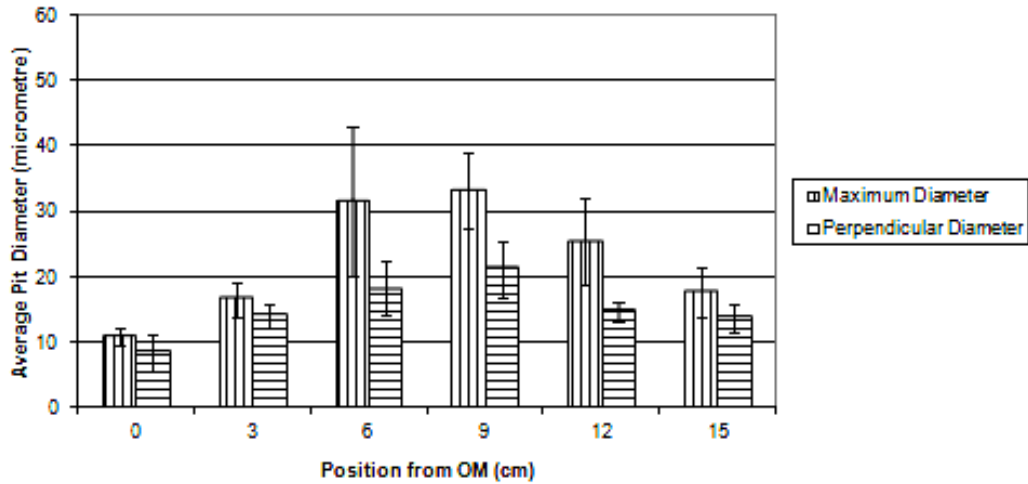
5-6), as a result of oxygen in the testing environment. Similar to the Reference Test, surface deposits mainly consisting of CaCO_3 were formed close to the OM.



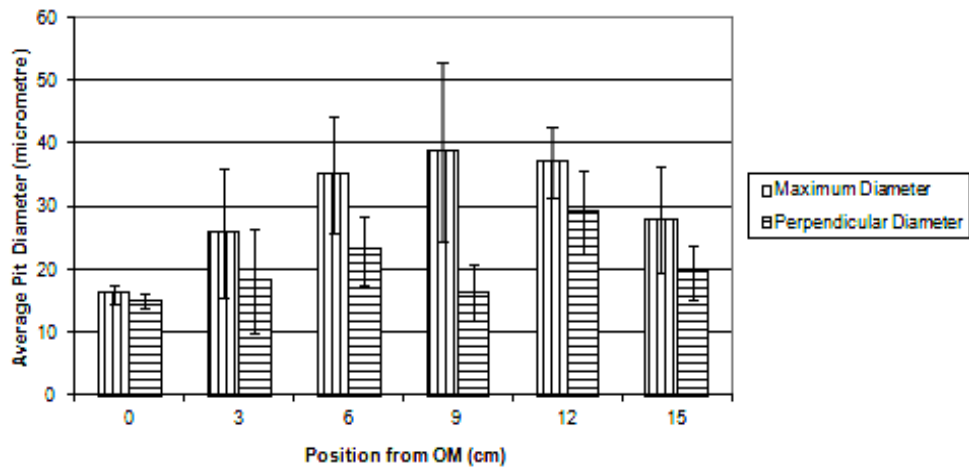
Figure 5.6: Digital camera image of the specimen inside the corrosion cell at the end of Test B (the test with 1% oxygen).

5.3.2.3. Stress corrosion cracking initiation

When the surface of the specimen was characterized, as in the Reference Test, corrosion features with different distribution were observed on the steel surface. Pit distribution at different positions from the OM as compared to the Reference Test, is shown in Figure 5.7.



(a)



(b)

Figure 5.7: (a) Average pit diameter at different positions from the OM in Test A (the Reference Test), (b) Average pit diameter at different positions from the OM in Test B (the test with the effect of 1% oxygen).

As can be seen from this figure, the presence of oxygen has increased the average pit size especially at locations away from the OM. The reason for the increase in pitting size is complicated, and could be caused by:

1. Higher corrosion rate of the pipeline steel due to the presence of oxygen. The corrosion rate of X-65 pipeline steel obtained from the Tafel slopes (Figure 5.8) in the test with 1% oxygen and without any oxygen was 0.47

mm/year and 0.41 mm/year, respectively¹. Therefore, at locations where localized corrosion could occur, the higher corrosion rate of the pipeline steel could generate larger pits.

2. Changes in CP distribution by the presence of oxygen at each particular location inside the disbondment (see Figure 5.5). The change in CP potential protection range, could affect the corrosion rate and therefore the pitting size.

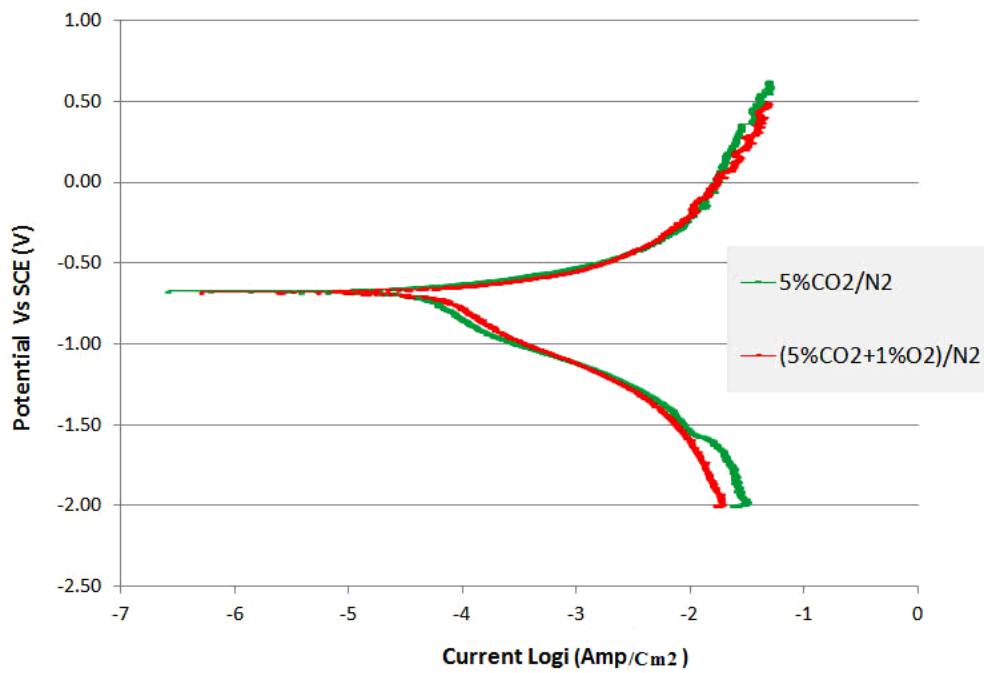
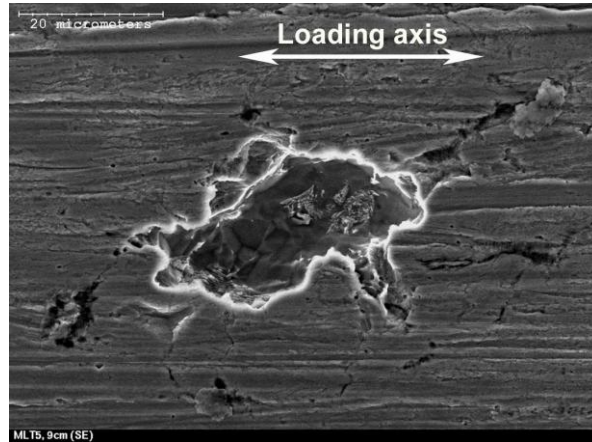


Figure 5.8: Potentiodynamic polarization curves for X-65 steel in test environments with and without any oxygen (C2 solution purged with (5%CO₂+1%O₂)/N₂ and C2 solution purged with 5%CO₂/N₂).

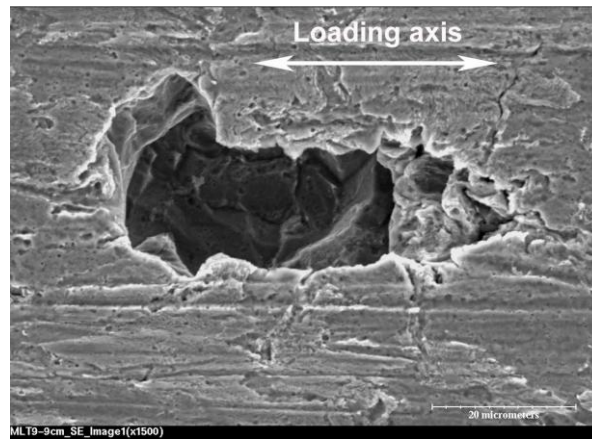
The pits in Test B were elongated particularly at 9 cm from the OM when compared to the Reference Test (see Figure 5.7). This could have been caused by the enhanced anodic dissolution in the presence of oxygen, and at regions of stress concentration [19, 20]. Typical images of the specimen surface showing a pit

¹ This is equivalent to corrosion of pipeline steel in mildly corrosive soil environments, i.e. between 0.2- 0.5 mm/year [18].

formed at 9 cm from the OM in Reference Test and in Test B are shown in Figure 5.9.



(a)



(b)

Figure 5.9: Typical image of the specimen surface showing a pit at 9 cm from the OM in: (a) Test A (the Reference Test), (b) Test B (the test with the effect of 1% oxygen).

As in the Reference Test, a few micro-cracks were initiated from the mouth of the large pits located between the OM and deep inside the disbondment. Micro-cracks were not initiated from the mouth of pits located close to the OM, where the pit size should not have been large enough to initiate surface cracks (see Figure 5.7b), or from those pits located at the far end from the OM where general corrosion had polished the surface. It's worth mentioning that some of the initiated micro-cracks were considerably longer than those in the Reference Test (see Figure 5.10).

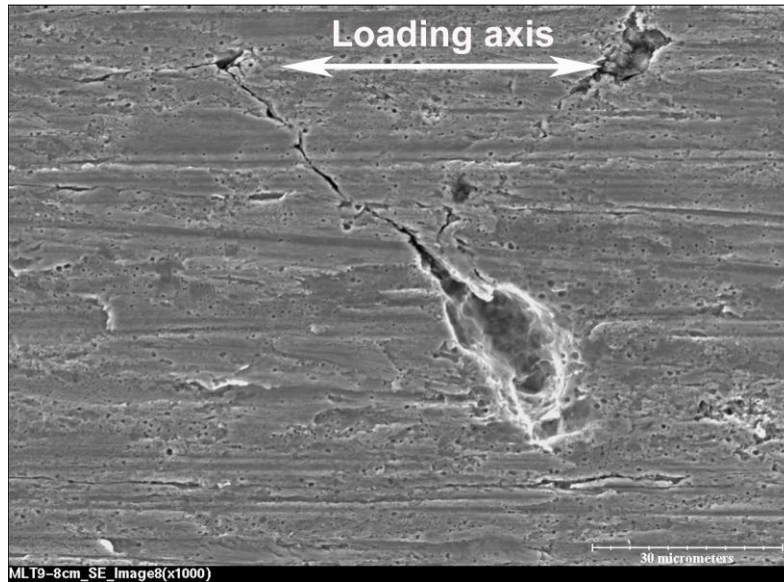
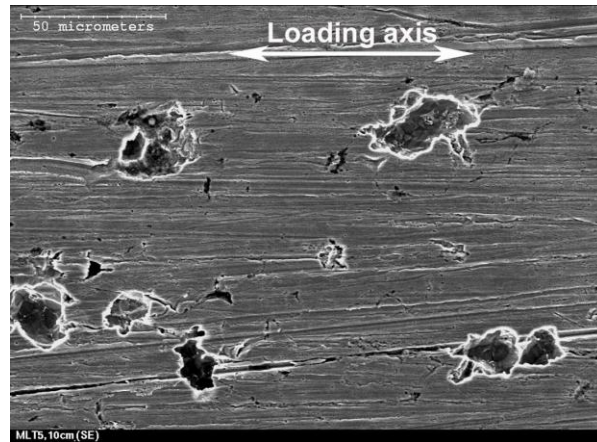
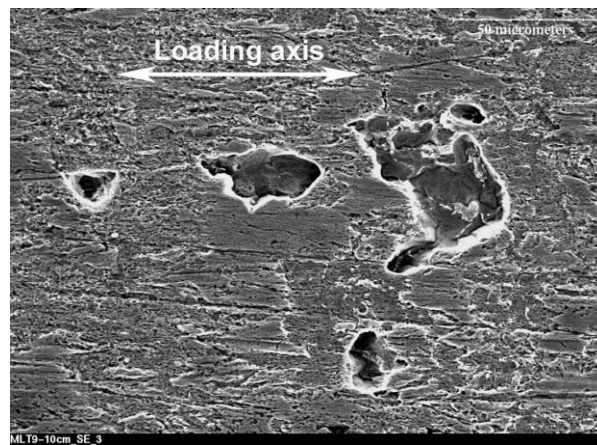


Figure 5.10: A relatively long micro-crack initiated from the mouth of a pit at 8 cm from the OM in Test B (the test with the effect of 1% oxygen).

The general corroded region had extended further towards the OM in Test B compared to the Reference Test. The extended general corrosion region mitigated the surface micro-crack initiation. For instance, while micro-cracks were initiated at 10 cm from the OM in the Reference Test, they were not observed in Test B (the test with the effect of 1% oxygen) due to general corrosion occurring at this location. General corrosion should have polished away/prevented the formation of surface micro-cracks, which are only few micro-meters deep (see Figure 5.11) [4]. This is an important finding showing how the change in the extent of general corrosion region could be beneficial in mitigating the surface crack initiation under disbonded coatings.



(a)



(b)

Figure 5.11: Typical pit formed at 10 cm from the OM in: (a) Test A (the Reference Test), (b) Test B (the test with the effect of 1% oxygen).

When the cross section of the specimen was characterized, the pitting depth had increased considerably at locations away from the OM in Test B as compared to the Reference Test (see Figure 5.12). As shown in Chapter 3 the increase in pitting depth could be a sign of an increase in crack initiation susceptibility [5]. The increased oxidizing condition of the solution and lower CP potential protection range from the presence of oxygen should have caused the increase in pitting depth. The insignificant change in pitting depth at the OM should have been due to the effective CP protection at this location (see Figure 5.5).

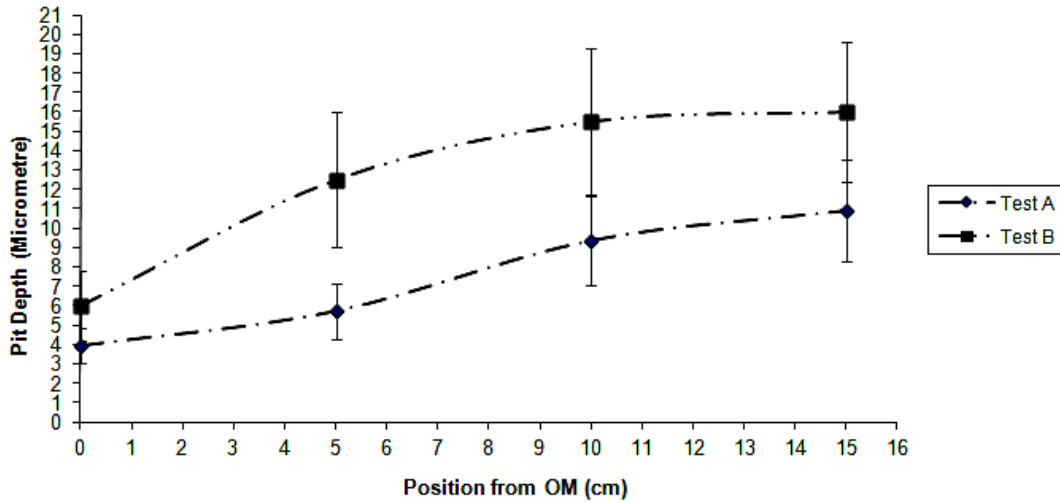


Figure 5.12: Average pit depth as a function of position from the OM in Test A (the Reference Test), compared to Test B (the test with the effect of 1% oxygen).

Although the pitting depth had increased¹, no cracks were initiated in the cross sectional view. If longer testing time and/or more aggressive loading condition were used cracks may have been initiated from the bottom of pits [5].

5.4. Summary and Conclusion

Oxygen affected near-neutral pH SCC initiation under the simulated disbanded coating, both on the surface and cross section of the specimen. While the susceptibility to crack initiation increased in the cross section of the specimen due to the formation of deeper corrosion pits at locations remote from the OM, the situation was complicated on the surface, and is summarized in Figure 5.13.

¹ Increasing in pitting depth could raise the stress concentration at the bottom of a pit enhancing the possibility of crack initiation [21].

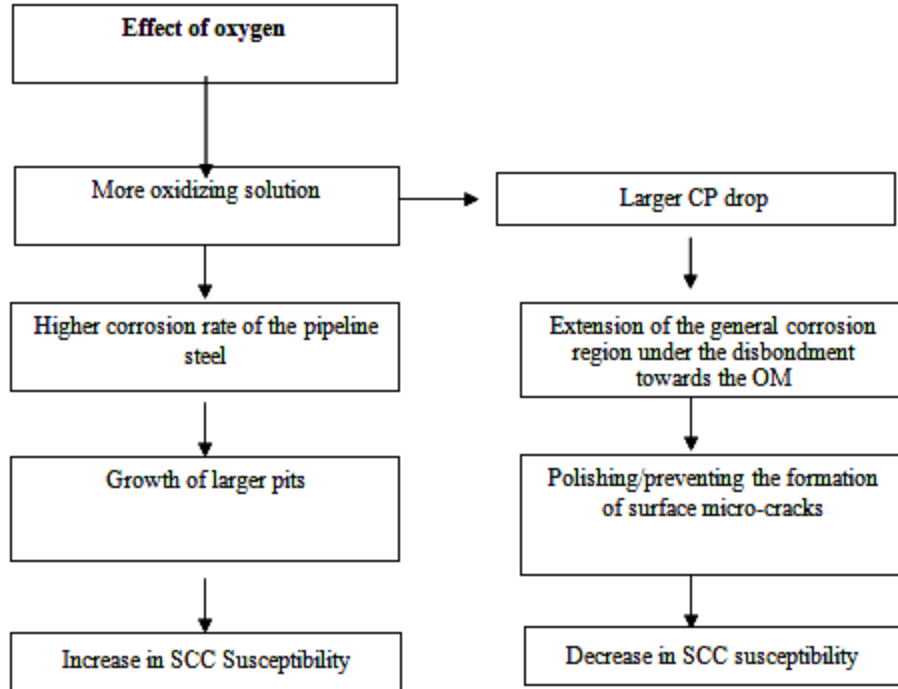


Figure 5.13: Effect of oxygen on crack initiation on pipeline steel surface under the coating disbondment.

As can be seen from this figure, the more oxidizing condition of the solution has caused different effects on pipe surface. On one side, the more oxidizing condition of the soil solution has caused formation of larger corrosion pits which could be formed at locations away from the OM of the simulated coating disbondment. This is a sign of increase in crack initiation susceptibility. On the other side, the more oxidizing condition of the solution has caused larger CP drop inside the simulated coating disbondment. This has extended the general corrosion region from deep inside the disbondment more towards the OM. As a consequence of this, surface micro-cracks were either prevented or polished away from the surface of pipeline steel, in the extended general corrosion region. This means decrease in crack initiation susceptibility.

5.5. References

- [1] NEB Report, Public Inquiry Concerning Stress Corrosion Cracking on Canadian Oil and Gas Pipelines, 1996.
- [2] B.N. Leis and R.J. Eiber, Stress-Corrosion Cracking on Gas-Transmission Pipelines: History, Causes, and Mitigation, Proceedings, First International Business Conference on Onshore Pipelines, Berlin, December 1997.
- [3] A. Eslami, B. Worthingham, R. Kania, R. Eadie, W. Chen, Corrosion of X-65 Pipeline Steel under A Simulated Disbonded Coating, Submitted to Corrosion, 2012.
- [4] A. Eslami, R. Kania, B. Worthingham, G.V. Boven, R. Eadie, W. Chen, Effect of CO₂ and R-Ratio on Near-neutral pH Stress Corrosion Cracking Initiation Under a Disbonded Coating of Pipeline Steel, Corrosion Science, 53 (2011) 2318-2327.
- [5] A. Eslami, B. Fang, R. Kania, B. Worthingham, J. Been, R. Eadie, W. Chen, Stress Corrosion Cracking Initiation under the Disbonded Coating of Pipeline Steel in Near-neutral pH Environment, Corrosion Science, 52 (2010) 3750-3756.
- [6] B.S. Delanty, J. O'Beirne, Major Field Study Compares Pipeline SCC with Coatings, Oil & Gas Journal, 15 (1992) 39-44.
- [7] H. Wang, Effect of Environment on Near-neutral pH Stress Corrosion Cracking of X-52 Pipeline Steel, M.Sc Thesis, University of Alberta, 2009.
- [8] Z.Y. Liu, X.G. Li., C.W. Du, L.X. Wang, and Y.Z. Huang, Effect of Dissolved Oxygen on Stress Corrosion Cracking of X70 Pipeline Steel in Near-Neutral pH Solution, Corrosion, 66-1 (2010) 15006/1-15006/6.
- [9] T.M. Ahmed, S.B. Lambert, R. Sutherby, A. Plumtree, Cyclic Crack Growth Rates of X-60 Pipeline Steel in a Near-Neutral Dilute Solution, Corrosion, 53-7 (1997) 581-590.
- [10] X. Chen, C. Du, X. Li, Effect of Cathodic Potential on the Local Electrochemical Environment under a Disbonded Coating, Journal of Applied Electrochemistry, 39 (2009) 697-704.
- [11] M. Yan, J. Wang, E. Han, W. Ke, Local Environment under Disbonded Coating on Steel Pipelines in Soil Solution, Corrosion Science, 50 (2008) 1331-1339.
- [12] M.C. Yan, J.Q. Wang, E.H. Han, Electrochemical Measurements Using Combination Microelectrodes in Crevice Simulating Disbonded of Pipeline Coatings under Cathodic Protection, Corrosion Engineering, Science and Technology, 42 (2007) 42-49.
- [13] X. Chen, X.G. Li, C.W. Du, Y.F. Cheng, Effect of Cathodic Protection on Corrosion of Pipeline Steel under Disbonded Coating, Corrosion Science, 51 (2009) 2242-2245.
- [14] D. X. He, W. Chen and J. L. Luo, Cathodic Potential Dependent Hydrogen Content in A Pipeline Steel Exposed to NS4 Near-Neutral pH Soil Solution, Corrosion, 60-8 (2004) 778-786.
- [15] D.W. Hoepfner, Model for Prediction of Fatigue Lives Based upon a Pitting Corrosion Fatigue Process, Fatigue Mechanisms, ASTM STP, 675 (1979) 841-870.
- [16] J.A. Colwell, B.N. Leis, P.M. Singh, Crack Initiation of Line Pipe Steel in Near-neutral pH Environments,

- [17] D.A. Jones, Principles and Prevention of Corrosion, 2nd Edition, Prentice Hall, 1995.
- [18] Mitigation of External Corrosion on Buried Pipeline Systems, Canadian Association of Petroleum Products (CAPP), 2009.
- [19] Y.F. Cheng, Thermodynamically Modeling the Interaction of Hydrogen Stress, and Anodic Dissolution at the Crack Tip During Near-neutral pH SCC in Pipelines, J. Mater.Sci., 42 (2007) 2701-2705.
- [20] F. King, T. Jack, W. Chen, M. Wilmott, R.R. Fessler, K. Krist, Mechanistic Studies of Initiation and Early Stages Crack Growth for NNpHSCC on Pipelines, Corrosion 2000, Huston-Texas, USA, 2001.
- [21] Y. Kondo, Prediction of Fatigue Crack Initiation Life Based on Pit Growth, Corrosion, 45 (1989) 7-11.

Chapter 6: Corrosion of Pipeline Steel under the Simulated Coating Disbondment¹

¹ A version of this chapter has been submitted to journal of **Corrosion** for publication.

6.1. Introduction

Pipelines can corrode when buried under ground. To mitigate corrosion, protective coatings in combination with cathodic protection (CP) are applied to the outer surface of the buried pipelines [1]. In ideal situations, while coatings isolate the pipe surface from its external environment, CP protects the pipe at regions where faults in the coating occur. In reality, at regions with coating defects ground water may penetrate under the coating, and if the CP is blocked by the coating, different forms of corrosion could be formed at locations under the coating with insufficient CP protection.

Disbonded coatings (Figure 6.1) are one of the most common types of pipeline tape coating failures, which can form along the weld seam of some welds, particularly longitudinal DSAW (Double Submerged Arc Welds) [1]. Although there has been considerable research on different forms of corrosion of pipeline steels [2-6], there is limited research considering the effect of coating disbondments on external corrosion of pipeline steels. Having a better understanding of this issue could be important for pipeline integrity management and safe operation.



Figure 6.1: Typical image of coating disbondments formed on a seam weld of a pipe section.

There are different methods for evaluating the corrosion rate of pipeline steels. Weight loss measurements and electrochemical measurements are the most common methods in this regard [7-11].

This study primarily investigates the corrosion of X-65 pipeline steel at the free corrosion condition without considering the effect of coating disbondment and CP. Since most pipes become corroded under coating disbondments, even when protected by CP, the effect of these parameters on corrosion of the pipeline steel is also investigated. It's worth mentioning that this study mainly deals with general corrosion of the pipeline steel under a disbonded coating, while the pitting corrosion and near-neutral pH stress corrosion cracking initiation of the pipeline steel have been investigated in the previous chapters. New findings about the corrosion rate of pipeline steels under coating disbondments are presented in this chapter, which could assist in the understanding and modeling of near-neutral pH crack initiation and growth.

6.2. Experimental

6.2.1. Specimen and solution

X-65 pipeline steel with a chemical composition same to that presented in section 3.2.1 was used for this study. Coupons with dimensions of 2×2×0.5 cm were machined from an X-65 pipe section. The coupons were ground to 600 grit, and then cleaned in acetone and ethanol prior to each test.

C2 solution with a chemical composition same to that presented in section 3.2.1 was used as the simulated ground water solution for this study. The solution was continuously purged for 2 days with 5%CO₂/N₂ prior to each test, reaching a stable pH of 6.29. For tests where high-pH solution was used, the pH of the C2 solution was adjusted by addition of NaOH solution.

6.2.2. Corrosion cell and coupon holder

In order to simulate the corrosion of X-65 pipeline steel under a disbanded coating, a corrosion cell similar to that explained in section 2.2.1, was designed and built (Figure 6.2a). The cell was made from PMMA¹ material. A shielding made from the same material with a gap distance of 1 cm was placed in the corrosion cell in order to simulate the coating disbondment. As shown in Figure 6.2a, only the upper end of the shielding was open to the outside environment, which was named the Open Mouth (OM). This simulated the OM of a large coating disbondment under a holiday.

Prior to each test, coupons were placed inside a coupon holder similar to that explained in section 2.2.3, and schematically shown in Figure 6.2b. The coupon holder was then placed inside the shielding of the corrosion cell. The corrosion cell was then filled with the simulated soil solution. Only the front sides of the coupons were exposed to the soil solution, while other surfaces were covered by the coupon holder.

¹ Poly (methyl methacrylate)

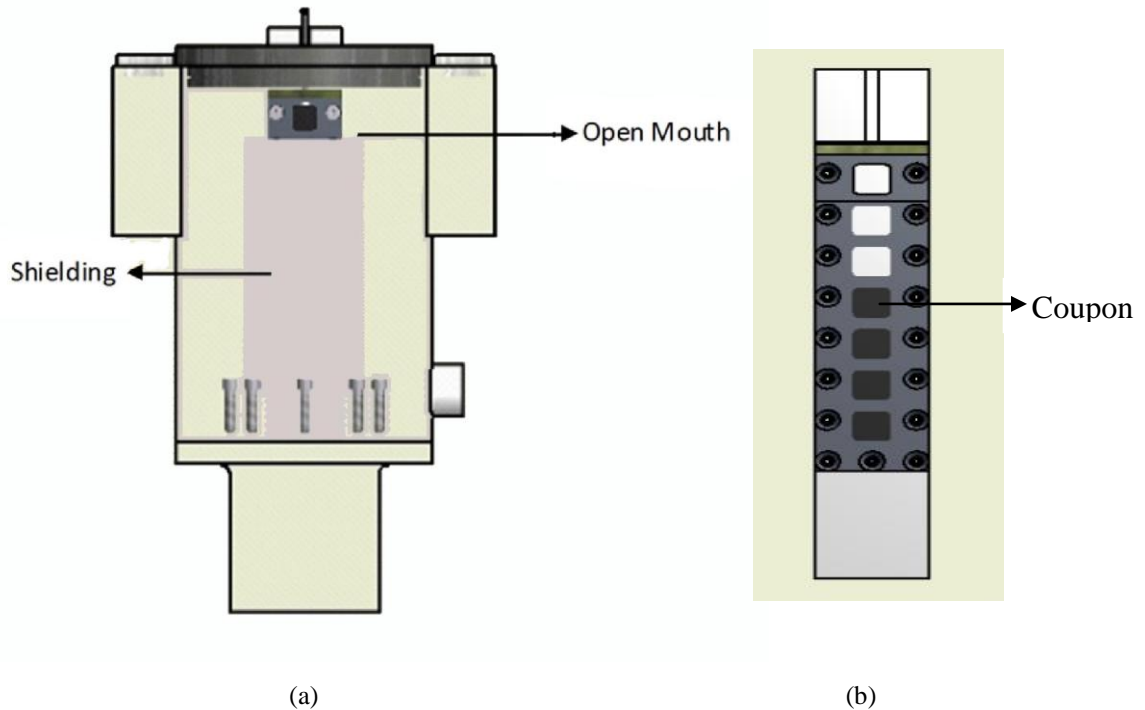


Figure 6.2: (a) Schematic of the corrosion cell with the shielding, (b) schematic of the coupon holder with coupons.

6.2.3. Corrosion tests

6.2.3.1. Electrochemical test

A Gamry PC4/300 potentiostat was used to study the corrosion behaviour of X-65 pipeline steel in C2 solution using the potentiodynamic polarization method. In this regard, a piece of X-65 pipeline steel with a surface area of 1 cm^2 was used as the working electrode. The working electrode was ground to 600 grit and cleaned in acetone and ethanol prior to each test. Standard saturated calomel electrode was used as the reference electrode, while two platinum meshes (5×5) cm were used as counter electrodes for the electrochemical test. C2 solution with an initial pH value of 6.29 and adjusted values of 8.3, 10.3, and 11.3 (by addition of NaOH solution) was used for the polarization tests. The scanning rate for the potentiodynamic polarization tests was 0.5 mV/s .

6.2.3.2. Weight loss corrosion tests

Weight loss tests were performed under three different testing conditions as shown in Table 6.1. During each test the C2 solution was continuously purged with 5% CO₂/N₂ in order to maintain a near-neutral pH anaerobic environment. In tests for which the effect of CP was to be considered a potentiostat model EG&G 363 was used to apply the CP potential of -1.2 V_{SCE} to the steel surface located at the OM of the simulated disbondment. In order to apply the CP potential, counter and reference electrodes similar to those used for the electrochemical tests were used. The detailed procedure for applying CP was similar to that explained in section 2.2.1.

Table 6.1: Weight loss corrosion tests performed in this study.

Test	Condition
A	Without considering coating disbondment; OCP ¹ condition; 30 day test in C2 solution continuously purged with 5% CO ₂ /N ₂
B	With considering coating disbondment; OCP condition; 30 day test in C2 solution continuously purged with 5% CO ₂ /N ₂
C	With considering coating disbondment and CP; 30 day test in C2 solution continuously purged with 5% CO ₂ /N ₂

6.2.4. Characterization

During weight loss corrosion tests, combination micro-electrodes were used to record the pH at different positions from the OM under the simulated coating disbondment. The micro-electrodes had a diameter less than 1.6 mm and were carefully calibrated in buffer solutions of pH 4, 7, and 10 prior to the pH measurements. After the weight loss corrosion tests, the coupons were removed from the corrosion cell and immediately dried. They were then weighed in order to determine their weight loss during the corrosion test. Prior to weighting, a rust remover solution with the chemical composition same to that given in Table 3.4

¹ Open Circuit Potential

was used in order to remove possible surface deposits. The corrosion rate on each coupon was calculated from its weight loss using the following Equation:

$$CR = \frac{W_2 - W_1}{t \times \rho \times A} \quad (6-1)$$

Where W_2 and W_1 are the initial weight and final weights, respectively; t is the time, ρ is the density of steel, and A is the surface area of the coupon exposed to the simulated soil solution.

Scanning Electron Microscope (SEM) equipped with Energy Dispersive X-ray analyzer (EDX) and X-ray Diffraction (XRD) technique were used for surface observation and characterization.

6.3. Results and Discussions

6.3.1. X-65 pipeline steel

Figure 6.3, shows the X-65 pipeline steel microstructure investigated in this study. As can be seen from this figure, the steel has a ferrite-pearlite microstructure with some inclusions and a grain size in the range of 10-20 micrometer. The pearlite formed around 25% of the microstructure. Previous studies have shown that this microstructure is more susceptible to corrosion and cracking compared to steels with a more uniform structure [12, 13].

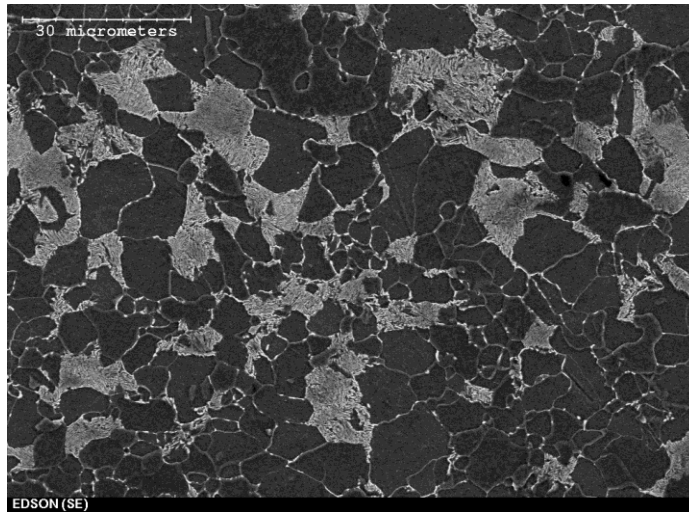


Figure 6.3: Typical microstructure of the X-65 pipeline steel investigated in this study.

6.3.2. Corrosion of X-65 pipeline steel

6.3.2.1. Electrochemical tests

Figure 6.4 shows the potentiodynamic polarization scan for the X-65 pipeline steel in C2 solution. As can be seen from this figure, with the increase in the pH of the simulated trapped solution inside the disbondment a narrow passive region starts to form, and at a pH of 11.3 complete passivation has occurred.

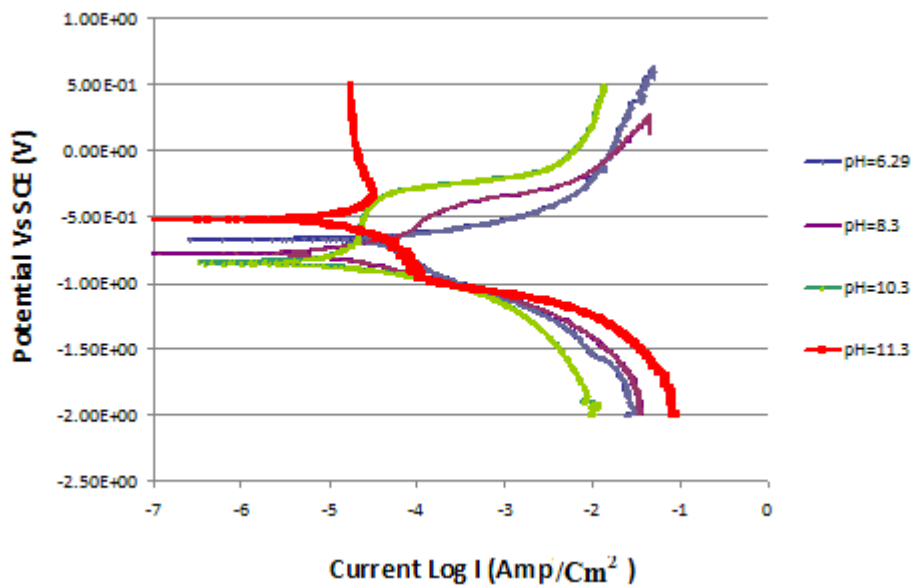


Figure 6.4: Diagram of the potentiodynamic scanning for the X-65 pipeline steel at different pH values.

The corrosion rate for the X-65 pipeline steel in C2 solution continuously purged with 5%CO₂/N₂ (with an initial pH value of 6.29) determined from the polarization curve was 14.9 mils/year (0.373 mm/year)¹. The passivation of steel in the high-pH solution significantly reduces the corrosion rate of the pipeline steel during the polarization tests when compared to the near-neutral pH state (See Figure 6.4). This can also be seen from Figure 6.5, which is in agreement with the findings of Zhang et al. [10], Niu and Cheng [14], and Park et al. [15].

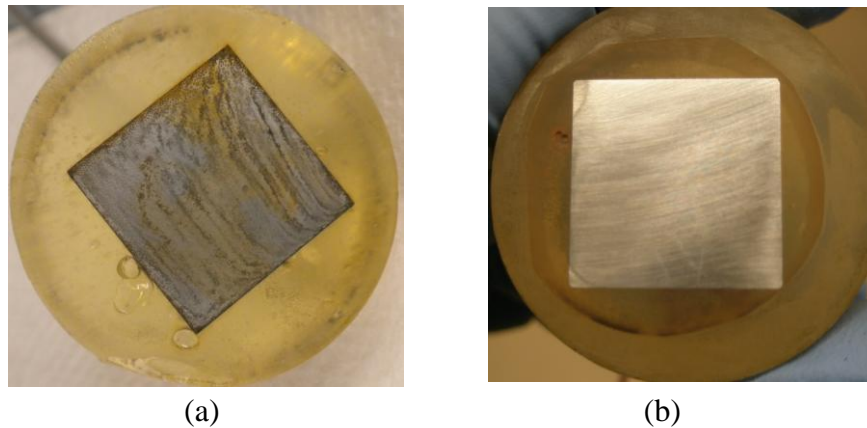


Figure 6.5: Digital camera image showing X-65 pipeline steel surface 3after the potentiodynamic polarization scan at different pH values: (a) at pH=6.29, and (b) at pH=11.

The alkalinity of the solution was initially adjusted by adding NaOH to the simulated soil solution (C2 solution). With the ion transportation occurring in the high-pH environment a concentrated carbonate-bicarbonate solution could form with time (see Figure 1.12). Passivation of the steel surface does not occur in the localized high-pH environment when the pipe is protected at cathodic potentials. It may occur in the high-pH environment when CP is shielded or when CP is turned off [16]. One occasion where shielding of CP is very common, is deep under the tape coating disbondments on the pipe surface [1].

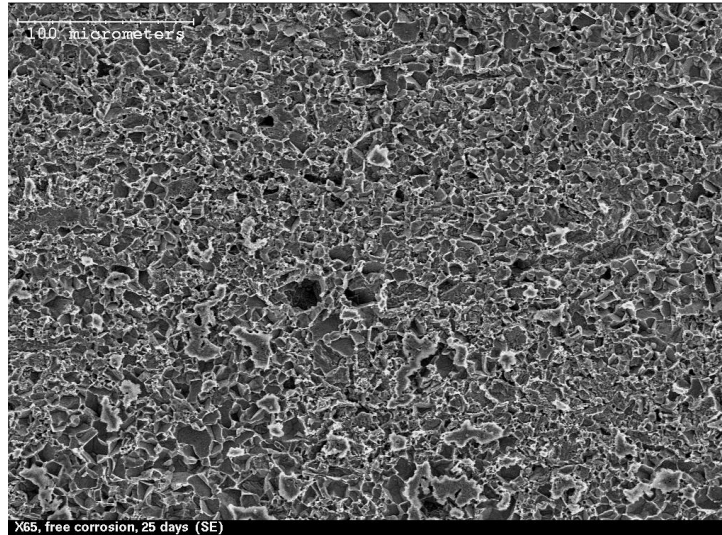
¹ 1 mil = 0.0254 millimeters.

6.3.2.2. Weight loss corrosion test without considering coating disbondment at OCP (Test A) ¹

The corrosion rate obtained for the X-65 pipeline steel after the 30 day weight loss test in near-neutral pH environment (C2 solution continuously purged with 5%CO₂/N₂ with an initial pH of 6.29) was 1.7 mils/year (0.043 mm/year). This is significantly lower than that determined by the potentiodynamic polarization test method. As investigated by Wang, one reason for the lower corrosion rate obtained in the weight loss method might be the formation of surface scales and products on the steel surface during longer exposure times [17]. The surface deposits can then reduce the general corrosion rate, by partially protecting the surface and reducing the corrosion sites on the surface of the pipeline steel. This statement is in agreement with other study showing that the corrosion rate of pipeline steel in simulated soil solutions was higher at the initial stages of the weight loss corrosion tests [13].

A typical image of the steel surface after the 30 day weight loss test in the near-neutral pH environment is shown in Figure 6.6a. As can be seen from this figure, the steel surface has been corroded with pits on the surface. Different mechanisms could be responsible for the pitting corrosion on the steel surface in the simulated near-neutral pH soil solutions. Preferential corrosion of crystallographic planes having different orientations, galvanic coupling between different phases in the steel microstructure and dissolution of inclusions are some of the mechanisms identified in a previous study [18]. Figure 6.6b shows how ferrite could selectively be corroded around pearlite on the steel surface.

¹ Due to insignificant level of general corrosion in the localized high-pH environments the weight loss corrosion test was only performed in the near-neutral pH environment with initial pH of 6.29.



(a)



(b)

Figure 6.6: (a) Typical image of the steel surface after Test A (30 day test without considering coating disbondment at OCP), (b) high magnification image showing selective corrosion of ferrite after Test A.

6.3.2.3. Weight loss corrosion test considering coating disbondment at OCP (Test B)¹

Figure 6.7 shows corrosion rate of pipeline steel at OCP conditions in a near-neutral pH environment under the simulated coating disbondment after the 30 day

¹ Due to insignificant level of general corrosion in the localized high-pH environments the weight loss corrosion test was only performed in the near-neutral pH environment with the initial pH of 6.29 and continuously purged with 5% CO₂/N₂.

weight loss corrosion test, as compared to the test at OCP without coating disbondment. As can be seen from this figure, the corrosion rate of pipeline steel has dropped under the coating disbondment, with only the OM showing corrosion rate close to what was seen in the test at OCP with no coating disbondment being considered. Typical steel microstructure after the weight loss test at different positions from the OM inside the simulated coating disbondment is also shown in Figure 6.8. As can be seen from this figure, the steel is increasingly corroded at locations close to the OM, compared to locations at the end far from the OM.

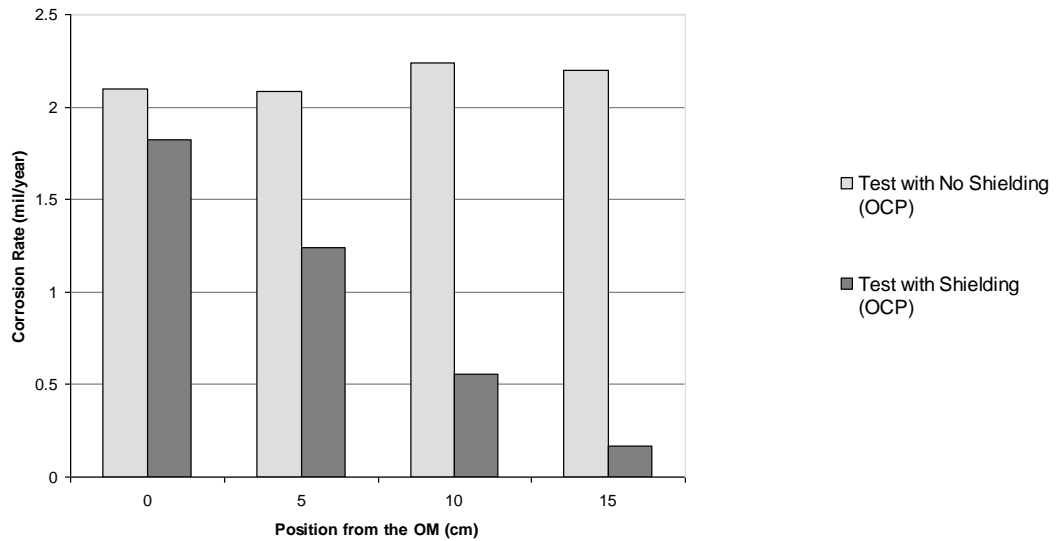


Figure 6.7: Corrosion rate of X-65 pipeline steel after the 30 day weight loss corrosion tests at OCP condition at different positions from the OM inside the simulated coating disbondment compared with test at OCP where no coating disbondment was used.

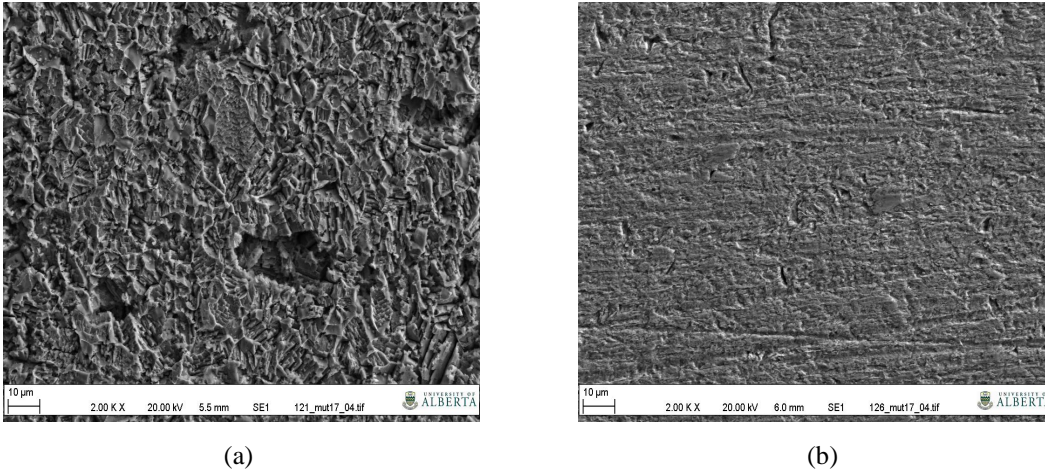
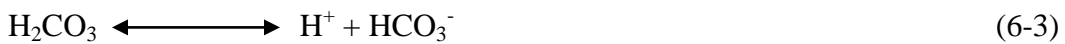


Figure 6.8: Typical images showing the X-65 pipeline steel microstructure at: a) close to OM, b) far end from the OM, after the 30 day weight loss corrosion test.

In order to determine the cause of higher corrosion rates close to the OM under the coating disbondment, pH measurements were carried out. As shown in Figure 6.9, locations close to the OM showed slightly lower pH values compared to locations far away from the OM. Since the OM was the only place where CO₂ could enter inside the disbondment, the lower pH at this location can be explained by higher levels of dissolved CO₂ at this location due to the difference in mass transfer rate of CO₂ towards deep inside the disbondment. The higher level of dissolved CO₂ could generate more hydrogen ions, and therefore could reduce the pH as the result of the following reactions:



Although the small difference in pH could be responsible for the reduced corrosion rates inside the coating disbondment, it may not be the only factor. There may be other factors involved (such as variation of Cl⁻ level inside the coating disbondment), which we have not considered in this study. They could be subject of future investigations.

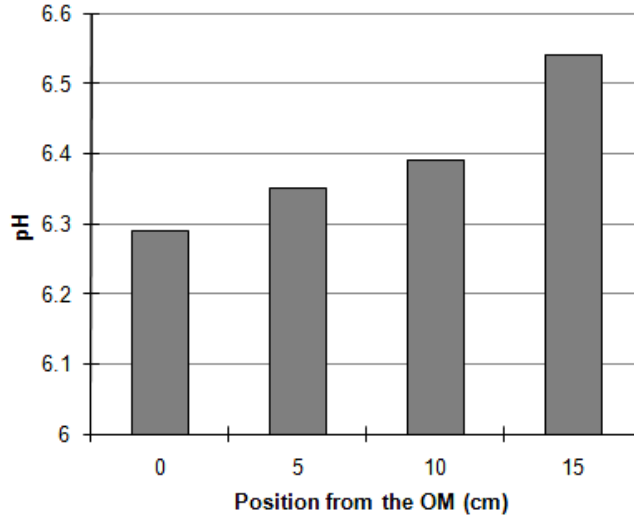


Figure 6.9: pH distribution under the simulated coating disbondment at different positions from the OM.

Further studies using coating disbondments with smaller gap size (gap size of 0.2 and 0.5 cm) showed evidence of galvanic corrosion [19]. In more detail, enhanced corrosion was observed for the coupons located at the OM, while the coupons located at the bottom of the coating disbondment were protected. The galvanic effect could possibly have been caused by the concentration cell which may have resulted from the reduced gap size [19]. No significant evidence of galvanic corrosion was observed for the coating disbondment investigated in this study.

6.3.2.4. Weight loss corrosion test considering coating disbondment and CP (Test C)¹

CP potential distribution at different positions from the OM under the simulated coating disbondment in the near-neutral pH environment is shown in Figure 6.10².

¹ Due to insignificant level of corrosion in the localized high-pH environment, the weight loss corrosion tests were only performed in the near-neutral pH environment with the initial pH of 6.29 and continuously purged with 5% CO₂/N₂.

² There is slight difference between CP distribution observed for the specimens used in the current test setup, with that observed for the tensile specimen used in previous studies. This should be due to the small differences in surface area of the specimens used for the two test setups. The effect of steel exposed surface area on CP distribution under coating a disbondment is investigated in Chapter 7.

As can be seen from this figure the level of CP has dropped from full protection at the OM to values close to OCP at the far end from the OM. The discussion of the CP drop as you move away from the OM can be found in Chapter 3 section 3.3.2.

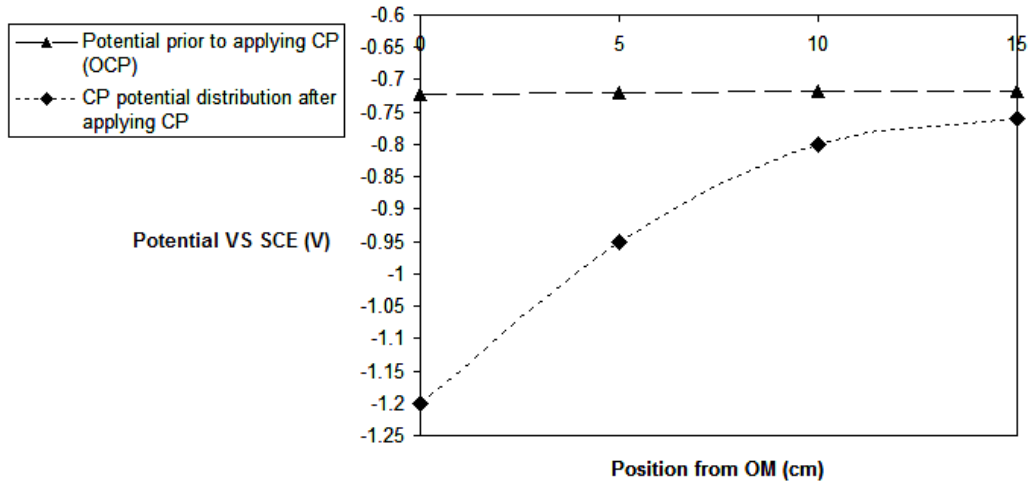


Figure 6.10: Potentials distribution at different positions from the OM, before and after a CP of $-1.2V_{SCE}$ was applied to the OM.

Figure 6.11 shows the effect of CP on corrosion rate of pipeline steel under the simulated coating disbondment.

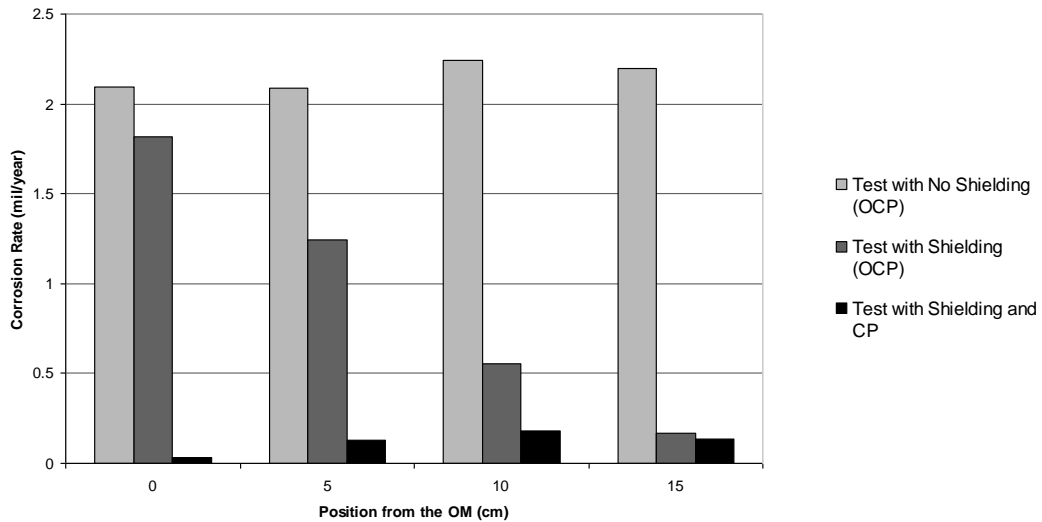


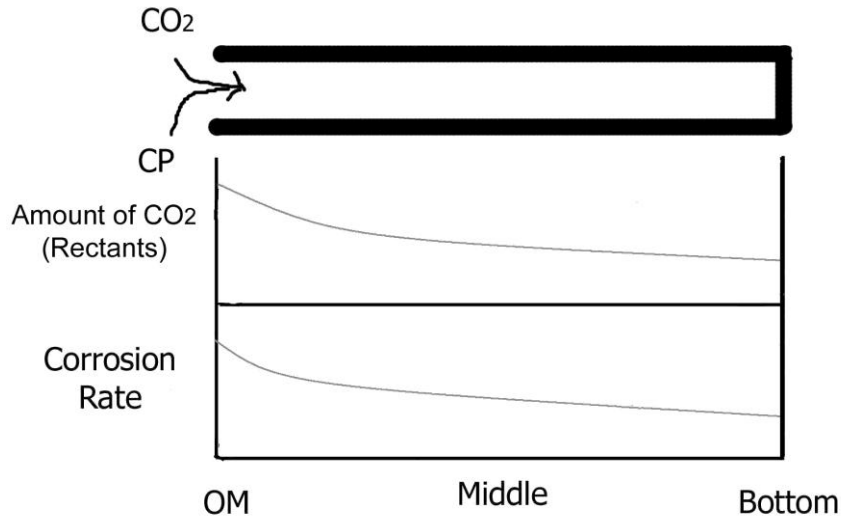
Figure 6.11: Effect of CP on corrosion mitigation under the coating disbondment at different positions from the OM, compared with OCP tests at situation with and without the shielding effect of the simulated coating disbondment after the 30 day weight loss corrosion tests.

As can be seen from this figure, the corrosion rate of the pipeline steel is significantly reduced especially at locations close to OM when compared to the OCP test. At the far end from the OM, where the CP effect diminished (see Figure 6.10), the corrosion rate is close to values determined in the OCP test (Test B).

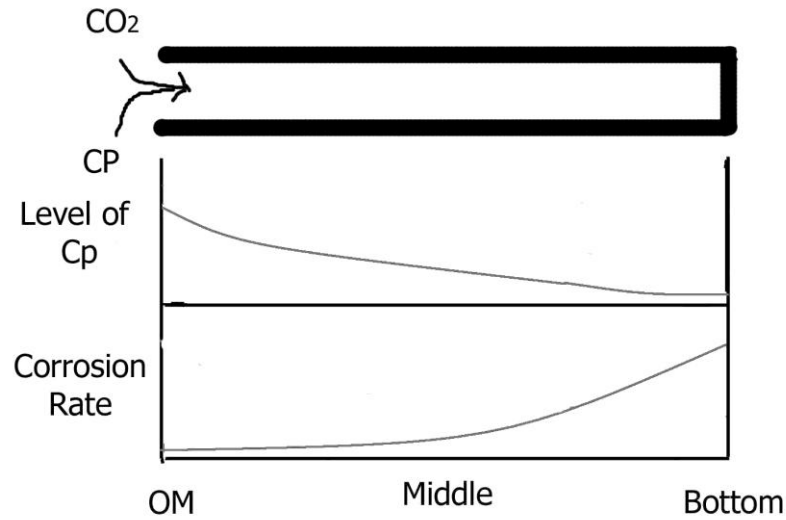
From Figure 6.11, it could be concluded that the corrosion rate of pipeline steel under the coating disbondment investigated in this study is affected by at least the following two factors:

1. Amount of CO₂: the corrosion rate of pipeline steel decreases towards the bottom of a coating disbondment with reduced amount of CO₂ (schematically shown in Figure 6.12a).
2. Level of CP potential: the corrosion rate of pipeline steel increases towards the bottom of a coating disbondment as the level of CP potential drops (schematically shown in Figure 6.12b).

When both CP and coating disbondment are present (such as that observed in Test C), the corrosion rate of pipeline steel at each particular location under the coating disbondment would be determined by the balance between level of CP potential and amount of CO₂ inside the coating disbondment. In more detail, when moving towards the bottom of the coating disbondment the corrosion rate of the pipeline steel would decrease due to reduced amount of CO₂ on one side (schematically shown in 6.12a), and on the other it would increase due to CP potential drop inside the coating disbondment (schematically shown in Figure 6.12b). This further explains the existence of a “sweet region” between the OM and deep inside the coating disbondment, where conditions for formation of large corrosion pits and surface micro-cracks are favorable (see Chapters 3 - 5).



(a)



(b)

Figure 6.12: Schematic showing corrosion rate of pipeline steel at different positions under a coating disbondment as a function of: (a) amount of CO₂ (reactants), (b) level of CP.

6.4. Conclusions

1. The corrosion rate of X-65 pipeline steel in simulated near-neutral pH soil solution determined by the potentiodynamic polarization test method was significantly higher than that determined from the long term weight loss corrosion test.

2. X-65 pipeline steel showed active corrosion behavior in simulated near-neutral pH environment, while passivation was observed in localized high-pH environments.
3. The corrosion rate of the pipeline steel under the simulated coating disbondment was reduced by the shielding effect of the coating disbondment.
4. For the test where both coating disbondment and CP were considered, the corrosion rate of pipeline steel was determined by level of CP and amount of CO₂ under the coating disbondment. This further explains the existence of a “sweet region” under the coating disbondment, where conditions for formation of large corrosion pits and surface micro-cracks are favorable.

6.5. References

- [1] National Energy Board (NEB), Report of the Inquiry - Stress Corrosion Cracking on Canadian Oil and Gas Pipelines, 1996.
- [2] J.A. Beavers, B.A. Harle, Mechanisms of High pH and Near-neutral-pH SCC of Underground Pipelines, *Journal of Offshore Mechanics and Arctic Engineering*, 123 (2001) 147-151.
- [3] M. Elboujdaini, R.W. Revie, Metallurgical Factors in Stress Corrosion Cracking (SCC) and Hydrogen-Induced Cracking (HIC), *Journal of Solid State Electrochemistry*, 13 (2009) 1091-1099.
- [4] R.L. Eadie, K.E. Szklarz, and R.L. Sutherby, Corrosion Fatigue and Near-neutral pH Stress Corrosion Cracking of Pipeline Steel and the Effect of Hydrogen Sulphide, *Corrosion*, 61, (2005) 167-173.
- [5] X. Mao, X. Liu, and R.W. Revie, Pitting Corrosion of Pipeline Steel in Dilute Bicarbonate Solution with Chloride Ions, *Corrosion*, 70 (1994) 651-657.
- [6] E. Ramirez, J.G. Gonzalez-Rodriguez, A. Torres-Islas, B. Campillo, G. Dominguez-Patino, Effect of Microstructure on the Sulphide Stress Cracking Susceptibility of a High Strength Pipeline Steel, *Corrosion Science*, 50 (2008) 3534-3541.
- [7] N. Guerhazi, A. Ibrahim, H.Hmidi, K.Elleuch, and H.F. Ayedi, Susceptibility to Corrosion Damage of Pipeline Steels under Coating Disbondments, *Materials and Corrosion*, 61 (2010) 43-50.
- [8] E.A. Noor, A.H. Al-Moubaraki, Corrosion Behaviour of Mild Steel in Hydrochloric Acid, *International Journal of Electrochemical Science*, 3 (2008) 806-818.

- [9] J.G. Gonzalez, M.A. Espinosa-Medina, C. Angeles-Chaves, and T. Zeferino-Rodriguez, SCC of X-52 and X-60 Weldments in Diluted NaHCO₃ Solutions with Chloride and Sulfate Ions, *Materials and Corrosion*, 58 (2007) 599-603.
- [10] L. Zhang, X.G. Li, C.W. Du, and Y.F. Cheng, Corrosion and Stress Corrosion Cracking Behaviour of X70 Pipeline Steel in a CO₂-Containing solution, *Journal of Materials Engineering and Performance*, 18(3) (2009) 319-323.
- [11] W. Chen, R.L. Sutherby, Crack Growth Behaviour of Pipeline Steel in Near-neutral pH Soil Environments, *Metallurgical and Materials Transaction A*, 38A (2007) 1260-1268.
- [12] R. Chu, W. Chen, S.H. Wang, F. King, T.R. Jack, R.R. Fessler, Microstructure Dependence of Stress Corrosion Cracking Initiation in X-65 Pipeline Steel Exposed to Near-Neutral pH Soil Environment, *Corrosion*, 60 (2004) 275- 282.
- [13] M.H Marvasti, Crack Growth Behavior of Pipeline Steels in Near-neutral pH Environment, M.Sc. Thesis, University of Alberta, 2010.
- [14] L. Niu, Y.F. Cheng, Corrosion Behavior of X-70 Pipe Steel in Near-Neutral pH Solution, *Applied Surface Science*, 253 (2007) 8626-8631.
- [15] J.J. Park, S.I. Puyan, K.H. Na, S. M. Lee, Y.T. Kho, Effect of Passivity of the Oxide Film on Low-pH Stress Corrosion Cracking of API 5L X-65 Pipeline Steel in Bicarbonate Solution, *Corrosion*, 58-4 (2002) 329-336.
- [16] M.C. Yan, J.Q. Wang, E.H. Han, W. Ke, Electrochemical Measurements Using Combination Micro-Electrodes in Crevice Simulating Disbonded of Pipeline Coatings under Cathodic Protection, *Corrosion Engineering Science and Technology*, 42-1 (2007) 42-49.
- [17] H. Wang, Effect of the Environment on Near-neutral pH Stress Corrosion Cracking of X-52 Pipeline Steel, M.Sc. Thesis, University of Alberta, 2009.
- [18] A. Eslami, M. Marvasti, W. Chen, R. Eadie, R. Kania, R. Worthingham, G. Boven, The Role of Electrochemical Conditions in Near-neutral pH SCC Initiation Mechanism(s), *Proceedings of the 8th International Pipeline Conference*, 2010, Calgary, Alberta, Canada.
- [19] K. Chevil, A. Eslami, W. Chen, R. Eadie, Development of Cathodic Protection Based on Disbondment Geometry, Accepted at the 9th International Pipeline Conference, 2012, Calgary, Alberta, Canada.

Chapter 7: Electrochemical Processes under Simulated Coating Disbondments¹

¹ A version of this chapter has been submitted to **Journal of The Electrochemical Society** for publication.

7.1. Introduction

A combination of coatings and cathodic protection (CP) is a common practice utilized to protect underground pipelines [1]. In an ideal situation, if a coating becomes damaged and/or disbonded, CP would prevent the pipe surface from external corrosion by changing the equilibrium between the metal and environment through the application of direct electrical current. 100mV of cathodic polarization can reduce external corrosion rates by 30 to 2000 times [2]. However, despite the very successful application of this technology, due to the shielding effect of some types of coatings, corrosion may occur when the coating disbonds from the pipe surface.

Different types of coatings currently exist on the external surface of high pressure transmission oil and gas pipelines. Coatings like polyethylene tape (PE tape), fusion-bonded Epoxy (FBE), coal tar enamel, and asphalt are the most common ones. While some block CP, others permit CP to reach the pipe surface. Of the most commonly used pipeline coatings, asphalt, coal-tar enamel and FBE are generally considered to be CP compatible [3], while the PE Tape coatings are considered to be shielding type coatings [4]. The PE tape coatings are a major concern to the pipeline industry when a holiday occurs, due to their shielding effect [5].

PE tape coated pipes are exposed to different types of environmental degradation. For instance, they can become disbonded at the pipe surface due to soil stresses or at the longitudinal seam welds where a gap between the coating and the pipe surface is created. In this situation, if a defect (such as a pinhole) is formed at the disbonded region, ground water could penetrate and become trapped inside the disbondment. Due to the high resistivity of the ground water and the shielding effect of the coating, CP penetration under the disbondment could then be limited. Therefore, a local environment suitable for corrosion and cracking is formed. Several types of corrosion including general corrosion, stress corrosion cracking

(SCC), pitting corrosion, and microbiological induced corrosion (MIC) have been observed under PE Tape coating disbondments [6-11].

In order to understand corrosion under disbonded coatings, it is important to understand the exact electrochemical conditions causing the corrosion. Several attempts have been made in this regard. Chen et al. [12] investigated the effect of cathodic potentials, bubbling CO₂, and pre-corrosion of the steel surface on the local environment under a disbonded coating. Yan et al. [13] obtained the experimental potential-pH (E-pH) diagrams for the pipeline steel surface in a crevice. Perdomo et al. [14, 15] measured potential, pH and oxygen concentration within the crevice for pre-corroded and grit blasted pipeline steel plates in aerated water. Fessler et al. [16] showed that the potential in the disbonded crevice is always less negative than the applied cathodic potential, and the crevice bottom is thus insufficiently protected. Song et al. [17, 18], modeled the corrosion and electrochemical conditions under a disbonded coating.

Despite the considerable level of work several aspects of the subject, mainly related to field observations, are not yet well understood. For instance, some of the previous studies were done in a simple environment, ignoring the possible effects of CO₂ fluctuations and CP variation and interruptions¹. Also, in most studies the coating disbondments were simulated using small crevices with a gap size of 0.2 - 1.5 mm². This appears inconsistent with field observations that indicate that most coating failures in tape-coated pipes have a larger gap size.

Inspired by field observations, this study investigates the effect of CO₂ fluctuations, level of CP potential, disbondment gap size, exposed steel surface area, and coating disbondment material on the electrochemical conditions formed

¹ There could be significant variation in the level of CO₂ and CP potential in the underground environment [11]. For instance, CO₂ concentration could vary significantly due to seasonal changes while CP could also be interrupted by changes in soil resistivity or by operational factors at excavation times or when doing close interval surveys (CIS) in order to evaluate the CP performance [19].

² Using very narrow gap distance (below 1.5 mm) could simulate conditions causing crevice corrosion [20], which is not the significant threat for corrosion under PE tape coated pipes.

under disbonded coatings. Knowing the effect of these parameters on the electrochemical conditions under disbonded coatings is important. As observed in previous chapters, the electrochemical conditions under disbonded coatings could significantly affect the corrosion and near-neutral pH SCC initiation mechanisms.

7.2. Experimental

7.2.1. Pipeline steel and soil solution

X-65 pipeline steel with a chemical composition as that presented in section 3.2.1 was used for this study. The pipeline steel has been identified as susceptible to different types of corrosion such as general corrosion, MIC, pitting corrosion, high-pH SCC and near-neutral pH SCC [21-23]. Flat specimens were machined from an X-65 pipe section free from defects. The specimen surfaces were then ground to 600 grit and ultrasonically cleaned in acetone and ethanol before each test.

C2 solution¹ with the chemical composition presented in section 3.2.1 was used as the simulated soil environment in this study. In order to remove oxygen and obtain an anaerobic soil solution environment, the solution was continuously purged with 5%CO₂/N₂ for 48 hours prior to each test. The solution reached a stable pH of 6.29 during the purging.

7.2.2. Corrosion cell

In order to understand the electrochemical conditions under disbonded coatings protected by CP, a corrosion cell similar to that described in section 2.2.1 and schematically shown in Figure 2.2 was used. Using the corrosion cell, the level of applied CP potential, disbondment gap size, and disbondment material were

¹ A near-neutral pH soil solution, which simulated water from corrosion sites on TransCanada pipeline system [24].

adjustable. The coating disbondment inside the corrosion cell was simulated using a shielding plate (see Figure 2.2). Only the top part of the shielding was open to the surrounding environment, which was named the Open Mouth (OM). It represented the holiday region of the disbonded coating. Specimens made from the pipeline steel were sandwiched inside the shielding which was 15 cm deep. Poly(methyl methacrylate) (PMMA), high density polyethylene (HDPE) and low density polyethylene (LDPE) were the materials used for the disbondment in the corrosion cell.

Different levels of CP potential were applied right above the OM, through a three electrode system. In the three electrode system, two platinum gauzes were used as counter electrodes, while a standard saturated calomel electrode (SCE) was used as the reference electrode. More details regarding the process of applying CP potential can be found in section 2.2.1 [25].

7.2.3. Test conditions and measurements

Table 7.1 shows the test conditions used for investigating the effect of the level of applied CP potential, exposed pipe surface area, disbondment gap size, and disbondment material on the electrochemical conditions formed under disbonded coatings. For each test a different scenario combining varying levels of CO₂ and variations in the application of CP cycles was used (see Table 7.2).

During each test, steel surface potential, pH, and the conductivity of the solution trapped inside the disbondment were measured. In order to measure the steel surface potential at different positions from the OM, a portable custom-made reference electrode was used. To measure the pH and conductivity of the trapped solution inside the disbondment, commercial micro-electrodes and conductivity probes were used. They were all carefully calibrated before each use.

Table 7.1: Experimental conditions of tests investigated in this study.

Test	Experimental conditions
Reference Test	CP: $-1.2 V_{SCE}$; Gap Distance: 1 cm; Surface Area A (rectangular shape with a length of 15 cm and a width of 12 cm); Coating material: PMMA
Effect of level of applied CP potential	CP: $-1.0 V_{SCE}$ * CP: $-0.9 V_{SCE}$ *
Effect of exposed steel surface area	Surface Area: 2A (rectangular shape with a length of 15 cm and a width of 24 cm)*
Effect of disbondment gap size	Gap Distance 0.5 cm*
Effect of disbondment material	Coating material: High Density Polyethylene (HDP) * Coating material: Low Density Polyethylene (LDP) *

*All other experimental parameters were similar to the Reference Test.

Table 7.2: Different stages of the tests investigated in this study, representing CP and CO₂ cycles*.

Stage	I	II	III	IV	V
Environment	CP + purging 5% CO ₂ /N ₂	CP without purging 5% CO ₂ /N ₂	CP + purging 5% CO ₂ /N ₂	CP off + purging 5% CO ₂ /N ₂	CP off without purging 5% CO ₂ /N ₂

* In order to avoid repetition, stages IV and V were performed only for the Reference Test.

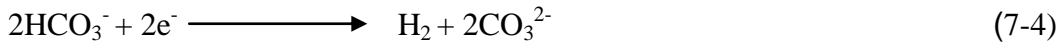
7.3. Results and Discussions

7.3.1. Reference Test

7.3.1.1. pH distribution

pH variation inside the simulated coating disbondment at different positions from the OM in Reference Test has been shown in Figure 7.1. The pH inside the disbondment is dictated by the balance between CO₂ availability and CP potential. At times when there was CP and a continuous supply of CO₂ the pH stayed near-neutral (stage I). When the purging of 5%CO₂/N₂ was stopped, the pH increased from near-neutral to high values above a pH of 10 (stage II). During stage II, higher pH values were observed closer to the OM (see Figure 7.1). This was due

to the increasingly negative CP potentials closer to the OM¹. The following reactions should have been responsible for the increase in pH, in the presence of CP and absence of CO₂ purging:



When 5%CO₂/N₂ purge was restored (stage III), despite the presence of CP the pH dropped back to near-neutral. The following reactions should have occurred when purging with CO₂:

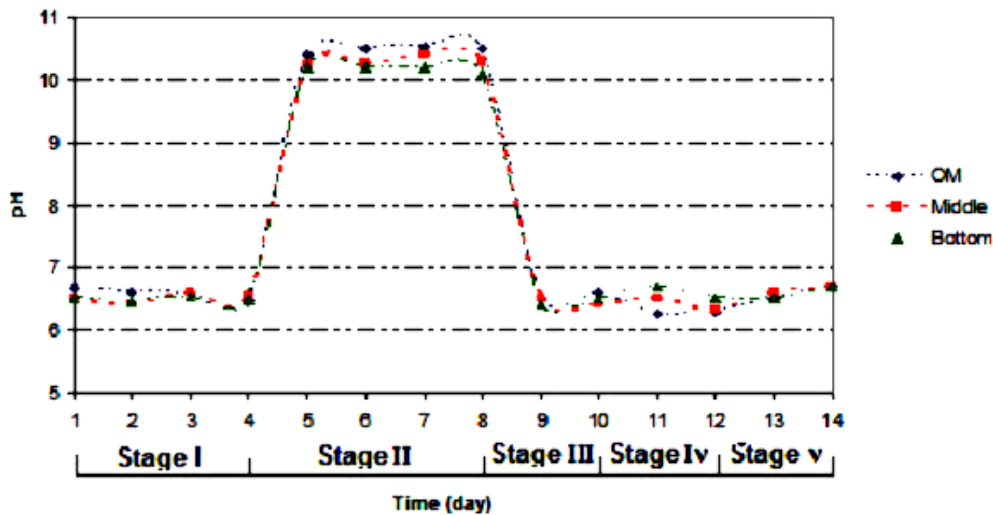


Figure 7.1: pH variation at different positions from the OM, in the Reference Test. Stage I experiences CP and gas containing 5%CO₂/N₂, stage II experiences CP while the gas has been turned off, stage III again experiences CP and gas containing 5% CO₂/N₂, stage IV experiences gas containing 5%CO₂/N₂ while the CP has been turned off, and Stage v experiences no CP and gas supply.

¹ In the current system ion migration from the near-neutral pH environment outside the OM, had negligible effect in preventing the increase in pH by CP.

Formation and dissociation of H_2CO_3 in addition to mixture of the solution should have prevented the increase in pH despite the presence of CP (see Equations 7-1 - 7-4)¹. When there was no CP, the pH stayed near-neutral independently of CO_2 purging (stages IV and V). More details regarding this can be found in the previous studies (Chapter 3 and Chapter 4, [25, 26]).

7.3.1.2. CP potential distribution

CP potential distribution at different position from the OM inside the disbondment in the near-neutral and high-pH environment is shown in Figure 7.2. As seen in this figure, the CP drops from full protection at close to the OM to less negative values further from the OM. This is due to both solution resistance and polarization resistance [27]. Also as seen in Figure 7.2, the potential drop in the near-neutral-pH environment is more than that observed in the high-pH environment. This should have been caused by the higher resistivity of the near-neutral pH soil solution when compared to the high pH soil solution (see Table 7.3).

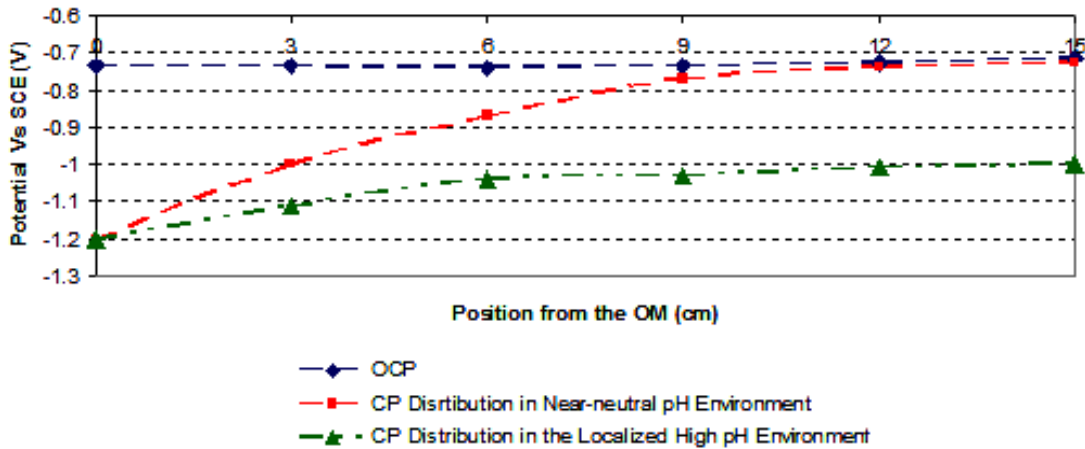


Figure 7.2: CP potential distribution in the Reference Test, at different positions from the OM in near-neutral pH and localized high and environment compared to the open circuit potential (OCP).

¹ In the study performed by M. Yan et al. [13] using a 0.5 mm crevice the pH remained high when purging with 5% CO_2/N_2 . This might be due to the considerable smaller gap size of the crevice.

Table 7.3: Resistivity of the near-neutral and high-pH solutions.

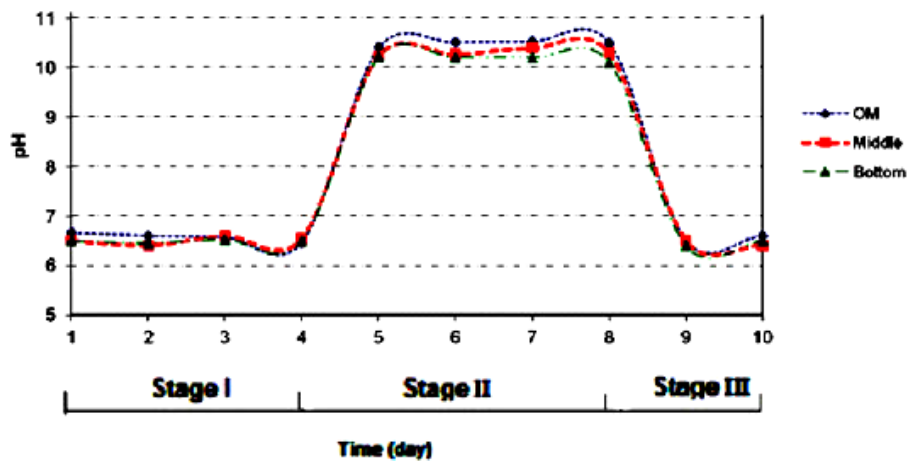
Environment	pH	Resistivity (ohm-cm)
Near-neutral pH	6.29	4730
High-pH	10.3	3304

A field implementation of the current observation is that coating disbondments containing near-neutral pH soil solution are less protected by CP, than those containing high-pH soil solutions (assuming all other affecting parameters are consistent).

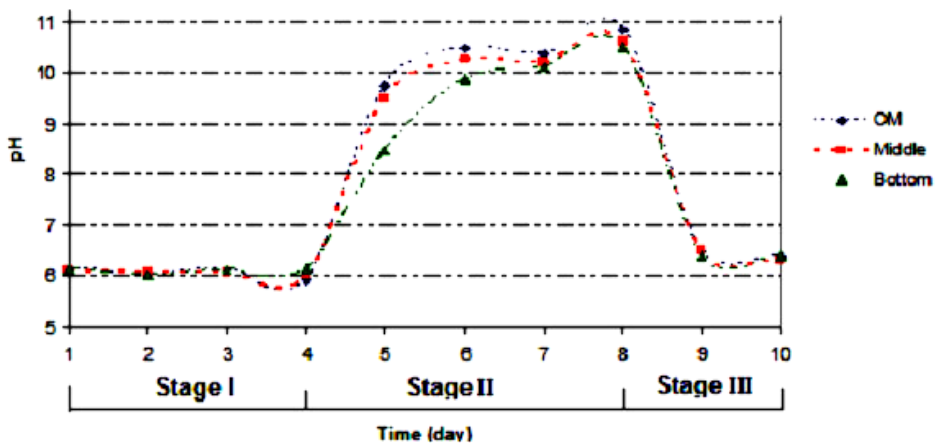
7.3.2. Effect of level of applied CP

7.3.2.1. pH distribution

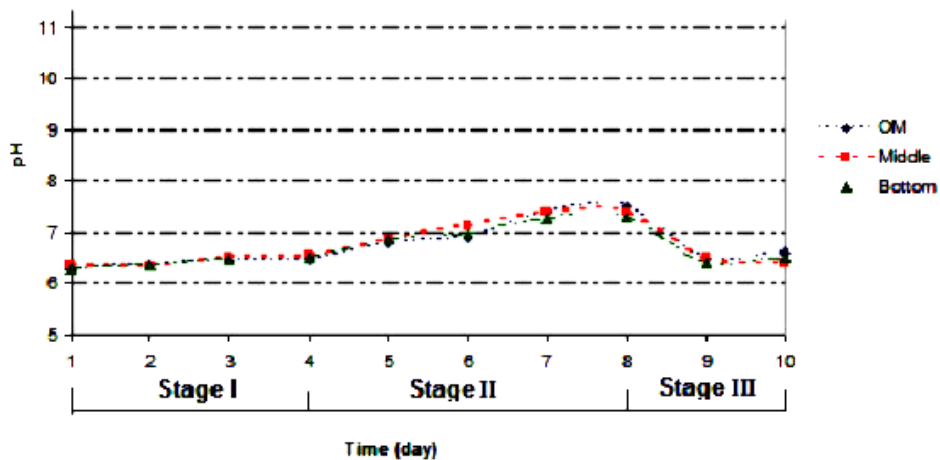
pH variation at different positions from the OM, when CP potentials of $-1.00 V_{SCE}$ and $-0.8 V_{SCE}$ were applied to the OM, compared to the Reference Test where a CP of $-1.2 V_{SCE}$ was applied to the OM are shown in Figure 7.3. As can be seen from this figure, as in the Reference Test, the pH is near-neutral at times when there is 5%CO₂/N₂ purging despite the level of CP (stages I and III). When the gas purging is stopped (stage II), the pH changes are determined by the level of applied CP. While in the Reference Test (with a CP potential of $-1.2 V_{SCE}$) it took only one day for the pH to increase to high values above 10 (see Figure 7.3a), for a CP potential of $-1.0 V_{SCE}$ it took 4 days for the pH to increase to high values above 10 (see Figure 7.3b), and for CP potential of $-0.8 V_{SCE}$ the pH stayed near-neutral for the test duration (see Figure 7.3c). This is related to the CP potential distribution under the coating disbondment which is explained in the next section.



(a)



(b)



(c)

Figure 7.3: pH variation at different positions from the OM when CP potentials of: (a) $-1.2 V_{SCE}$, (b) $-1.00 V_{SCE}$, and (c) $-0.8 V_{SCE}$ was applied to the OM. Gas containing 5% CO_2/N_2 is being supplied in stages I, and is turned off at the beginning of stage II, and turned on again in stage III.

7.3.2.2. CP potential distribution

CP potential distribution in the near-neutral pH environment when CP potentials of $-0.8 V_{SCE}$ and $-1.00 V_{SCE}$ were applied to the OM, as compared to the Reference Test is shown in Figure 7.4. As can be seen from this figure, the more negative level of applied CP potential has caused more negative CP potentials inside the disbondment (until reaching values close to OCP)¹. According to Nernstian behaviour of hydrogen reaction on steel surface (E-pH diagram), more negative CP potentials inside the disbondment would be in equilibrium with the higher pH environment [14]. Therefore it is reasonable to see more rapid pH increase inside the disbondment at more negative applied potentials, at times when there is no CO_2 being purged in the solution.

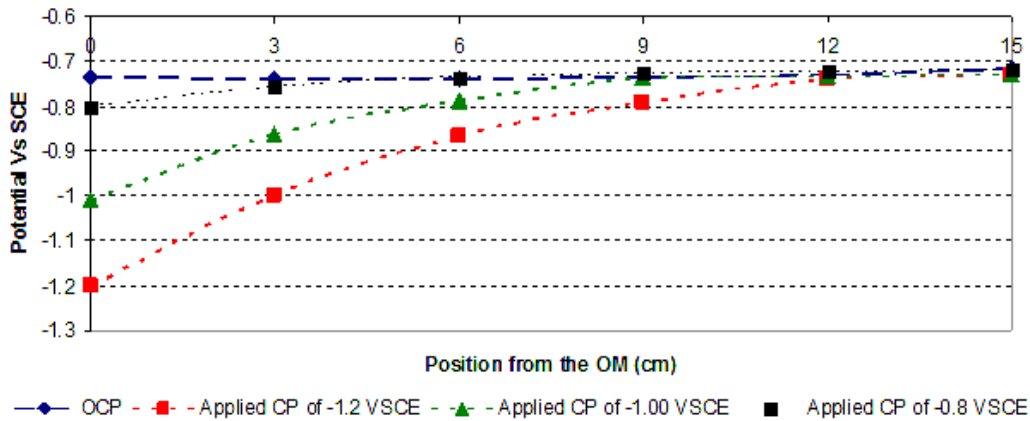


Figure 7.4: CP potential distribution at different positions from the OM in near-neutral pH environment, when CP potentials of $-1.2 V_{SCE}$, $-1.00 V_{SCE}$ and $-0.8 V_{SCE}$ were applied to the OM, compared to the OCP.

A field implementation of the current observation is that pipes having more negative instant off potentials², are better protected under the disbondments than those with less negative instant off potentials (assuming all other affecting parameters are consistent).

¹ The same trend was observed for the high-pH environment. In order to avoid repetition, it is not presented here.

² Instant off potentials are used as a reference showing the level of CP potential at the pipe surface [2].

7.3.3. Effect of exposed steel surface area

7.3.3.1. pH distribution

pH distribution in the test with double the exposed steel surface area compared to the Reference Test is shown in Figure 7.5. Just like the Reference Test, the pH has stayed near-neutral when there was a continuous supply of CO₂ (stage I, Figure 7.5). When the CO₂ supply was stopped it took a longer time for the pH to increase at all locations inside the simulated coating disbondment from near-neutral to higher pH values above 10, than the Reference Test (see stage II, Figure 7.5). This is related to the CP potential distribution inside the disbondment, which is explained in the next section (section 7.3.3.2).

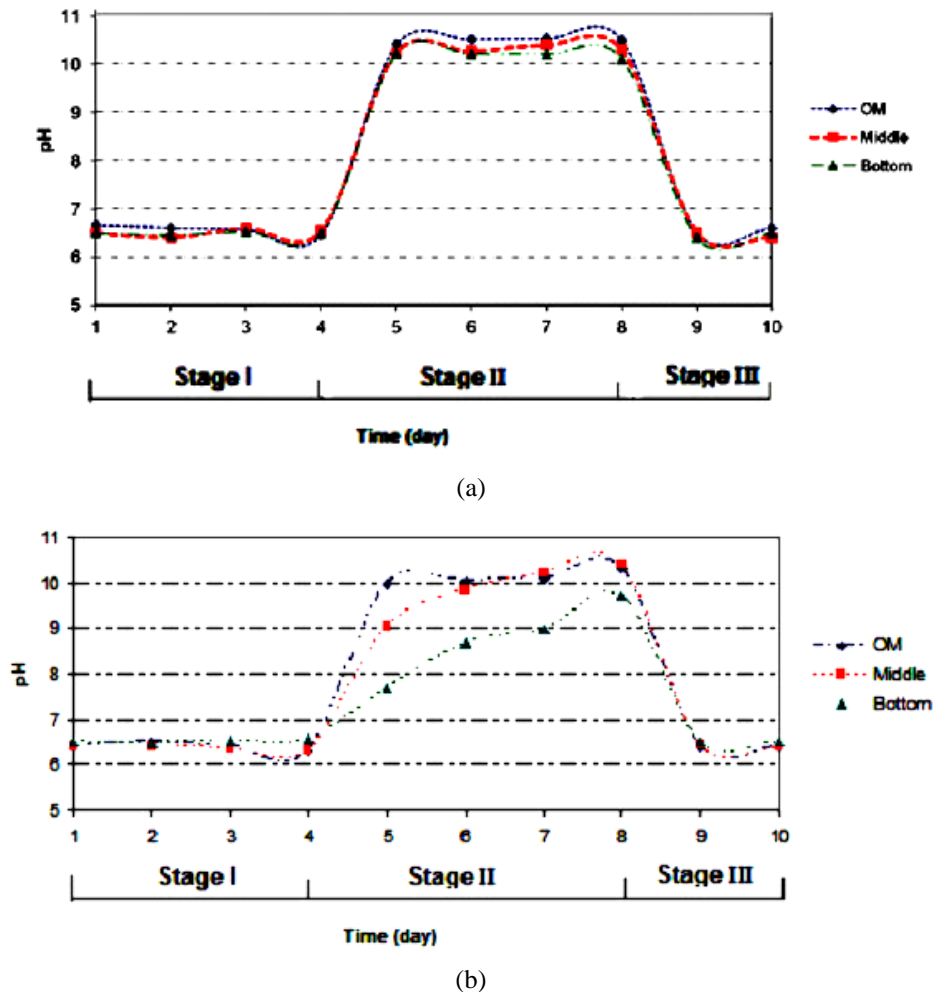


Figure 7.5: pH variation at different positions from the OM in: (a) the Reference Test, (b) the test with double exposed steel surface area. Gas containing 5% CO₂/N₂ is being supplied in stages I, and is turned off at the beginning of stage II, and turned on again in stage III.

7.3.3.2. CP potential distribution

Figure 7.6 shows the CP potential distribution inside the disbondment at different positions from the OM, as a function of exposed steel surface area in the near-neutral pH environment. As can be seen from this figure, more rapid CP potential drop has occurred with the increase in exposed steel surface area¹. This should be related to the decrease in surface current density with increase in steel exposed surface area, affecting the CP potential distribution.

Similar to the explanation in the previous section (section 7.3.1.1), the CP potential distribution inside the disbondment could then affect the pH inside the disbondment. A field implication of the current experiment is that disbondments containing larger surface areas of steel are less protected by CP. This could happen at longitudinal seam welds on pipes, where more metal is exposed to the solution compared to disbondments located at the pipe body (assuming all other affecting parameters are consistent).

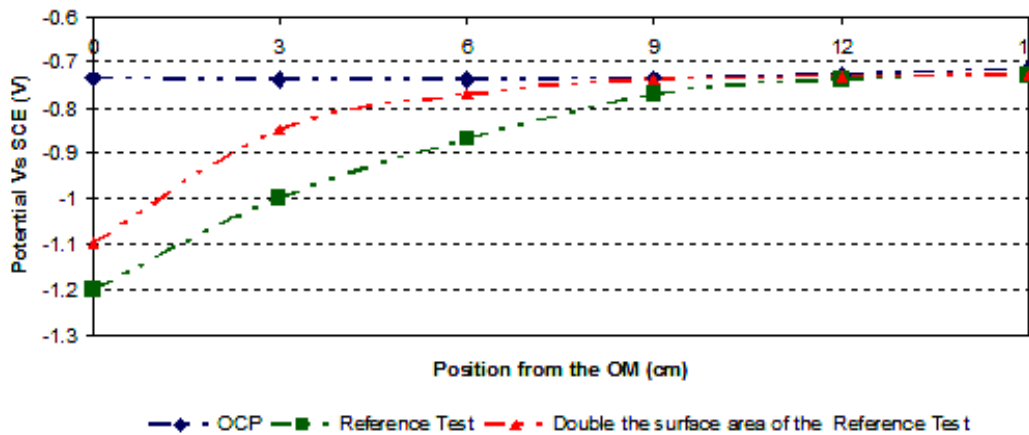


Figure 7.6: OCP and CP potential distribution at different positions from the OM in near-neutral pH environment in the test with double the surface area compared to the Reference Test².

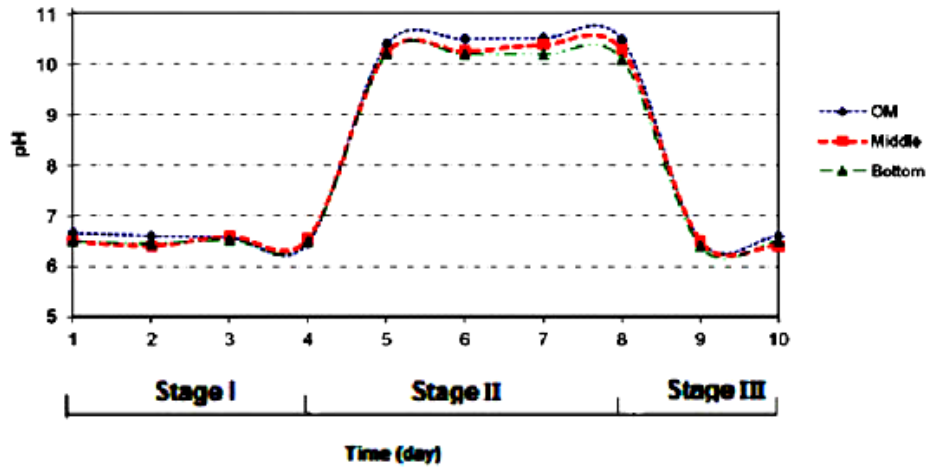
¹ The same trend was observed for the localized high-pH environment.

² The OCP was not affected by the change in steel exposed surface area.

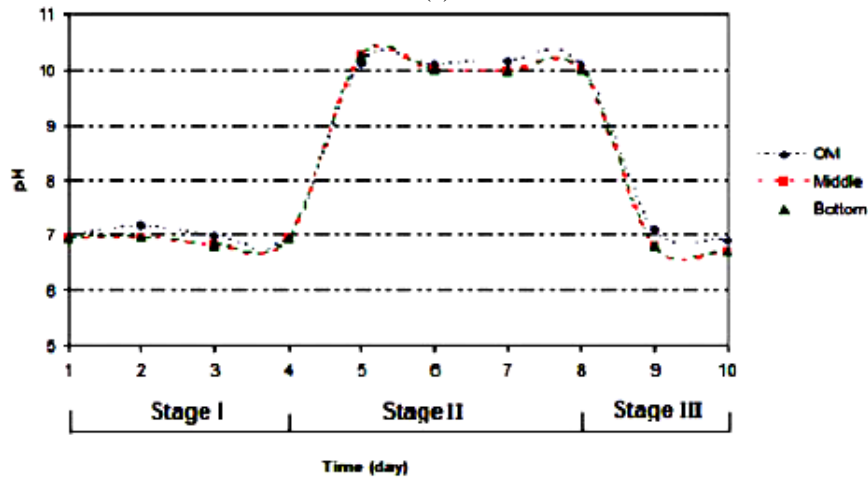
7.3.4. Effect of disbondment gap size

7.3.4.1. pH distribution

pH distribution for the test with reduced disbondment gap size compared to the Reference Test is shown in Figure 7.7. Comparing to the Reference Test, similar trends in pH distribution can be observed. As will be explained in the following section, this is related to the CP potential distribution inside the disbondment in addition to the reduced volume of the trapped soil solution when compared to the Reference Test.



(a)



(b)

Figure 7.7: pH variation at different positions from the OM in: (a) the Reference Test, (b) in the test with reduced disbondment gap size. Gas containing 5% CO₂/N₂ is being supplied in stages I, and is turned off at the beginning of stage II, and turned on again in stage III.

7.3.4.2. CP potential distribution

CP potential distribution in the test with reduced disbondment gap size, measured at different positions from the OM as compared to the Reference Test has been shown in Figure 7.8. As can be seen from this figure, reducing the disbondment gap size has caused rapid potential drop inside the disbondment at the different positions from the OM¹. This is due to the shielding effect of the coating disbondment. By reducing the disbondment gap size, the more negative CP potentials around the OM of the disbondment, are blocked as a result of the shielding effect of the disbondment parapet (schematically shown in Figure 7.9). The blockage of CP potential around the disbondment OM, should have affected the resistivity of the trapped solution inside the disbondment, affecting the CP potential drop inside the disbondment.

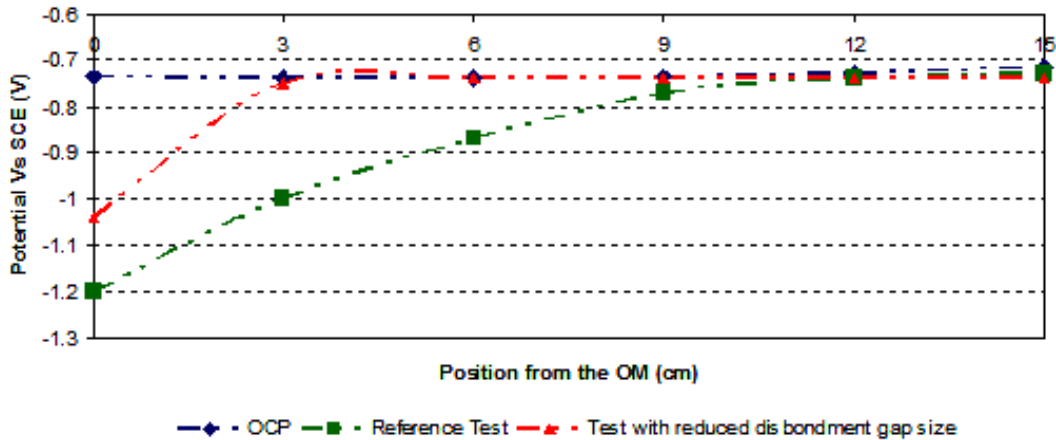


Figure 7.8: OCP and CP potential distribution at different positions from the OM in near-neutral pH environment in the test with reduced disbondment gap size compared to the Reference Test².

¹ The same trend was observed in the localized high-pH environment.

² The OCP was not significantly affected when reducing the disbondment gap size.

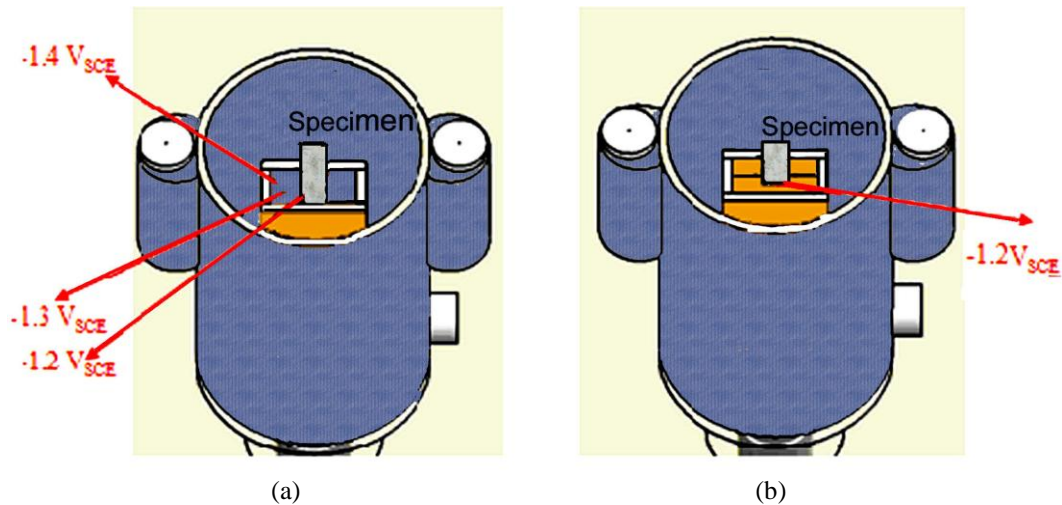


Figure 7.9: CP potential distribution around the OM of the simulated coating disbondment: a) in the Reference Test, b) in the test with reduced disbondment gap size.

Assuming all other parameters are held constant, the pH change of the trapped solution inside the disbondment is dictated by the level of CP potential as well as the volume of trapped solution [14]. When compared to the Reference Test, despite the more rapid CP potential drop inside the disbondment in the test with reduced disbondment gap size, the pH changes were quite consistent (see Figures 7.7 and 7.8). This should be related to the lower volume of the trapped solution inside the reduced gap size disbondment.

A field implication of the current investigation is that the pipe under a coating disbondment with narrower gap is less protected by the CP, as compared to disbondments with larger gap size.

7.3.5. Effect of various factors

As observed in this study, different factors could affect the CP and pH distribution under a coating disbondment. Dynamic and complicated field conditions, such as variation in coating disbondment gap size, exposed steel surface area, level of applied CP, CO₂ gas flow etc, make predicting the exact level of pH and CP potential inside a coating disbondment difficult. Despite this, based on the

practical knowledge obtained from the single factor investigations for C2 solution (sections 7.3.1-7.3.4), effect of various factors on CP and pH distribution under a coating disbondment could be roughly interpreted using Equations 7-7 and 7-8.

$$CP(x) = f(CP_{OM}) + f(SA) + f(GS) + f(SR) \quad (7-7)$$

$$pH(x) = f(CPx) + f(VS) + f(CO_2) \quad (7-8)$$

Where “CP_{OM}” is the level of CP at the OM of the coating disbondment, “SA” is the exposed steel surface area, “GS” is the disbondment gap size, “SR” is the soil solution resistance, and “VS” is the volume of the trapped solution.

According to Equation 7-7, the level of CP at a distance “x” inside a coating disbondment is a function of the level of applied CP at the OM, disbondment gap size, pipe exposed surface area, and the resistivity of the trapped soil solution inside a coating disbondment. In more detail:

- The higher the level of applied CP, the higher the CP potential level at each particular distance under a coating disbondment until reaching OCP.
- The greater the exposed the steel surface area, the larger the CP potential drop at each particular distance under a coating disbondment until reaching OCP.
- The smaller the disbondment gap size, the larger the CP potential drop at each particular distance under a coating disbondment until reaching OCP.
- The lower the resistivity of the trapped soil solution inside a coating disbondment, the lower the CP potential drop at each particular distance until reaching values close to OCP.

As shown in previous sections in addition to CP other factors affect the pH inside a coating disbondment. As shown in Equation 7-8, the level of pH inside a coating disbondment at distance “x” from the OM is a function of level of CP potential at

that location, volume of trapped solution, and CO₂ diffusion inside the coating disbondment. In more detail:

- CP could reduce hydrogen and bicarbonate ions, and increase the pH inside a coating disbondment. Higher level of CP potential under a coating disbondment would be more effective in this regard.
- CO₂ could mix with the solution inside a coating disbondment, and generate hydrogen and bicarbonate ions, and prevent the raise in pH by the presence of CP. Higher CO₂ diffusion could be more effective in this regard.
- Lower volume of trapped solution under a coating disbondment would undergo more abrupt changes due to CP reactions or CO₂ fluctuations.

The final pH and potential at each particular location inside a coating disbondment is a function of each individual factor affecting the pH and potential inside the disbondment.

7.3.6. Effect of coating disbondment material

As mentioned earlier, PE tape coated pipes are a major concern to the pipeline industry. Therefore, in order to validate the laboratory experiments done using Poly(methyl methacrylate) (PMMA) as the coating material, two new tests using high density polyethylene (HDPE) and low density polyethylene (LDPE) were performed. Results showed no significant difference in terms of the electrochemical conditions formed under simulated coating disbondments made from these materials when compared to PMMA. As can be seen from Table 7.4, this could be explained by the low CO₂ permeability, and high electrical resistivity of all these materials.

Table 7.4: CO₂ permeability and electrical resistivity of the materials used for the simulated coating disbondment in this study, T=25 °C [28, 29].

Material \ Property	Permeability ($\times 10^{13}$) $\frac{[cm^3][cm]}{[cm^2][s][cmHg]}$	Resistivity ohm-cm
Poly(methyl methacrylate) (PMMA)	3.79	10^{13}
Low Density Polyethylene (LDPE)	9.5	10^{14}
High Density Polyethylene (HDPE)	0.27	10^{15}

7.3.7. Corrosion and near-neutral pH SCC initiation

Electrochemical conditions under a coating disbondment could guide in identifying regions of higher susceptibility to corrosion and near-neutral pH SCC. For instance as determined in Chapter 3, for a coating disbondment containing near-neutral pH soil solution at regions with partial CP protection (less than 100 mV_{SCE}), the formation of large corrosion pits and surface micro-cracks is more probable. However, at OCP conditions for the same coating disbondment formation of large corrosion pits and surface micro-cracks is less probable. Further details about the electrochemical conditions causing corrosion and near-neutral pH SCC may be found in Chapters 3, and 4.

7.4. Conclusions

1. Coating disbondments do not completely shield the CP as commonly believed. Depending on the pH of the soil solution, the level of applied CP potential, the disbondment gap size, and the exposed steel surface area, the CP penetration depth may vary.
2. The CP penetration depth was greater for the localized high-pH environment compared to the near-neutral pH environment. The more negative the CP potential at the OM, the deeper was the CP penetration depth.

3. Increase in the exposed steel surface area, caused lower CP penetration depth inside the disbondment.
4. CP penetration depth decreased for the disbondment with reduced gap size. This was due to the blockage of the more negative CP potentials around the OM for the small gap disbondment.
5. The final pH and potential at each particular location inside a coating disbondment, is a function of combination of several individual factors affecting the pH and potential inside the disbondment.
6. The electrochemical conditions under disbondments made from PMMA, HDPE and LDPE were similar. While this validates the laboratory experiments done using PMMA as the coating material, it also shows that HDPE and LDPE coatings could be treated similarly in terms of electrochemical conditions formed under these coatings.

7.5. References

- [1] A.W Peabody, Peabody's Control of Pipeline Corrosion, Second Edition, NACE International, 2001.
- [2] NACE International Publication 35108, One Hundred Millivolt (mV) Cathodic Polarization Criterion.
- [3] F. King, T.R. Jack, M. Kolar, R. Worthingham, A Permeable Coating Model for Predicting the Environment at the Pipe Surface under CP-Compatible Coatings, Corrosion, New Orleans, Los Angeles, USA, 2004.
- [4] Canadian Association of Petroleum Producers (CAPP), Mitigation of External Corrosion on Buried Pipelines, June 2009.
- [5] S. Papavinasam, M. Attard, and R. Winston Revie, External Polymeric Pipeline Coating Failure Modes, Materials Performance, 4-45 (2006) 28-30.
- [6] A. Cosham, P. Hopkins, The Assessment of Corrosion in Pipelines- Guidance in the Pipeline Defect Assessment Manual (PDAM), Pipeline Pigging and Integrity Management Conference, Amsterdam, The Netherlands, 2004.
- [7] S.Y. Li, Y.G. Kim, Y.T. Kho, and T. Kang, Statistical Approach to Corrosion under Disbonded Coating on Cathodically Protected Line Pipe Steel, Corrosion, 60 (2004) 1058.

- [8] S.Y. Li, Y.G. Kim, K.S. Jeon, and Y.T. Kho, Microbiologically Induced Corrosion of Underground Pipelines under the Disbonded Coatings, *Metals and Materials*, 6 (2000) 281-286.
- [9] F.M. Song, D.W. Kirk, J.W. Graydon, D.E. Cormack, D. Wong, Corrosion under Disbonded Coatings Having Cathodic Protection, *Materials Performance*, 42 (2003) 24-26.
- [10] National Energy Board (NEB), Report of the Inquiry- Stress Corrosion Cracking on Canadian Oil and Gas Pipelines, 1996.
- [11] B.S. Delanty, J. O'Beirne, Major Field Study Compares Pipeline SCC with Coatings, *Oil & Gas Journal*, 15 (1992) 39-44.
- [12] X. Chen, C. Du, X. Li, Effects of Cathodic Potential on the Local Electrochemical Environment under a Disbonded Coating, *Journal of Applied Electrochemistry*, 39 (2009) 697-704.
- [13] M. Yan, J. Wang, E. Han, W. Ke, Local Environment under Simulated Disbonded Coating on Steel Pipelines in Soil Solution, *Corrosion Science*, 50 (2008) 1331-1339.
- [14] J.J. Perdomo, I. Song, Chemical and Electrochemical Conditions on Steel under Disbonded Coatings: the Effect of Applied Potential, Solution Resistivity, Crevice Thickness and Holiday Size, *Corrosion Science*, 42 (2000) 1389-1415.
- [15] J.J. Perdomo, I. Song, Chemical and Electrochemical Conditions on Steel under Disbonded Coatings: The Effect of Previously Corroded Surface and Wet and Dry Cycles, *Corrosion Science*, 43 (2001) 515-532.
- [16] R.R. Fessler, A.J. Markworth, and R.N. Parkins, Cathodic Protection Levels under Disbonded Coatings, *Corrosion*, 39 (1983) 20-25.
- [17] F.M. Song, N. Sridhar, A Two-Dimensional Model for Steel Corrosion under a Disbonded Coating Due to Oxygen With or Without Cathodic Protection Part 1: Full Numerical Solution, *Corrosion*, 62 (2006) 676-686.
- [18] F.M. Song, N. Sridhar, A Two-Dimensional Model for Steel Corrosion under a Disbonded Coating Due to Oxygen with or without Cathodic Protection—Part 2: Model Simplification for Practical Application, *Corrosion*, 62 (2006) 873-883.
- [19] NACE RP 0169-02, Standard Recommended Practice: Control of External Corrosion on Underground Submerged Metallic Piping Systems.
- [20] D.A. Jones, Principles and Prevention of Corrosion, Second Edition, 1996.
- [21] M. Amaya, E. Sosa, Jose L. Garcia Villalobos, and J.M. Romero, Corrosion Behaviour of API X52 and API X65 Pipeline Steels in the Presence of Bacteria Consortia Using Electrochemical Noise, *Corrosion 2003*, San Diego, California, USA, 2003.
- [22] A.Eslami, W.Chen, R.Eadie, Corrosion of X-65 Pipeline Steel under a Simulated Coating Disbondment, Submitted to *Corrosion*, 2012.
- [23] W. Chen, S.H. Wang, R. Chu, F. King, T.R. Jack, R.R. Fessler, Effect of Precyclic Loading on Stress-Corrosion-Cracking Initiation in an X-65 Pipeline Steel Exposed to Near-Neutral pH Soil Environment, *Metallurgical and Materials Transactions A*, 34A (2003) 2601-2608.
- [24] W. Chen, F. King, T.R. Jack, and M.J. Wilmott, Environmental Aspects of Near-neutral pH Stress Corrosion Cracking of Pipeline Steel, *Metallurgical and Materials Transaction A*, 33A (2002) 1429-1436.

- [25] A. Eslami, B. Fang, R. Kania, B. Worthingham, J. Been, R. Eadie, W. Chen, Stress Corrosion Cracking Initiation under the Disbonded Coating of Pipeline Steel in Near-neutral pH Environment, *Corrosion Science*, 52 (2010) 3750-3756.
- [26] A. Eslami, R. Kania, B. Worthingham, G.V. Boven, R. Eadie, W. Chen, Effect of CO₂ and R-Ratio on Near-neutral pH Stress Corrosion Cracking Initiation Under a Disbonded Coating of Pipeline Steel, *Corrosion Science*, 53 (2011) 2318-2327.
- [27] A. J. Bard, L. R. Faulkner, *Electrochemical Methods Fundamentals and Applications*, Second Edition, John Wiley and Sons INC., 2000.
- [28] S. Pauly, Permeability and diffusion data, in: J. Brandrup and E.H. Immergut (Eds.), *Polymer Handbook*, 3rd Edition., John Wiley & Sons, New York, NY, 1989
- [29] T.A. Oswald, G. Menges, *Materials Science of Polymers for Engineers*, 2nd Edition, Hanser Gardeners Publications Inc., 2003.

Chapter 8: Conclusions, Research Impact, and Recommendations

8.1. Conclusions

The objective of this thesis was to increase our understanding of near-neutral pH SCC initiation mechanism(s) and the effect of different environmental and mechanical factors on crack initiation. In this regard a novel testing setup was designed and built (Chapter 2). Using the setup, and by utilizing other techniques, different aspects of near-neutral pH SCC initiation were investigated. Near-neutral pH SCC initiation under a disbonded coating and the effect of different environmental and operational factors on crack initiation were covered in Chapters 3-5. Corrosion of pipeline steel under the simulated coating disbondment was covered in Chapter 6. The effect of CP, pH, disbondment gap size, pipeline exposed steel surface area, and disbondment material on electrochemical conditions formed under coating disbondments were covered in Chapter 7. The main conclusions obtained from these studies are summarized below.

8.1.1. Near-neutral pH SCC initiation under the simulated coating disbondment and effect of environmental and operational factors

1. The combination of CP and coating disbondment generated a localized environment under the simulated disbonded coating with a gap size of 1 cm. CP potential dropped from full protection at the open mouth of the disbondment to values close to free corrosion potential deep inside the disbondment at around 12 cm from the OM.
2. Despite the pH of the bulk soil solution being near-neutral, the pH of the trapped solution inside the simulated coating disbondment was not persistently near-neutral as commonly believed. It varied significantly depending on CO₂ concentration and level of CP. When the CO₂ supply was limited and there was adequate CP in the testing environment, the pH increased from near-neutral to higher values above 10. The closer to the OM of the disbondment, the more significant was the increase in pH. In

the presence of 5%CO₂/N₂ in the testing environment, independent of the level of CP, the pH of the trapped soil solution inside the simulated coating disbondment stayed near-neutral.

3. When cyclic loading was applied, depending on the pH of the localized environment inside the simulated coating disbondment, different crack initiation mechanisms were involved. In the near-neutral pH environment micro-cracks were mainly generated from the mouth and bottom of large individual pits, whereas, in the localized high-pH environment several surface micro-cracks were initiated from the linkage of sub-micrometer pits.
4. In the near-neutral pH environment the corrosion severity depended on the position from the OM. Close to the OM of the disbondment, where the region had full CP protection minor corrosion and/or pitting had occurred. At the far end from the OM where no/limited CP protection was present, general corrosion had occurred. In the region between the OM and the far end from the OM where only a little CP protection (less than 100 mV_{SCE}), large individual corrosion pits were formed. When sufficient time had passed, micro-cracks were initiated both from the surface and cross sections of some of the large individual corrosion pits.
5. In high-pH environments the corrosion severity was insignificant compared to the near-neutral pH environment. Pitting corrosion was different from that observed in the near-neutral pH environment. Several sub-micrometer pits were formed particularly in the region between the OM and the far end. Surface shallow micro-cracks were initiated from linkage of these pits. The region between the OM and the far end away from the OM had the highest number of the surface micro-cracks. Sufficient CP close to the OM, or slight corrosion at the far end from the OM had mitigated the formation of the micro-cracks.

6. Reducing the R-ratio (increasing the stress change) had different effects on the crack initiation mechanism depending on the pH of the localized environment inside the simulated coating disbondment. In the near-neutral pH environment, reducing R-ratio from R=0.8 to R=0.4 enhanced the crack initiation from the mouth of large pits. However it did not significantly affect the crack initiation in the localized high-pH environment, where the crack initiation mechanism was driven by formation of several shallow surface micro-cracks.
7. Near-neutral pH SCC initiation was affected by the presence of 1% O₂ in the near-neutral pH environment testing environment. Due to the formation of deeper corrosion pits, crack initiation was enhanced in the cross section of the specimen; however, the situation was complicated on the surface. On the surface, crack initiation was affected by the change in CP distribution under the simulated coating disbondment.

8.1.2. Corrosion of pipeline steel under the simulated coating disbondment

1. X-65 pipeline steel showed active corrosion behavior in the near-neutral pH environment, while passivation behavior was observed in the localized high-pH environment. This caused the corrosion rate of the pipeline steel to be significantly lower in the high-pH environment compared to the near-neutral pH environment.
2. Preferential corrosion of crystallographic planes having different orientations, dissolution of inclusions, and galvanic coupling between different phases in the steel microstructure were some of the corrosion mechanism observed in the investigations. It was discovered that dissolution from inclusions could initiate large corrosion pits, while dissolution of sub-micrometer constituents could result in formation of sub-micrometer pits.

3. The corrosion rate of pipeline steel was significantly affected by the effect of CP and coating disbondment. While CP reduced the corrosion rate of the pipeline steel especially at locations close to the OM of the coating disbondment by providing electrons to the surface, coating disbondment reduced the corrosion rate of the pipeline steel deeper in the disbondment by forming a barrier against CO₂ diffusion and hence causing the pH to increase slightly deep inside disbondment. This explains the existence of a “sweet region” between the OM and the far end where the conditions for formation of large corrosion pits as the results of high localized corrosion rates in the presence of partial CP potential is favorable.

8.1.3. Electrochemical conditions under coating disbondments of pipelines

1. Near-neutral pH SCC initiation was a function of electrochemical conditions formed under coating disbondments.
2. Coating disbondments do not completely shield CP as commonly believed. CP penetration under the coating disbondment was a function of the pH of the trapped soil solution, level of applied CP potential, disbondment gap size, and exposed steel surface under the coating disbondment.
3. CP penetration depth under coating disbondment was more in the localized high-pH environment than the near-neutral pH environment. This was due to the higher resistivity of near-neutral pH soil solution, as compared to the high-pH soil solution.
4. An increase in pipeline steel exposed surface area caused a larger CP potential drop inside the simulated coating disbondment. This was explained by the decrease in current density with increase in the exposed steel surface area. With an increase in the level of applied CP potential, the CP penetration depth increased.

5. CP penetration depth decreased for simulated coating disbondment with reduced gap size. This was due to the shielding effect of the coating at the OM the reduced gap size disbondment, as compared to disbondments with larger gap distances.
6. The electrochemical conditions under simulated coating disbondments made from real coating materials (High Density Polyethylene (HDPE) and Low Density Polyethylene (LDPE)), were similar to that under coatings made from Poly(methyl methacrylate) PMMA. While this validates all the laboratory experiments done in this research using PMMA, it also shows that HDPE and LDPE coating could be treated similarly in terms of electrochemical conditions formed under these coatings.

8.2. Research Impact

This work has significant impact in understanding near-neutral pH SCC initiation under disbonded coatings of pipelines. No prior work has been able to simulate near-neutral pH SCC initiation by considering the synergistic effects of coating disbondment, CP and cyclic loading as has been observed in the field investigation. Using the novel testing setup described, this was achieved. The true effects of CP, coating materials and disbondment geometry, loading cycles, soil solution chemistry and gas concentrations on near-neutral pH SCC initiation were investigated. By understanding the true effects of these parameters on near-neutral pH SCC initiation, effective steps in mitigating this form of cracking on currently existing buried pipes can be taken. Also, actions to prevent this form of cracking for future pipeline installations can be implemented.

It is worth mentioning that the novel testing setup used for near-neutral pH SCC initiation investigations, could be used as a powerful tool not only for crack initiation studies, but also for further crack growth studies. In fact, this testing

setup has already been used for crack growth studies. So far the results using this setup have shown significant improvement in understanding near-neutral pH SCC crack growth behavior¹.

8.3. Recommendations

1. While the role of some environmental and operational factors on near-neutral pH SCC initiation using realistic testing conditions were investigated, the effect of other parameters such as pipe steel surface condition, microstructure, yield strength, residual stresses, sulfur and bacteria in the testing environment could also be investigated.
2. Cracks were initiated at different environmental and loading conditions through long term tests. While understanding the initiation is important, performing longer term tests in order to better understand the condition(s) of crack propagation is also suggested.
3. Reducing the stress ratio (R-ratio) affected crack initiation from deep corrosion pits, while it had minor effects on crack initiation where corrosion features were shallow. This could be important for pipeline integrity management and safe operation. Therefore full scale validation tests are suggested.
4. It was discovered that general corrosion could mitigate surface crack initiation. This could be the basis of a remedy for the shallow near-neutral pH SCC crack treatment. Full scale investigation in controlled corrosion condition is suggested in this regard

¹ A.T. Egbewande, A. Eslami, W. Chen, R. Worthingham, R. Kania, G.V. Boven, Growth of Surface-type Stress Corrosion Cracks in Near-neutral pH Environments under Disbonded Coatings, In Proceedings of the 8th International Pipeline Conference IPC2010, Calgary, Alberta, Canada, 2010.

5. Every disbondment (almost) has a region where the gap narrows down to nothing. The effects of other disbondment geometries and particularly this tapered region would be something that should be studied in future.
6. Modeling of the corrosion and near-neutral pH SCC initiation under disbonded coatings is recommended. The results of the models could be compared with the current laboratory findings.

Appendix A: Experimental Setups

A.1. Mechanical loading testing frame



A. 2. Potentiostat



A.3. Reference Electrodes

A.3.1. Permanent reference electrode



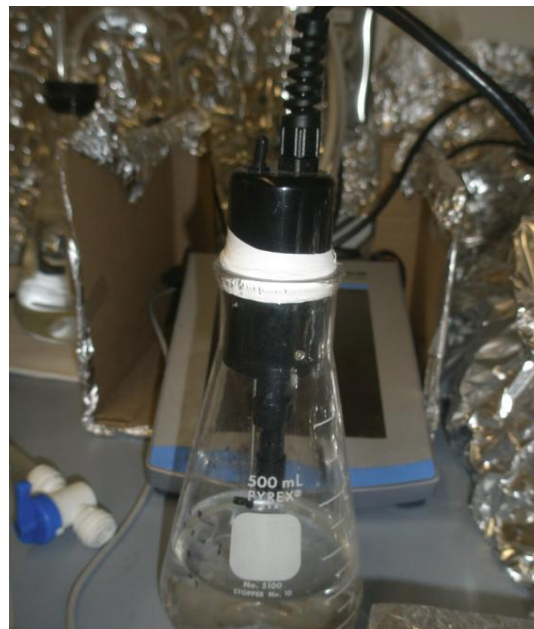
A.3.2. Portable reference electrode



A.4. Micro-electrodes used for determining the pH inside coating disbondments



A.5. Oxygen probe used for determining oxygen concentration in soil solution



A.6. Conductivity probe used for determining the conductivity and resistivity of soil solutions



Appendix B: Experimental Procedures

B.1. Nickel plating procedure for cross sectional characterization

In nickel plating with Watts type solution, the plating bath was filled in a beaker. The pH of the bath was controlled at 4.0 and the temperature was maintained at 40 °C. A stirrer was employed in the experiment to provide agitation. It is common that the pH and the nickel ion concentration of the bath increase slowly during electroplating. Therefore, checking and adjusting pH value of the solution regularly in plating is necessary [1]. The polished specimen surface was cleaned in acetone then ethanol, and placed inside the plating bath. The time and current for plating were adjusted according to Faraday's law [2].

B.2. References

[1] ASM Handbook, Surface Engineering Volume 5, ASM International, 1996.

[2] V.S. Bagotsky, Electrochemistry and Environment, in Fundamentals of electrochemistry 2nd Edition, John Wiley & Sons, 2005.